UC Berkeley
UC Berkeley Electronic Theses and Dissertations

Title

Geometric insights into speed, efficiency, and optimal control of nonequilibrium systems

Permalink

https://escholarship.org/uc/item/7mp4f15p

Author

Frim, Adam

Publication Date

2024

Peer reviewed|Thesis/dissertation

eScholarship.org Powered by the California Digital Library
University of California

Geometric insights into speed, efficiency, and optimal control of nonequilibrium systems

by

Adam Frim

A dissertation submitted in partial satisfaction of the

requirements for the degree of

Doctor of Philosophy

in

Physics

in the

Graduate Division

of the

University of California, Berkeley

Committee in charge:

Professor Michael DeWeese, Chair
Professor Hernan Garcia
Professor Michael Lindsey

Summer 2024

Geometric insights into speed, efficiency, and optimal control of nonequilibrium systems

Copyright 2024
by
Adam Frim

Abstract

Geometric insights into speed, efficiency, and optimal control of nonequilibrium systems

by

Adam Frim

Doctor of Philosophy in Physics

University of California, Berkeley

Professor Michael DeWeese, Chair

The last several decades have seen revolutionary advances in our understanding of nonequilibrium thermodynamics. Designed originally to study macroscopic systems manipulated slowly, these new approaches to thermodynamics have extended the applicability of the theory to the small, fluctuating systems most relevant to biology and nanoscale engineering. With this powerful framework in place, a significant effort has been made to not only understand but control and manipulate such systems to achieve desired goals, and to do so optimally. In this thesis, after summarizing relevant history and background, we explore two major facets of this thermodynamic control problem. First, we investigate shortcut engineering, a control problem aimed at addressing rapid system transformation from an initial state to a target state. Second, utilizing a geometric approach, we study the control of slowly-driven systems, with particular focus on the optimal, i.e. maximally efficient, control of mesoscale thermal machines. Finally, we demonstrate a novel connection between these two disparate topics: although seemingly disconnected, the optimal control problem for certain shortcutting settings is *identical* to that of slowly-driven systems. We conclude by commenting on both the scientific merit and pragmatic calculational utility of this connection and on potential implications for future work.

To my parents

Contents

Contents **ii**

List of Figures **v**

I Introduction 1

1 An invitation to the nonequilibrium world **2**

2 Review of classical thermodynamics and statistical mechanics **4**
2.1 Classical thermodynamics 4
2.2 Statistical mechanics 5
2.3 Limitations of the classical theory 8

3 Stochastic thermodynamics **9**
3.1 Precursors 9
3.2 Fluctuation theorems 12
3.3 Stochastic energetics 14
3.4 A modern outlook 16

4 Thermodynamic control of nonequilibrium systems **18**
4.1 Preliminaries 18
4.2 The general thermodynamic control problem 19
4.3 Full and parametric control 20
4.4 Approximation schemes and regimes of applicability 21

II Shortcut engineering and rapid control 23

5 Shortcut engineering **24**
5.1 Shortcuts to adiabaticity 24
5.2 Broader escorted dynamics 26
5.3 Outlook 27

6 Engineered swift equilibration for arbitrary geometries **28**
6.1 Introduction . . . 28
6.2 Theory . . . 29
6.3 Practical examples . . . 30
6.4 Discussion . . . 35
6.5 Conclusion . . . 36
6.A High temperature limit of dipole model . . . 36
6.B Simulation details . . . 37

7 Shortcut engineering active matter: run-and-tumble particles **38**
7.1 Introduction . . . 38
7.2 Run-and-tumble dynamics in 1D . . . 39
7.3 Shortcut solution . . . 41
7.4 Explicit protocols . . . 42
7.5 Minimal work protocol . . . 44
7.6 Discussion . . . 45
7.A Derivation . . . 48
7.B Athermal Shortcut . . . 51
7.C Average external work . . . 52

III Thermodynamic geometry and optimal control **55**

8 Thermodynamic geometry **56**
8.1 Early geometric approaches . . . 56
8.2 Thermodynamic length and dissipation . . . 57
8.3 Geometric optimal control . . . 57

9 Optimal finite-time Brownian Carnot Engine **59**
9.1 Introduction . . . 59
9.2 Thermodynamic geometry . . . 60
9.3 Brownian working substance . . . 62
9.4 Optimal Brownian Carnot engine . . . 62
9.5 Engine performance . . . 66
9.6 Discussion . . . 68
9.7 Conclusion . . . 69
9.A Thermodynamic metric for the parametric harmonic oscillator . . . 69
9.B Fokker-Planck dynamics of the harmonic oscillator and simulations . . . 72
9.C Numerical validation of slow-driving approximation . . . 73
9.D Comparison of simulated results to experiment . . . 76

10 A geometric bound on the efficiency of irreversible thermodynamic cycles **79**

10.1 Introduction . . . 79
10.2 Efficiency of irreversible engines . . . 80
10.3 Isoperimetric bound on efficiency . . . 81
10.4 Construction of optimal cycles. . . . 83
10.5 Parametric harmonic oscillator . . . 83
10.6 Discussion . . . 86
10.7 Conclusion . . . 89
10.A Isoperimetric bound on efficiency for arbitrary thermodynamic manifolds . . . 89
10.B Isoperimetrically optimal Brownian protocols . . . 90
10.C Classical Brownian protocols . . . 93
10.D Construction of Fig. 10.3 . . . 96
10.E Isoperimetric inequalities with density . . . 97

IVBringing the slow up to speed: connecting thermodynamic geometry and shortcut engineering 99

11 The equilibrium manifold: bridging thermodynamic and shortcut geometries 100
11.1 Kolmogorov operators . . . 100
11.2 Shortcuts to Isothermality . . . 102
11.3 Optimal shortcut geometry . . . 105
11.4 Unifying thermodynamic geometries . . . 105
11.5 Thermodynamic geometry and the equilibrium Wasserstein manifold . . . 107
11.6 Outlook . . . 108

Bibliography 110

List of Figures

6.1 Demonstration of Engineered Swift Equilibration for non-Euclidean configuration space 32

7.1 Steady-state distribution of run-and-tumble particles for a variety of parameter values 40
7.2 Shortcut protocols can outperform quenched protocols in Langevin dynamics simulations 43
7.3 Minimal work (solid blue) and Minimal time (dashed orange) protocols for $k(t)$ and $v_0(t)$ 46

9.1 Shape and temporal parametrization of a previously tested Brownian Carnot cycle, the optimized Brownian Carnot cycle, and an optimal geodesic cycle matched to the Carnot cycle 63
9.2 Performance of various engines considered in the main text as a function of protocol duration τ 65
9.3 The thermodynamic cycles and parametrizations considered 68
9.4 Comparison of full numerical results to linear response 75
9.5 Comparison of simulated results to experiment 77

10.1 Comparison of Brownian Carnot cycle and optimal isoperimetric cycles 85
10.2 Examples of numerically constructed optimal isoperimetric cycles 87
10.3 Optimally constructed cycles strongly outperform Carnot and all other cycles tested 88
10.4 Characteristic example of optimal cycle construction 90
10.5 Plots of optimally constructed cycles for a variety of material parameters and in a variety of regions of Clausius space 92
10.6 Quasistatic profiles of classical thermodynamic cycles in various spaces 95

Acknowledgments

This work was made possible in no small part from the aid, support, friendship, and love of the many people I have had the pleasure of calling advisors, colleagues, collaborators, and friends over the course of my PhD. After six wonderful years in Berkeley, I fear I must preface any acknowledgements by myself acknowledging that there are in fact far far too many people to thank and I apologize to any I omit.

I will start by thanking my many mentors and advisors over the years. First and foremost, none of what follows would be possible without the kindness, patience, passion, enthusiasm and support of my advisor, Michael DeWeese. Your constant encouragement and excitement, even at times when they did not exactly seem warranted, has been integral to the success of my program and will forever inform how I view mentorship, and your methods for uncovering and tackling good questions have already influenced how I approach science. I wish also to thank my thesis committee members, Hernan Garcia and Michael Lindsey, whose expertise and advice have been very helpful, and Ori Ganor for agreeing to sit on my qualifying committee. I would like to give a special thanks to David Limmer of the Chemistry department who has served as something of an external advisor at times during my PhD and for whose support I am grateful. Finally, I wish to thank my previous mentors over the whole course of my academic career, with particular appreciation to Howard Georgi, who showed me the curiosity and wonder physics can elicit, and Mark Vondracek, who first demonstrated to me the joys of studying and interacting with the natural world.

Over the years, I have been very lucky to have had wonderful scientists with which to work through hard problems. I wish first to acknowledge my coauthors: Stephen Chen, Ethan Evans, Etienne Fodor, Dibyendu Mandal, Evangelos Theodorou, and Ziyi Wang. Over the last year, I have also very much enjoyed my collaboration with Hana Mir. I have great faith in the future of optimal control in nonequilibrium stat mech in her hands. I would also like to thank the DeWeese group as a whole over the last several years, who have been wonderful colleagues, friends, and made my academic life all the more fun. Whether talking about science, life, or whatever struck our fancy, I am very grateful to especially to Sam D'ambrosia,, Dhruva Karkada, Steven Lee, Eduardo Sandoval, and Jamie Simon for making the office both a place full of curiosity but also full of fun. Finally, I would like to give very special recognition to Adrianne Zhong who has been my closest colleague and collaborator essentially from the start of my work in nonequilibrium physics, and who continues to push the boundary of our (and certainly my) understanding on a seemingly daily basis. I have benefited immensely from our professional work, and I am grateful that there is only more to come (and all the more grateful to call her a friend)!

Six years ago, I moved across the country to the Bay Area not knowing a soul; I have been remarkably fortunate to have made some of my closest friends since then. I wish to thank, among many others, Elizabeth and Clara Dresselhaus, Chitraang Murdia and Jack Spilecki, Dahlia Davidovits, Talia Wiskind, and Daniella Rosen, Roy Abdollahi and Jade Cohen, Noa Dahan, Yael Saiger and Matt Jelen, and David Dunsky for being patient, loyal, and truly dear friends. Without their support, I most certainly would not have finished this

thesis (and debatably kept my sanity). I would also like to recognize Michael Greenwald and Ronna Bach who have been incredibly generous hosts over the years, and the whole Bach-Greenwald family for serving as a welcoming home away from home. I would be remiss if I did not also thank Rabbi Gil and Bracha Leeds and the entire Leeds family, from whom I have learned a great deal and for whom I am truly grateful for the truly unimaginable time and effort they sacrifice to serve as spiritual leaders and as the keepers of a *heimishe* space at Cal. Finally, I wish to thank the entire community of Congregation Beth Israel which has served as a welcoming and kind spiritual home from my earliest days in Berkeley, though especially over the last year.

As a final acknowledgment, I thank my family immensely. To Daniel, I am grateful for the many paths you blazed so I could more easily traverse them. To Michael, I am so grateful for your kindness, humor, mathematical support, and mind-boggling Mathematica mastery. I would like to thank you both for the time, counsel, and friendship you have given, from childhood all the way up. To my mother, you have given so much of yourself for our sakes. Especially over the last few years, I could never overstate my appreciation and my awe of your kindness, patience, consideration, and ability to handle so much to ensure that we could continue to pursue our dreams. And finally, to my father of blessed memory: you served as my original scientific and academic hero, teaching me so much about the value of curiosity, scholarship, education, hard work, the pursuit of excellence, and, above all, decency. Without these many lessons over the years and the inspiration and support you always showed in the path I chose to follow, I would certainly not be where I am today. Much as I am saddened you are not able to be join us in this moment, I hope this achievement in part carries on the legacy of the values you instilled.

Part I

Introduction

Chapter 1

An invitation to the nonequilibrium world

Across numerous timescales and spatial resolutions, the observable physical universe is in flux. Systems organize, move, disassemble, and transform. At the smallest scales, nuclear forces drive motion, charged particles attract and repel, atoms bond, and molecules associate; at the largest scales, celestial bodies, galaxies, and even the cosmos as a whole evolve. A unifying theme is change: Nature is decidedly not static.

When viewing macroscopic systems composed of many constituent parts, the most relevant and successful physical theories have to date been thermodynamics and statistical mechanics. These theories were designed explicitly to describe and explain the macroscopic observable properties of such complex systems without full access to their unimaginably intricate microscopic details. However, a key weakness of the classical "textbook" versions of these theories is their frequent reliance on an equilibrium assumption. That is, for the sake of theoretical development and pragmatism, one often assumes a system is, and remains, in equilibrium at all times. Although this assumption can explain the properties of certain physical systems, especially those at or near equilibrium, with outstanding accuracy, it fails to faithfully describe systems significantly away from equilibrium. And, as we have just emphasized, nearly all processes in the natural world are *not* in equilibrium.

These issues particularly come to a head when undertaking a quantitative, physically-consistent study of biological systems. Living systems by definition explicitly maintain their existence out of equilibrium. In a particularly prescient 1944 manuscript [1], in addition to postulating an early precursor of genetics, Erwin Schrödinger discussed the constant battle biological systems face in their struggle for survival. In his own words, "Living matter evades the decay to equilibrium"; in a popular paraphrase: "equilibrium means death." Nonequilibrium physics provides an important lens to study living organisms in their ever-changing environment.

Inspired by these issues, the last several decades have seen an explosion of literature focused on tackling a consistent understanding of thermodynamics, statistical mechanics, and more broadly, stochastic dynamics for systems not necessarily in, or near, equilibrium. These

studies have led to numerous advances, discovering novel results that apply to all systems regardless of their specific dynamics or the degree to which they are out of equilibrium, and have fundamentally revolutionized the state of the art in the study of such systems.

In this dissertation, we approach these problems with particular focus on external control and optimization. The manuscript is organized as follows:

- In Part I, we introduce the topics of this thesis and briefly review relevant background information. In Chapter 2, we discuss classical thermodynamics and statistical mechanics including a brief history before delving into the main weaknesses of this classical theory. In Chapter 3, we introduce stochastic thermodynamics, a revolutionary new approach to the nonequilibrium thermodynamics of the fluctuating systems, as frequently encountered in nanoscale thermodynamics or when studying externally driven systems. Finally, in Chapter 4, we introduce and contextualize our main focus by discussing prior work on optimal control of nonequilibrium thermodynamic systems.

- In Part II, we consider *shortcut engineering*, a series of techniques for rapid control and manipulation of complex physical systems. In Chapter 5, we introduce shortcut engineering in greater detail and overview its history. In Chapters 6 and 7 we demonstrate examples of important novel advances to these techniques. In Chapter 6, we consider a specific type of shortcut engineering, *engineered swift equilibration*, that allows for rapid equilibration of a classical physical system. We derive a method to carry out this technique for an overdamped classical system with a generic configuration space. In Chapter 7, we consider a specific instance of shortcut engineering applied to *active matter*, arriving at a method to steer this intrinsically nonequilibrium matter to a desired state in finite-time.

- In Part III, we consider *thermodynamic geometry*, an approach to studying thermodynamics through the lens of differential geometry. In particular, in a modern formulation of thermodynamic geometry, one can draw a direct link between a notion of geometric length and dissipation, thus allowing for shortest-length, geometric optimization to be utilized in optimal control of thermodynamic systems. In Chapter 8, we introduce this approach and these concepts in more rigorous detail and discuss their history. In Chapter 9, we demonstrate the successful application of these methods to an important model engine, demonstrating the strengths of these methods in practical, experimentally relevant systems. In Chapter 10, we use this theory to derive a novel and universal geometric bound on efficiency for irreversible thermodynamic cycles acting as heat engines. We also construct optimal cycles that demonstrate the tightness of this bound and prove its utility in engine design at the nanoscale.

- Finally, in Part IV, we connect the major focuses of this dissertation. In particular, in Chapter 11 we will demonstrate that, although historically developed independently and seemingly disparate topics, shortcut engineering and thermodynamic geometry are intimately connected.

Chapter 2

Review of classical thermodynamics and statistical mechanics

2.1 Classical thermodynamics

Classical thermodynamics, and arguably modern physics, was born in the early 19th century when, inspired by the then recent advent of the steam engine, leading polymaths and engineers first delved into questions of heat and work. At the time, kinetic energy, *vis viva*, or *motive power* were all understood to be various forms of some motional conserved quantity [2, 3, 4], precursors to what would later be understood as *mechanical work*. Heat, in contrast, was far less well understood: the flow of heat was associated with changes in temperature, but there was no deeper understanding at the time of what exactly heat, or temperature for that matter, was [5]. These issues came to a head with the development of the engine, a system capable of utilizing a transfer of heat to enact work.

The theory grew over the next century to explain these and related issues. By the early 20th century, due to significant contributions by, among many others, Sadi Carnot [4], Emile Clapeyron [6], Hermann von Helmholtz [7], and Rudolf Clausius [8], the theory at the level of physical understanding was largely established through two major empirical laws. The first law of thermodynamics posited that heat and work were both forms of by which the *internal energy* in a system, U, could be exchanged with some environment:

$$dU = \delta Q + \delta W, \tag{2.1}$$

where δQ is the amount of heat injected into the system by its environment and δW is the amount of work done on the system by the environment. Fundamentally, this law mandates that for an isolated system, the sum total internal energy must be conserved. The second law of thermodynamics is slightly more opaque. At the level of classical thermodynamics, it essentially mandates the empirically-informed observation that heat does not flow from colder to hotter substances [9, 10]. In its more modern formulation due primarily to Clausius, one considers the quantity *entropy* S. In classical thermodynamics, entropy is a state function

defined as the sum of all incremental heat flow into a system divided by the system's current temperature, assuming that all processes are carried out reversibly [10]

$$dS_{\text{sys}} = \frac{\delta Q}{T}. \tag{2.2}$$

It bears mentioning, this definition holds even if an actual physical process is *not* reversible: the entropy is a function of the state defined via a "virtual" reversible process. However, if the system is in contact with its surroundings at some temperature T_{surr} and some not-necessarily reversible cyclic process is carried out, Clausius proved [11]:

$$\oint dS_{\text{surr}} = -\oint \frac{\delta Q}{T_{\text{surr}}} \geq 0, \tag{2.3}$$

where equality is only achieved for a reversible process. Altogether then,

$$\oint dS_{\text{tot}} = \oint (dS_{\text{sys}} + dS_{\text{surr}}) \geq 0, \tag{2.4}$$

which follows as $\oint dS_{\text{sys}} = 0$ as entropy is a function of state. Recognizing this is true for *all* cycles, one can conclude total entropy production is positive even for non-cyclic paths. This is the development of the modern formulation of the classical second law of thermodynamics: for an isolated system the total entropy must increase. Following the establishment and acceptance of these two laws of nature, the next several decades saw the addition of two empirical laws that mainly served to make the theory of thermodynamics well-defined, though we will not focus on their history here.

2.2 Statistical mechanics

In the later 19th century, initially growing out of the nascent kinetic theory of gases, James Clerk Maxwell and Ludwig Boltzmann made a first attempt at a microscopic explanation for thermodynamics. First, following prior work by Clausius [12], Maxwell considered a collection of N small particles interacting by perfectly elastic collisions. Applying this form of a kinetic theory and symmetry arguments, he arrived at a formula for the fraction of particles that existed in a given infinitesimal range of velocities when the system was stationary, effectively deriving the equilibrium distribution of velocities for a system [13], now universally known as the Maxwell distribution. Boltzmann, inspired by Maxwell's work, first generalized the distribution to a number of more complicated cases and began considering its temporal evolution [14, 15]. Next, both to answer these questions and as an early attempt for a microscopic understanding of entropy, Boltzmann defined a quantity H[1], with

[1]To connect with entropy, Boltzmann initially used the symbol E. The usage of H derives from a critical review of Boltzmann's work by Samuel Burbury [16]. The origin of the H is debated, though it is likely derived from a Hellenized E: the capital Greek Eta is indistiguishable from a capital Latin "H."

the following form [15]:

$$H = \int f(E) \left(\ln \frac{f(E)}{\sqrt{E}} - 1 \right) dE, \tag{2.5}$$

where E is the energy of the system and $f(E)$ is the energy distribution. By then considering collisions between idealized particles and, critically, assuming all particles and collisions were uncorrelated, an assumption he called "molecular chaos," Boltzmann was able to show that H should always decrease for any collision. Boltzmann further showed that H would attain a minimum value when the system is in the equilibrium Maxwell-Boltzmann distribution, thus providing further confirmation of the previous mechanical derivations. This result, now universally known as Boltzmann's H-Theorem, was an early and critical success of the nascent statistical theory: at least at the level of suggestion, it gave a microscopic explanation for the second law for nearly-ideal gases.

Boltzmann's work was the subject of notable criticisms at the time of its publication for a variety of reasons. Philosophically, Boltzmann adopted a particle theory in describing gases, which, although popularly accepted among chemists at the time, was still unpopular and highly controversial among physicists [17]. Further, Johann Lochschmidt pointed out that the underlying mechanical dynamics were time symmetric, though Botlzmann was deriving a time-irreversible result at the macroscopic level, a seeming paradox [18]. Boltzmann's attempt to resolve this paradox led to his next most significant result: a fundamental connection between microscopic dynamics and macroscopic phenomena. We highlight here only the ultimate result and refer the interested reader to the more comprehensive history [19]: Botlzmann derived that entropy of a macroscopic state was related logarithmically to the microscopic combinatorial multiplicity of a macroscopic state. In more modern language [10], a given observed macroscopic state is referred to as a *macrostate*. This, for example, could correspond to an ideal gas with a given, fixed energy E, number of particles N, and volume V. At the same time, that gas is made up of N particles each with a momentum, such that one could specify the state of the gas microscopically with all such positions and momenta: this detailed microscopic configuration is referred to as a *microstate*. Importantly, for any given macrostate, there are typically a large number of such microstates that the system could assume: we refer to this number as the multiplicity, W, of the macrostate. Boltzmann considered a system at a fixed energy and made a key assumption that, for a given macrostate at this energy, all such possible microstates were equally likely, and derived the critical equation

$$S = k_B \log W, \tag{2.6}$$

where $k_B = 1.380649 \times 10^{-23}$ J/K is a constant with dimension[2]. This is one of the earliest major tenets of statistical mechanics: a relation linking macroscopic thermodynamic entropy to the microscopic details of the system.

The next several decades of development carried on this legacy, extending bridges between empirical, macroscopic thermodynamic laws, and theoretically derived, microscopic

[2]Boltzmann actually only derived the logarithmic dependence on W. Planck was the first to study the constant in detail, coming up with the first estimate in 1900 while studying black-body radiation [20].

statistical mechanical results, though to ever more complicated systems. Here, we will highlight some of the major contributions of J. Willard Gibbs, particularly as his perspective informs modern statistical mechanics even today [21, 22, 10]

Rather than focussing only on an ideal gas, Gibbs considered a general ensemble of system states. In particular, rather than the actual system that was observed, Gibbs envisioned carrying out an experiment a large (technically infinite) number of times [21, 22]. In each run of this experiment, the system would assume a specific microstate, and Gibbs defined an ensemble as the complete set of all possible microstates when a given experiment is repeated infinite times. Of particular interest are experiments repeated with a certain set of macroscopic observables held fixed: that is an experiment in which the system assumes a fixed macrostate. With these definitions, Gibbs defined unique ensembles corresponding to a given set of fixed observables, and a number of historically significant such ensembles are named. For the macrostate given by a fixed number of particles N, fixed volume V and a total measurable macroscopic energy E, the corresponding ensemble of microstates as the *Microcanonical ensemble* or N, V, E *ensemble*. This is the ensemble for which Boltzmann's entropy equation, Eq. 2.6, is valid. In contrast, for fixed N, V, and temperature T, the ensemble is referred to as the *Canonical ensemble* or NVT *ensemble*. Gibbs studied this ensemble extensively, arriving at the general distribution of energies for such a system given by:

$$p(E_i) = \frac{1}{Z} e^{-\beta E_i}, \tag{2.7}$$

where i labels a given energy level, E_i is the corresponding energy, and Z, called the *partition function* is a normalization constant:

$$Z = \sum_i e^{-\beta E_i}. \tag{2.8}$$

Boltzmann's initial derivation for the energy distribution of a gas assumed this form, however Gibbs's result holds for *any* system in equilibrium at a fixed temperature, volume, and particle number.

Gibbs also, importantly, derived the form of entropy for an arbitrary ensemble [22]:

$$S_{\text{Gibbs}} = -k_B \sum_i \rho_i \log \rho_i, \tag{2.9}$$

where ρ_i is the probability to be in the ith (micro)state. This formula, to which we will refer as *Gibbs entropy*, is general for *any* distribution over microstates. In the special case where the distribution is uniform over microstates, as occurs in the fixed-energy microcanonical ensemble, Eq. (2.9) degenerates to Eq. (2.6) as it must. Further, one should observe this formula is quite similar to Botlzmann's H, Eq. (2.5).

With these and subsequent major developments from Boltzmann, Gibbs, and others, one is able to recapitulate the major results of classical thermodynamics as well as give a microscopically-informed, statistical interpretation of these laws.

2.3 Limitations of the classical theory

Thermodynamics and statistical mechanics have proven hugely influential over the last century, providing fundamental physical constraints on all systems and disciplines with particular influence on the development of quantitative approaches to chemistry and biology. From a physicist's standpoint, studies in statistical mechanics led to the so-called ultraviolet catastrophe in the early 20th century [23], whose resolution spurred the early quantum theory. Even today, the laws of thermodynamics, as a whole, remain entirely applicable and correct as far as we know.

Nevertheless, throughout the entirety of the development of both thermodynamics and statistical mechanics, the focus generally assumed two major requirements: 1) systems were very large and 2) systems were to be manipulated slowly. In particular, these conditions are often necessary for the unambiguous definition of macroscopic observables in the first place. For example, as now understood through statistical mechanics, the pressure of a gas, the force felt on a given wall per unit area, is an emergent quantity, due ultimately to the many rapid and minute collisions of the microscopic particles making up the gas. If the gas were to instead consist only of a small number of particles, the pressure of the gas would vary significantly spatially and temporally and cease to be a well-defined quantity. Further, from a pragmatic standpoint, to make calculations accessible and experimentally relevant, a quasistatic, equilibrium assumption proved to be sufficient.

Under these assumptions, one is able to describe very accurately large assemblies of particles, such as an ideal gas with Avogadro's number of particles, as exists in one mole of gas. Further, due to the law of the large numbers, the fluctuations of such a system are so small as to be negligible for most practical purposes. This makes these theories both accurate and predictive for such equilibrium systems. However, as we clarified in Chapter 1, many interesting phenomena in the natural world are *not* in equilibrium and many systems, especially those most relevant to biophysics, biochemistry, and engineering at the nanoscale, consist of far smaller numbers of constituent and occur over rapid timescales. For such systems, fluctuations are hugely important to the fundamental physics of the problem and the paradigm of classical, equilibrium thermodynamics and statistical mechanics is no longer strictly applicable. Over the last several decades, attempts to extend the approach of thermodynamics and statistical mechanics to such fluctuating, small systems led to the development of new approaches to thermodynamics of nonequilibrium systems, as we detail in the next chapter.

Chapter 3

Stochastic thermodynamics

3.1 Precursors

Even from the young days of thermodynamics, its limited focus on equilibrium systems was recognized and numerous scholars made attempts at extensions. Some of the first successes in nonequilibrium thermodynamics came in the early 20th century by studying systems perturbed from equilibrium, though generally weakly. First, utilizing this approach, Lars Onsager was able to prove a remarkably general statement relating generalized thermodynamic flows and forces for systems out of equilibrium [24]. In particular, equilibrium systems are stationary and therefore do not exhibit flows of thermodynamic variables: this does not apply for systems driven from equilibrium.

Onsager considered a thermodynamic variable B_i. We can define the conjugate force to B_i as

$$X_i = \frac{\partial S}{\partial B_i}, \tag{3.1}$$

where S is the entropy. We also define the conjugate flux,

$$J_i = \frac{dB_i}{dt}. \tag{3.2}$$

Note that we are assuming the system is in steady state such that J_i is well-defined. Combining these two equations, we may write

$$\frac{dS}{dt} = \sum_i J_i X_i. \tag{3.3}$$

The flows, Eq. (3.2) are due ultimately to the conjugate forces, such that if there are no forces, the system is in equilibrium. In contrast, if the forces exist but are sufficiently small, we can accurately account for the flows by means of a linear approximation:

$$J_i = \frac{dB_i}{dt} = \sum_j L_{ij} X_j, \tag{3.4}$$

where L_{ij} is known as the *phenomenological matrix* or the *Onsager matrix*. Combining Eqs. (3.3) and (3.4), we have

$$\frac{dS}{dt} = \sum_i J_i X_i = \sum_{ij} L_{ij} X_i X_j. \tag{3.5}$$

By the Second Law, this quantity must be positive and therefore thermodynamics immediately asserts that L_{ij} is a positive-definite matrix. Onsager's key contribution was to show that not only was this matrix positive-definite, but further, it was symmetric. That is: $L_{ij} = L_{ji}$. Given that L_{ij} ultimately linked the flow of a thermodynamic quantity to conjugate thermodynamic forces, Onsager demonstrated a form of reciprocity between flows and forces.

As an example, let us consider the thermoelectric effect. For our starting point consider a fluid in contact with hot plates at different temperatures. If the two temperatures deviate by an amount ΔT that is sufficiently small relative to other temperature scales, the fluid will develop a temperature gradient and heat will flow from the hot plate to the cold plate. More generally, in the presence of a temperature gradient, heat will flow according to Fourier's law of heating, a phenomenological constitutive relation,

$$\mathbf{q} = -k_T \nabla T, \tag{3.6}$$

where $\mathbf{q}$ is the heat flux density, ∇T is the local temperature gradient, and k_T is the *thermal conductivity*. Similarly, if the fluid were to be electrically conductive and we placed an electric current across it, we would find the production of a current. Locally, due to Ohm's law, which is again a phenomenological constitutive relation, we may write

$$\mathbf{J} = -\sigma \nabla \phi, \tag{3.7}$$

where $\mathbf{J}$ is the current density, ϕ is the electrostatic potential, and σ is the conductivity of the fluid. Both Fourier's Law and Ohm's Law are frequently introduced in introductory physics. Slightly less well known are their corresponding reciprocal constitutive relations: due to experiments by Seebeck [25] and Peltier [26], respectively, there are likewise linear relations between temperature gradients and resultant current flow and voltage gradients and resultant heat flow. We may write

$$\mathbf{J} = -\sigma \nabla \phi - \sigma \mathcal{S} \nabla T, \tag{3.8a}$$

$$\mathbf{q} = -\sigma \Pi \nabla \phi - k_T \nabla T, \tag{3.8b}$$

where $\mathcal{S}$ is the *Seebeck coefficient* and Π is the *Peltier coefficient*. It may be tempting to immediately apply reciprocity to yield a relation between the Seebeck and Peltier coefficients, though reviewing Eqs. (3.1) and (3.3), to apply the reciprocity, we require the relevant thermodynamic forces be conjugate with respect to the entropy. A more detailed derivation

is beyond the scope of this work, though one can ultimately show these two reciprocal constitutive coefficients are indeed intimately connected [27]

$$\Pi = T\mathcal{S}. \tag{3.9}$$

This relation is known as the second Thomson relation and was first derived in 1854 by Lord Kelvin, utilizing a convoluted argument based on Carnot's work that was specific only to this system [27]. Onsager was aware of this, as well as many similar relations, but his reciprocity theorem therefore not only demonstrated this known relation but generalized it to a host of reciprocal transport problems. Onsager was awarded a Nobel prize in Chemistry in 1968 for this discovery [28].

Ilya Prigogine, working in Brussels, utilized Onsager's reciprocity to demonstrate an important principle for systems well-described by the linear relations. In particular, considering a certain set of thermodynamic forces $\{X_i^f\}$ as free and a certain set as fixed $\{X_i^b\}$, one can minimize the total entropy production with respect to the free forces [29, 30, 31]:

$$0 = \frac{\partial \dot{S}}{\partial X_a^f} = \frac{\partial}{\partial X_a^f} \sum_{ij} L_{ij} X_i X_j = \sum_j (L_{aj} + L_{ja}) X_j = 2 \sum_j L_{aj} X_j = 2J_a, \tag{3.10}$$

where the penultimate equality invokes Onsager reciprocity. Eq. (3.10) states that, for minimal entropy production, the free forces arrange themselves such that there are no flows in the free variables. This is *synonymous* with the steady state [31]. In essence, Prigogine demonstrated that steady state nonequilibrium systems act to minimize their entropy production. This was one of the first major extremal principles in nonequilibrium thermodynamics, following in the long legacy of such extremal principles in classical thermodynamics due to Maxwell, Boltzmann, Gibbs, etc.

There were other notable early successes in nonequilibrium thermodyanmics which are somewhat beyond the scope. As brief highlights, we mention the Onsager-Machlup formalism and the principle of least energy dissipation [32, 33], the general fluctuation-dissipation theorem [34], Green-Kubo relations [35, 36, 37, 38], and more broadly static and dynamic linear response [39]. All of these results were novel and inspired great interest both in their time and for decades following their discovery [31]. However, generically, they required the systems to remain sufficiently close to equilibrium such that the linear approximations of, for example, Eq. (3.3) hold. Further, the inherently thermodynamic formalism in which most were derived requires that the forces and flows, which are in turn defined in terms of macroscopic thermodynamic variables, be well-defined. In Onsager's own words, this is a "local equilibrium" assumption [31], which, as stated previously, is not inherently accurate for highly fluctuating systems. In fact, various attempts to generalize Onsager's and Prigogine's results beyond the linear regime actually proved that the *opposite* of their implications can be realized [40]. Prigogine spent much of his later career studying chemical thermodynamics far from equilibrium, and, with increasingly complexity, Prigogine observed increasing richness [40]. In essence, attempts at nonequilibrium thermodynamics of the early and mid 20th

century showed general, powerful results for systems near equilibrium, but were not able to handle systems far from equilibrium broadly. It was not until the late 20th century that fresh perspectives on nonequilibrium thermodynamics led to very general conclusions for arbitrary systems far from equilibrium, as we will detail below.

3.2 Fluctuation theorems

A more modern approach was spurred largely by the development of a series of *Fluctuation theorems* in the late 20th century. Arising initially out of studies of constantly sheared fluids [41], one of the early major results in what was to become stochastic thermodynamics was a series of results pertaining to the probability distribution of entropy production in a nonequilibrium steady state. First proposed and studied numerically by Evans, Cohen and Morris [41], and later proven in a variety of contexts by Gallavotti and Cohen [42], Kurchan [43], and Lebowitz and Spohn [44], this first fluctuation theorem considered the time averaged entropy produced over some duration in a nonequilibrium steady state: Σ_t. For such a nonequilibrium steady state, entropy is constantly produced, however, the specific amount of entropy produced will vary in each run of an experiment due to underlying fluctuations. This earliest modern fluctuation theorem, now typically called the *Steady-state fluctuation theorem*, showed that distribution of measured entropy production must follow a specific symmetry [45]:

$$\frac{P(\Sigma_t)}{P(-\Sigma_t)} = e^{\Sigma_t t} \tag{3.11}$$

where $P(X)$ is the probability of finding X and t is the duration of the experiment. Importantly, if t is large or the system size is macroscopic then typically Σ_t will be large, and this equation effectively mandates that Σ_t is exponentially more likely to be positive than negative, highly suggestive of the second law. In fact, we can make this more rigorous:

$$\begin{aligned} \frac{P(\Sigma_t)}{P(-\Sigma_t)} = e^{\Sigma_t} &\implies P(\Sigma_t)e^{-\Sigma_t t} = P(-\Sigma_t) \\ &\implies \int P(\Sigma_t)e^{-\Sigma_t t}d\Sigma_t = \int P(-\Sigma_t)d\Sigma_t \implies \left\langle e^{-\Sigma_t t}\right\rangle = 1, \end{aligned} \tag{3.12}$$

where $\langle\cdot\rangle$ represents an ensemble average, i.e. the average upon carrying out the same experiment repeatedly. Recognizing the convexity of the negative exponential and appealing to Jensen's inequality, Eq. (3.12) implies

$$\left\langle e^{-\Sigma_t t}\right\rangle = 1 \implies \langle\Sigma_t\rangle\, t \geq 0 \implies \langle\Sigma_t\rangle \geq 0, \tag{3.13}$$

which mandates that the ensemble average of the time-averaged entropy production of a nonequilibrium steady state *must* be positive. This result, of course, is also mandated by the second law but the form of Eq. (3.12) places a stricter constraint on the entirety of the entropy production probability distribution. Importantly, for sufficiently small systems,

fluctuations might occasionally lead to an experiment in which the entropy production is measured to be *negative*, a so-called "violation" of the second law. However, the second law strictly applies only at the level of an average: classical thermodynamics does not explicitly clarify this distinction as its focus is systems for which the law of large numbers guarantees all experimental outcomes *are* precisely the averages, though the fluctuation theorem demonstrates the possibility and likelihood of such rare outcomes.

Simultaneous to the development of the steady state fluctuation theorem, Christopher Jarzynski arrived at a very general fluctuation theorem for general nonequilibrium transformations [46]. Following a relatively simple argument, Jarzynski was able to prove that, for any system starting in canonical equilibrium at temperature T and that undergoes an arbitrary transformation, the transformation must satisfy

$$\left\langle e^{-\beta(W-\Delta F)} \right\rangle = 1, \tag{3.14}$$

where $\beta = (k_B T)^{-1}$ is the inverse temperature, W is the work performed on the system and measured in the experiment, and ΔF is the change in Helmholtz free energy associated with the transformation. Recognizing the convexity of the negative exponential and appealing to Jensen's inequality, Eq. (3.14) implies

$$\left\langle e^{-\beta(W-\Delta F)} \right\rangle = 1 \implies \langle \beta(W - \Delta F) \rangle \geq 0 \implies \langle W \rangle \geq \Delta F, \tag{3.15}$$

where we recognize that β and ΔF are features of the experimental setup and therefore will *not* vary across a given run. The final inequality in Eq. (3.15) is itself a form of the second law of thermodynamics for systems at fixed temperature. It bears emphasizing Jarzynski's accomplishment: whereas the second law amounted to an inequality guaranteeing that the work, on average, must be greater than the change in free energy, Jarzynski found a strict *equality* constraining the entirety of the nonequilibrium work distribution. Further, Jarzynski made no assumption about the protocol duration and no requirement that the system end in equilibrium. Therefore, beyond its fundamental importance as a further, very general fluctuation theorem, Jarzynski's equality allowed for a measurement of the equilibrium free energy change associated with a transformation simply by recording sufficient number of nonequilibrium work measurements [46, 47].

Jarzynski's result was a huge advance but was not met without controversy [48, 49]. Further credence was lent through the work of Gavin Crooks in the later 1990's and early 2000s. Following arguments pertaining to reversibility of dynamics at the microscopic level, Crooks was able to derive the relation [50]:

$$\frac{P_F(W)}{P_R(-W)} = e^{\beta(W-\Delta F)}, \tag{3.16}$$

where $P_F(W)$ is the probability to measure a given nonequilibrium work value W in some experiment starting at equilibrium and $P_R(-W)$ is the probability to measure a nonequilibrium work value of $-W$ when carrying out the same experiment in reverse (i.e., beginning

in the final equilibrium distribution and running the protocol backwards). Importantly, one can transform Eq. (3.16) as follows,

$$\begin{aligned} \frac{P_F(W)}{P_R(-W)} = e^{\beta(W-\Delta F)} &\implies P_F(W)e^{-\beta(W-\Delta F)} = P_R(-W) \\ &\implies \int P_F(W)e^{-\beta(W-\Delta F)}dW = \int P_R(-W)dW \\ &\implies \left\langle e^{-\beta(W-\Delta F)} \right\rangle = 1, \end{aligned} \tag{3.17}$$

which is precisely Eq. (3.14). Crooks therefore derived a yet stricter requirement on the nonequilibrium work distribution of a completely general system starting in thermal equilibrium.

These fluctuation theorems have now been verified experimentally [51] and generalized extensively [45]. From a phenomenological standpoint, these two fluctuation theorems demonstrate the general form one typically observes: the Jarzynski Equality, Eq. (3.14), is an *integral fluctuation theorem* (IFT), which generically takes the form $\langle e^R \rangle = 1$ for some quantity R, whereas the Crooks Fluctuation Theorem, Eq. (3.16), is a *detailed fluctuation theorem* (DFT), which takes the form $P(R)/\tilde{P}(\bar{R}) = e^R$ for some alternative ensemble $\tilde{P}$ and some transformation of R given by $\bar{R}$. Following Esposito and Van den Broeck [52], corresponding to every IFT is a DFT and vice versa. Following Seifert [45], a large number of fluctuation theorems can be derived from one master fluctuation theorem encoding different dynamics, initial conditions, and protocols. In all cases, fluctuation theorems place strict constraints on the measured distribution of some fluctuating thermodynamic quantity of interest.

It bears highlighting a final time the significance of these earliest fluctuation theorems. For a century, thermodynamics had largely been focused on equilibrium systems with certain extensions to general phenomena near equilibrium or occasional bespoke theories for individual systems out of equilibrium. The fluctuation theorems upended this paradigm: these results were completely general for any system arbitrarily far from equilibrium, ushering in a new era of nonequilibrium physics.

3.3 Stochastic energetics

Although preceded by the earliest work on fluctuation theorems, stochastic thermodynamics as a coherent field essentially began with the work of Ken Sekimoto in 1998 [53]. Sekimoto constructed consistent definitions for a large number of thermodynamic variables even for small, nonequilibrium systems subject to inherent stochasticity. As a model system, Sekimoto considered a one-dimensional overdamped Brownian particle, therefore subject to the following stochastic Langevin equation:

$$\dot{x} = -V_\lambda'(x) + \eta, \tag{3.18}$$

where $V_\lambda(x)$ is a potential energy function parametrized by some externally controlled λ and η encodes thermal noise due to the surrounding medium at temperature T. For such

an overdamped particle, the total energy is simply the potential. Considering the time derivative of the energy, then

$$\frac{dV_\lambda}{dt} = \frac{\partial V_\lambda}{\partial \lambda}\frac{d\lambda}{dt} + \frac{\partial V_\lambda}{\partial x} \circ \frac{dx}{dt}, \tag{3.19}$$

where $\circ$ represents the Stratonovich product between random variables. The first term on the RHS of Eq. (3.19) is the rate of change of the energy due to the externally varied parameter $\lambda(t)$ and can therefore be identified with work rate. By drawing an analogy to classical thermodynamics, the residual term must therefore be identified with the heat rate:

$$\dot{W} \equiv \frac{\partial V_\lambda}{\partial \lambda}\frac{d\lambda}{dt}, \tag{3.20a}$$

$$\dot{Q} \equiv \frac{\partial V_\lambda}{\partial x} \circ \frac{dx}{dt}, \tag{3.20b}$$

$$\dot{E} = \dot{W} + \dot{Q} = \frac{\partial V_\lambda}{\partial \lambda}\frac{d\lambda}{dt} + \frac{\partial V_\lambda}{\partial x} \circ \frac{dx}{dt}. \tag{3.20c}$$

Note that we follow the convention that work done on and heat added to the system are both positive. Importantly, under these identifications, one recapitulates a form of the first law of thermodynamics, even at the level of an individual fluctuating trajectory.

Following this work, Udo Seifert [54, 45] likewise arrived at a means of expressing the second law for such fluctuating trajectories. First, following standard statistical methods [55], the Langevin stochastic differential equation can be instead transformed into an equivalent Fokker-Planck deterministic partial differential equation for the time-varying probability position distribution of the particle $\rho(x,t)$. Under an information theoretic reinterpretation, one can now define the fluctuating system entropy as

$$s_{\text{sys}}(x,t) \equiv -k_B \log \rho(x,t), \tag{3.21}$$

which measures the information theoretic entropy of the particle at a given time. Importantly, upon ensemble averaging, we recover the Gibbs formula, Eq. (2.9):

$$S_{\text{sys}} = \langle s_{\text{sys}}(t) \rangle = -k_B \int dx \rho(x,t) \log \rho(x,t), \tag{3.22}$$

though we emphasize the form of Eq. (3.21) allows for the evaluation of the particle's entropy even along an individual fluctuating trajectory. Further, given that the particle is in contact with a heat bath at temperature T and the stochastic definition of heat from Eq. (3.20b), the entropy of the surroundings can also be consistently defined in the traditional thermodynamic sense

$$\Delta s_{\text{surr}} \equiv -\frac{Q}{T}. \tag{3.23}$$

With these definitions, we can now define the total entropy production rate, $\Delta s_{\rm tot} = \Delta s_{\rm sys} + \Delta s_{\rm surr}$. Upon careful evaluation of the stochastic products, one can derive an integral fluctuation theorem of the form [45]

$$\left\langle e^{-\Delta s_{\rm tot}} \right\rangle = 1, \tag{3.24}$$

which, following the discussion in Sec. 3.2 immediately implies

$$S_{\rm tot} = \langle \Delta s_{\rm tot} \rangle \geq 0, \tag{3.25}$$

a form of the second law of thermodynamics, though again for stochastic thermodynamic variables.

With the first two laws now derived for stochastic thermodynamic variables, one can follow the same development, and importantly, significant results, as classical thermodynamics, though now applied to systems far beyond the scope of the traditional treatment. We emphasize, although originally derived only for one-dimensional overdamped Langevin systems, the identification of stochastic thermodynamic variables has been extended widely, allowing for a thermodynamic treatment of a large number of stochastic, fluctuating systems at a variety of time and length scales.

3.4 A modern outlook

We presented an overview of the earliest developments in stochastic thermodynamics as a brief introduction to the field. Over the last few decades, however, the field has made major strides in a variety of related areas whose full treatment is well beyond the scope of this review. Nevertheless, we highlight some of the more notable directions in this section.

First, over the last several decades, our understanding of the relationships between thermodynamics, information, measurement, and feedback has grown dramatically. Since the early days of thermodynamics, paradoxes involving information-transducing demons [56] and, more generally, measurement-informed engines [57, 58] have served as a perplexing complication on the theory with no immediate contemporary resolutions. Recent studies on the thermodynamics of information, however, have clarified resolutions to these seeming paradoxes [59] while providing new ties between information theory and thermodynamics [60, 61]. These relations have given an inherent physical meaning to information and yield fundamental thermodynamic constraints on general logical operations relevant to computation [62] which may prove to inform the design of future generations of nanoscopic machines [63, 64, 60].

Second, following in the legacy of de Donder and the Brussels school [65] stochastic thermodynamics has contributed significantly to physical and thermodynamical understanding of discrete nanoscopic systems, which is particularly relevant to chemical and biomolecular systems [45]. Following Jarzynski and others, stochastic thermodynamics informed approaches now provide important numerical techniques for important but difficult problems, such as

estimating the free energy differences needed for drug discover [47] . Further, recently refinements of the second law for chemical reaction networks and potential implications in biophysical systems have been studied [66, 67].

Third, a major innovation in stochastic thermodynamics has been the study of nonequilibrium steady states from a thermodynamic standpoint. Advances have included consistent definitions of stochastic thermodynamic variables such as work, heat, and entropy [68, 69], generalizations of the fluctuation dissipation theorem [70], and, recently, relations constraining the fluctuations of currents in steady state [71, 72]. In particular, for a nonequilibrium steady state, although the distribution does not change, there remain nonzero, irreversible currents keeping the system out of equilibrium. *Thermodynamic uncertainty relations* (TUR) are thermodynamic bounds that place constraints on the ratio of variance to mean for the these fluctuating currents related to the entropy produced, generally assuming a heuristic form [73]

$$\frac{\mathrm{Var}(J_\tau)}{\langle J_\tau \rangle^2} \geq \frac{2k_B}{\Sigma_\tau}, \tag{3.26}$$

where J_τ is the net current under consideration over duration τ, $\mathrm{Var}(\cdot)$ is the variance and Σ_τ is the thermodynamic entropy dissipated over the duration τ. Importantly, if one desires for a high degree of precision, i.e. low variance to mean, the average dissipation necessarily must be large. This has implications for a wide range of settings, from molecular clocks to biological precision. The TUR has been generalized extensively to a variety of system dynamics and provides a fundamental physical trade-off between accuracy and thermodynamic cost.

Fourth, as we detailed in Sec. 3.3, stochastic thermodynamics takes a dynamical, time-dependent approach to the theory. Therefore, significant progress has been made over the last several decades on *finite-time thermodynamics*, for which thermodynamic systems are studied undergoing non-quasistatic manipulation [74, 75]. From an engineering standpoint, this allows for the rate of work extraction, the power, to be nonzero and therefore can yield bounds that are more relevant to existing thermal machines [74, 76]. Further, major advances have been made in the design of protocols that rapidly transform a system to some desired target [77, 78]. In this vein, the development of *optimal* manipulation schemes for nonequilibrium physical systems, which simultaneously accomplish some intended goal while minimizing some intrinsic cost, has also received substantial interest [79, 80, 81]. Such protocols are a main focus of this thesis and will be detailed further in the following chapter.

Finally, though the focus of this thesis will be primarily on classical dynamics, substantial headway has been made in the study of quantum thermodynamics using techniques similar to classical stochastic thermodynamics [82, 83]. Quantum generalizations now exist of many major results in stochastic thermodynamics, such as fluctuation theorems [84], steady-state thermodynamics [85], thermodynamic uncertainty relations [86] and optimal control [87, 88, 89]. Further, with the modern revolution in quantum information theory [90], the thermodynamics of quantum information has received considerable attention [91].

Chapter 4

Thermodynamic control of nonequilibrium systems

4.1 Preliminaries

Following the formalism of stochastic thermodynamics, we consider a physical system described by some dynamical variable x in contact with a heat bath at temperature T. For notional simplicity, we will consider only a singular dynamical variable and a singular heat bath, though one can extend to multiple of either.

The *state* of the system is described by the potentially time-varying probability distribution of dynamical variable $\rho(x,t)$. Generally, the dynamics are given by

$$\partial_t \rho(x,t) = \mathcal{L}^\dagger \rho(x,t), \tag{4.1}$$

where $\mathcal{L}^\dagger$ is the time-evolution Fokker-Planck operator [92], a, typically linear, differential operator.

As the paradigmatic example, let us consider the dynamics of an overdamped particle subject to a (controlled) potential $V(x,t)$. The dynamics follow the Smoluchowski equation [92]

$$\partial_t \rho = \partial_x[-D\partial_x(\beta V + \log\rho)\rho], \tag{4.2}$$

where D is the diffusion constant. Following Eq. (4.1), we can, therefore identify the overdamped dynamics as

$$\mathcal{L}^\dagger_{\text{over}} \equiv -(\partial_x v + v\partial_x), \tag{4.3}$$

where we define the *local mean velocity* [45]

$$v(x,t) \equiv -D\partial_x(\beta V + \log\rho). \tag{4.4}$$

With access to the probability distribution, we can define the average value, or more generally any moment, of an arbitrary quantity of interest. In particular, averaging Eq. (3.20),

the rates of work and heat at the level of ensemble averages are given by [45]

$$\langle \dot{W} \rangle \equiv \int dx \frac{\partial V(x,t)}{\partial t} \rho(x,t), \tag{4.5a}$$

$$\langle \dot{Q} \rangle \equiv \int dx V(x,t) \frac{\partial \rho(x,t)}{\partial t}, \tag{4.5b}$$

where again the work is identified as the energy exchange due to external manipulation of the potential whereas heat is identified as energy exchange due to internal rearrangement of the system at a fixed potential. Further, observe $\langle \dot{W} \rangle + \langle \dot{Q} \rangle = \frac{d}{dt} \langle V \rangle = \frac{dE}{dt}$ where $E(t) = \langle V(x,t) \rangle = \int dx V(x,t) \rho(x,t)$, a manifestation of the first law at the level of an ensemble average. For a given process of duration τ, we can then calculate $\langle W \rangle = \int_0^\tau \langle \dot{W} \rangle \, dt$ and $\langle Q \rangle = \int_0^\tau \langle \dot{Q} \rangle \, dt$. We can do the same for entropy:

$$S_{\text{sys}} = -k_B \int dx \rho(x,t) \log \rho(x,t) \tag{4.6a}$$

$$\Delta S_{\text{surr}} = -\frac{\Delta Q}{T} \tag{4.6b}$$

$$dS_{\text{tot}} = dS_{\text{sys}} + dS_{\text{surr}} > 0, \tag{4.6c}$$

which is the second law.

4.2 The general thermodynamic control problem

The general thermodynamic control problem typically involves the extremization of some objective function subject to a specific set of externally controlled dynamics with a given initial condition. For the model overdamped case, formally, we seek to find the optimal external control, encoded by the potential V,

$$V_*(x,t) = \left\{ \underset{V(x,t)}{\text{argmin}} \int_0^\tau L(x,t) dx dt \middle| \begin{array}{l} \partial_t \rho(x,t) = \mathcal{L}^\dagger_{\text{over}} \rho(x,t) = \partial_x (v(x,t) \rho(x,t)), \\ \rho(x,0) = \rho_0 \end{array} \right\}, \tag{4.7}$$

where L is a desired objective function density whose integral we seek to minimize and $\rho_0(x)$ is some given initial condition. Note, one can modify this in a variety of ways, for example, by adding some intended terminal condition on $\rho(x,\tau)$.

The form of Eq. (4.7) is modular, allowing for a variety of objective functions. In the typical thermodynamic context, one is interested in one of two major classes of problems. In the first major class, the objective is to end in some specified target state. This can be encoded in an objective function that is time local, for example

$$L_{\text{target}(x,t)} \sim \delta(t - \tau) D_{\text{KL}}(\rho(x,\tau) || \rho_{\text{target}}(x)), \tag{4.8}$$

where $D_{\mathrm{KL}}(P||Q)$ is the positive-definitie Kullback-Leibler (KL) divergence:

$$D_{\mathrm{KL}}(P||Q) = \int dx P(x) \log \frac{P(x)}{Q(x)}. \tag{4.9}$$

Note, one can use other measures of difference between the two distributions, though the KL divergence is common, historically significant, and physically relevant [93].

In the second major class, one seeks to minimize a measure of thermodynamic cost for a finite-time thermodynamic operation. Most often, the minimized cost is dissipated entropy, ΔS_{tot}, dissipated energy, or for isothermal processes, excess work, $W_{\mathrm{ex}} \equiv W - \Delta F$. Importantly, all of these quantities are positive definite and can be interpreted as wasted energy or effort such that their minimization is practically relevant.

Although we have focused on these two major classes, we note again the wide flexibility of the form of Eq. (4.7) and a variety of other optimization problems do arise. Most relevant to this thesis are the optimization of engines, which, following in the legacy of the earliest days of thermodynamics, typically involve maximizing various forms of efficiency or output power. This is decidedly related to both of these broader classes of optimization problems, though poses its own difficulties, as we will study.

4.3 Full and parametric control

In the thermodynamic control problem, we further distinguish between full and parametric control.

Full control

In the full control problem, the experimenter has control over the full potential function $V(x,t)$. For such a problem, the exact solution, $V_*(x,t)$, is known in one-dimension for the work-minimizing potential protocol connecting an initial distribution $\rho_0(x)$ and a target distribution $\rho_f(x)$ [94]. The solution is likewise known more generally for protocols beginning and ending in Gaussian distributions [95]. Beyond, these two cases, however, the exact solution is not known analytically and typically one must resort to numerical methods to make progress on exact optimal protocols [94, 96].

Recently, the full control problem has been shown to be equivalent to the problem of Optimal Transport [97, 98]. This realization has spurred significant progress on further finite-time refinements of thermodynamic bounds and allows for numerical methods for developing full-control optimal protocols [63, 64]. We will detail these connections further in Chapter 11.

Parametric control

The problem of parametric control instead assumes the experimenter only has control over a certain subset of control parameters, i.e. the experimenter has control over a finite set of

experimental "knobs." In particular, the potential $V(x,t) = V(x,\lambda(t))$ is now parametrized by a time-dependent externally manipulated control parameter $\lambda(t)$. For simplicity, we have focused on the case of a singular control parameter, but the extension to multiple is straightforward. One can further restrict to the case where the experimenter only has parametric control over a finite region of parameter space. The parametric control problem is therefore much more representative of an actual experimental apparatus and physical manipulation. However, its mathematical treatment does not neatly lend itself to exact results: the control may now not be sufficiently *expressive* to ensure the dynamics reach a target distribution at a given time and therefore possesses far fewer guarantees on optimal performance as compared to full control [99]. Nevertheless, due to its scientific importance, parametric control has been a major focus of study, both theoretically and experimentally [45, 89, 94], yielding the successful design of novel exact optimal protocols for a variety of physical systems [100].

4.4 Approximation schemes and regimes of applicability

As noted, it is typically analytically intractable to solve for the exact optimal protocols beyond overdamped systems in one-dimensions or transitions between Gaussian initial and final states. For this reason, approximation schemes have been developed that accurately characterize the system and control dynamics under certain limits. These approximation schemes can then be used to construct parametric optimal protocols *analytically* when considering experimental manipulation relevant to these regimes of applicability. From a theoretical standpoint, the use of approximation schemes serves to inform our understanding of the exact, numerically-constructed protocols, and can be used as an efficient ansatz for solving exact protocols variationally [96, 101]. From an experimental perspective, most present-day experimentally-tractable manipulation tasks are *well-described* by these approximate treatments, such that the optimal protocols designed in this manner are experimentally relevant [102]. Further, from a pragmatic standpoint, although only approximate in nature, many of the optimal protocols designed for use in limited experimental scope have proven to be highly effective even outside their strict regions of applicability [103]. Here, we detail a number of notable schemes.

Fast control

Optimal protocols in the limit of fast control were first studied by Blaber et al. [104]. In particular, they considered the control parameter changing from λ_i to λ_f over a rapid timescale τ_{fast}. By assumption $\tau_{\text{fast}} \ll \tau$, where τ represents any other timescale relevant to the system, most notably the intrinsic relaxation timescale for the system to respond to the transition and re-equilibrate. Under these assumptions, [104] showed the optimal protocol consists of a Short Time Efficient Protocol (STEP), for which $\lambda(t)$ is always a stepwise

function of the form

$$\lambda_{\text{STEP}}(t) = \begin{cases} \lambda_i, & t \leq 0 \\ \lambda_*, & 0 < t < \tau \\ \lambda_f, & t > \tau \end{cases}, \tag{4.10}$$

where λ_* is found by minimizing the work for such a protocol.

It bears mentioning, for sufficiently fast protocols, the system does not observe any intermediate control dynamics, i.e. the system does not have time to react to any control for times $0 < t < \tau$. As a result, in practice, although derived explicitly with fast control dynamics in mind, the STEP protocol performs only marginally better than generic protocols, such as a linear ramp [100].

Weak control

The weak control regime focuses on the case when all control variables are modulated only slightly: $|\delta\lambda(t)/\lambda_0| \ll 1$ for all times $0 < t < \tau$ where $\delta\lambda(t) = \lambda(t) - \lambda_0$ is change in a control parameter, λ_0 is its initial value, and τ is the duration of the external control. Following standard linear response theory [39], the excess work may be written as

$$W_{\text{ex}} = W - \Delta F = \frac{1}{2}\int_0^\tau dt \int_0^\tau dt' \Psi_0(t - t')\delta\dot{\lambda}(t)\delta\dot{\lambda}(t'), \tag{4.11}$$

from which one may then derive optimal protocols [105]. It bears highlighting that the weak control regime makes no assumption about the duration of the protocol, such that it can be highly predictive even for systems driven very rapidly [103], so long as all perturbations are small. The weak control regime has been studied for a number of different systems, both classical and quantum [89]. Further, recently, the weak control regime was shown to relatively predictive even beyond its regime of strict applicability [103].

Slow control

The slow control regime instead focuses on the case when control variables are modulated slowly: $|\dot{\lambda}/\lambda| \ll 1/\tau$ where τ again is used to represent all time scales relevant to the problem. That is, the timescale over which a control variable changes must be slower than all natural timescales for the system under study. However, unlike weak control, this regime does *not* limit the absolute scope of the allowed change over sufficiently long durations. Using dynamical linear response, [106] demonstrated a connection between slow control and geometric control, which has since paved the way for major efforts advancing optimal protocols in the slow regime [107, 87, 108, 109, 76, 110, 111]. The study of optimal protocols in this regime will form the main focus of Part III of this dissertation. We give a more in-depth overview of the slow control regime in Chapter 8.

Part II

Shortcut engineering and rapid control

Chapter 5

Shortcut engineering

Shortcut engineering is a broad series of techniques meant to enforce a desired set of dynamics on a system by means of external control. Typically, the aim of such control is to rapidly manipulate a system from an initial state ρ_0 to a final state ρ_f in a given duration. Such a transformation typically has some given relaxation timescale τ_r whereas shortcuts attempt to enact this state-to-state transformation in time $\tau < \tau_r$ such that these techniques *shortcut* the intrinsic timescale of the transformation. Here, we give a brief overview, though the interested reader is referred to the far more extensive reviews: [112, 78, 113].

5.1 Shortcuts to adiabaticity

The phrase "shortcut to adiabaticity" (STA) was coined initially in 2010 in [114], though conceptually similar methods had been developed over the previous decade [115, 116, 117, 118, 119, 120, 121]. The earliest works focused exclusively on quantum dynamics with a relatively simple question. The adiabatic theorem of quantum mechanics [122], ensures that if a Hamiltonian H is modulated *adiabitically*, i.e. very slowly, from $H(0) = H_0$ to $H(t_f) = H_f$ then all initial eigenstates of that system $|n(0)\rangle$ will likewise be modulated into the corresponding final eigenstates, $|n(t_f)\rangle$. This, for example, guarantees that if a system is initially in the ground state of the Hamiltonian $H(0)$, during an adiabatic transition it will remain in the ground state *at all times*, and same for the first excited state, second excited state, etc. In contrast, if a Hamiltonian is quenched from H_0 to H_f then the initial state of the system will remain unchanged during the quench and therefore, if initially an eigenstate, may *not* be eigenstates of H_f. The earliest shortcuts attempted to essentially replicate the results of the adiabatic theorem while manipulating the system *non-adiabatically*.

Mathematically, we consider a time-dependent Hamiltonian $H(t)$ and some corresponding eigenspectrum $\{|n(t)\rangle\}$, where $|n(t)\rangle$ is the nth excited eigenstate of the Hamiltonian at time t. We mandate the Hamiltonian begin at $t = 0$ in H_0 and end at $t = t_f$ in H_f and now seek some control scheme for intermediate times $H(t)$ such that if we start with an eigenstate $|n_0\rangle$ we will arrive at the corresponding eigenstate $|n_f\rangle$ at time $t = t_f$. Unlike the adiabatic

theorem, we generically make no demand on the state in the intermediate times, and it will typically *not* be an eigenstate of the instantaneous Hamiltonian $H(t)$, but if the state ends as an eigenstate, it will remain an eigenstate at later times. Therefore, we can *shortcut* the adiabatic theorem.

The earliest shortcut techniques focused on simple, two- and three-level quantum systems [114], for which authors were able to successfully derive methods to shortcut the adiabatic timescale. Since then, shortcuts to adiabatiicity have been extended broadly, first to more complicated quantum systems [112, 123, 124, 125, 126, 127] and then to classical discrete and continuous systems [128, 129] as well as stochastic systems [130, 77, 131, 132, 133, 134, 135] These extensions have included a large number of different, though connected techniques, such as inverse engineering, counterdiabatic driving, invariant-based design, and numerous other approaches [78, 113, 135]. We highlight inverse engineering and counterdiabiatic driving as they are most relevant to our later development.

Inverse engineering

Inverse engineering is essentially the broadest class of shortcut schemes, for which we impose a specific desired state trajectory, $|\psi(t)\rangle$, and simply invert the dynamics to find the necessary external control. So long as we mandate that the correct boundary conditions on the Hamiltonian, this technique ensures the initial and final desired states are imposed, though can further strongly enforce the dynamics at intermediate times. The major drawback of this technique, however, is that the necessary control to impose such a specific state trajectory may not always be realizable [131, 135]

Counterdiabatic driving

Counterdiabatic driving (CD) accomplishes a shortcut in a slightly more specific way by modifying the Hamiltonian with some auxiliary term. In particular, we write the total Hamiltonian as

$$H(t) = H_{\text{base}}(t) + H_{\text{aux}}(t), \tag{5.1}$$

where $H_{\text{base}}(0) = H_0$ and $H_{\text{base}}(t_f) = H_f$ whereas $H_{\text{aux}}(0) = H_{\text{aux}}(t_f) = 0$. In particular, if we desire the state to begin in an initial eigenstate $|n_0\rangle$ and arrive in the corresponding eigenstate at the end of protocol $|n_f\rangle$, we then design H_{aux} such that the state $|\psi(0)\rangle = |n_0\rangle$ is transformed into an eigenstate of $H_{\text{base}}(t)$ at all times: $|\psi(t)\rangle = |n_{\text{base}}(t)\rangle$. By the construction of Eq. (5.1), this immediately guarantees that the Hamiltonian enacts the desired shortcut. It is worthwhile to clarify that the state $|\psi(t)\rangle$ is *not* an eigenstate of the full Hamiltonian at intermediate times, $H(t) = H_{\text{base}}(t) + H_{\text{aux}}(t)$, only of the base Hamiltonian. Further, there are numerous choices of the base and auxiliary Hamiltonians, so long as they satisfy the necessary boundary conditions. The choice allows for flexibility in experimental design [124] and can lead to solutions of optimization problems for shortcut accuracy or time [125]

5.2 Broader escorted dynamics

Beyond their application in quantum systems, shortcutting techniques have now been extended quite widely. Here, we highlight extensions to both quantum and classical systems with either deterministic or stochastic dynamics.

Closed classical systems

The earliest extensions of shortcut engineering were for closed classical systems — isolated systems described by classical dynamics. Such systems are energy-conserving and the evolution of their distribution can be described by Liouville's equation. Classical shortcuts were developed later than their quantum counterparts but have now matured [128, 129, 136, 113].

Open classical systems

For classical open systems, engineered swift equilibration (ESE) and shortcuts to isothermality (STI) were first introduced in [130] and [77], respectively. and have since been extended widely [130, 77, 131, 132, 133, 134, 80, 137, 138]. Both strategies follow a similar philosophy to classical shortcuts to adiabaticity, though for the stochastic dynamics of a system in contact with a heat bath at temperature T. In particular ESE is an inverse-engineering based strategy to enact rapid distributional changes whereas STI is a CD-based strategy. Utilizing and extending the applicability of these strategies will be the focus of Ch. 6.

Open quantum systems

More recently, techniques have been developed for shortcutting open quantum systems. In particular, Shortcuts to Equilibration [127] rapidly transition between equilibrium states of quantum systems whose dynamics can be described by a nonadiabaitic master equation. With these methods, shortcuts have been designed to rapidly manipulate thermal quantum harmonic oscillators and can be used for studying thermalization properties more generally [127, 139]. Finally, quantum shortcuts have recently been implemented in designing finite-time quantum engines [140].

Complex and nonequilibrium dynamics

Initially, shortcuts were designed exclusively for single isolated particle or thermal systems that were being driven externally from their stationary distributions. Recently, shortcuts have been extended to a far wider range of systems. First, through creative mathematical transformations, novel shortcuts have been designed for complex many-body systems, both classical and quantum [129, 141]. In a similar vein, shortcut engineering can be interpreted

differently to suggest fundamental speed limits to physical phenomena, which has seen broad application including in the study of critical phenomena [142, 143]

Beyond these more complex systems, shortcut engineering approaches have been implemented for a far more general class of dynamical systems. First, shortcut designs were extended to evolutionary dynamics [144, 145]. These extensions allow both for the study of finite-time population genetics, but also introduce a physics-based approach toward controlling and manipulating evolving populations. These ideas could also have future implications for directed evolutionary design and even yield biomedical applications [145]. In addition, shortcut methods have very recently been extended to physical systems with explicitly nonequilibrium dynamics, such as nonequilibrium steady states [146] and active matter [147, 135]. An example of one such extension to a notable active system will be the focus of Chapter 7.

5.3 Outlook

Shortcut engineering is a relatively young field with the earliest direct references on the subject appearing only after the turn of the millennium. Arguably, shortcut design grew initially out of pure physical interest and curiosity: the ability to rapidly and faithfully manipulate quantum systems seems to contradict the "spirit" of the adiabatic theorem if not its literal implications. Nevertheless, with recent advances in experimental techniques, shortcut engineering has been successfully realized in laboratory settings and has been suggested for future technological design [78]. Especially in the current era of noisy intermediate-scale quantum technology [148], the ability to rapidly *prepare* quantum states by use of shortcuts before carrying out a quantum computation is worthwhile in and of itself [149, 150]. Further, various implications of shortcut techniques have now been recognized for optimal control of physical and dynamical systems [151] and will likely play a significant role in the field going forward. Finally, with the numerous extensions listed above, such as those to active matter or even evolutionary dynamics, shortcutting techniques are likely to influence the future of applied control theory in scientific settings.

Chapter 6

Engineered swift equilibration for arbitrary geometries

In this chapter, we extend shortcut engineering techniques to systems described by overdamped classical dynamics with arbitrary configuration spaces. It is adapted from [134] with the permission of all authors.

6.1 Introduction

As detailed in Chapter 5, in any transformation process, there exists some intrinsic relaxation time for the final distribution to be reached. Recently, a number of studies have attempted to manipulate or eliminate altogether this relaxation time by means of alternative driving protocols. These strategies are generally known as shortcuts to adiabaticity, in which one attempts to rapidly transform from a specified initial distribution to a target distribution in finite time, in either classical [128, 129, 136, 78] or quantum [152, 118, 112, 123, 128, 129, 124, 136, 153, 126, 78, 154] settings. In the context of open classical systems, protocols that shortcut the natural relaxation timescale of the system go by the name of Engineered Swift Equilibration (ESE) and focus on enforcing internal thermal equilibrium at specified initial and final times [130, 155]. This constraint is clearly satisfied when an instantaneous equilibrium distribution is maintained at *all times* during the protocol, rather than only at the beginning and the end, a strategy called shortcuts to isothermality introduced in [77]. This is achieved by adding external driving forces: by following a specified driving protocol, a rapidly-transforming system assumes the trajectory of a quasistatic transformation.

To be more concrete, consider a physical system described by some time-dependent Hamiltonian $H_0(\lambda_i(t))$, where t is time, and all time dependence is prescribed by parameters $\lambda_i(t)$. Following standard Boltzmann statistics [55], the equilibrium probability distribution corresponding to the control parameters at a given time is

$$\rho_{\text{eq}}(\mathbf{x};\lambda_i(t)) = \frac{\exp(-\beta H_0(\mathbf{x};\lambda_i(t)))}{Z(\lambda_i(t))}, \tag{6.1}$$

where $\beta = (k_B T)^{-1}$ is the inverse temperature, k_B is Boltzmann constant, and $Z(\lambda_i(t))$ is the partition function, explicitly dependent on parameters $\lambda_i(t)$. If the $\{\lambda_i(t)\}$ are changed quasistatically, the system will be well-described by Boltzmann statistics at all times. However, if $\lambda_i(t)$ changes too rapidly, the system deviates from its equilibrium distribution specified by Eq. (6.1). The ESE protocols we consider introduce a modified Hamiltonian $H(\mathbf{x}, t) = H_0(\mathbf{x}, \lambda_i(t)) + H_1(\mathbf{x}, t)$ such that under the full dynamics of H, the system assumes the internal equilibrium distribution of H_0 alone [Eq. (6.1)], at all times.

To date, ESE protocols have been successfully derived for a Brownian particle trapped in a variety of simple one-dimensional (1D) potentials [77, 131] and realized experimentally for a Brownian particle in a 1D harmonic trap [130]. This approach was also recently applied to the Brownian gyrator [133], a two-dimensional (Euclidean) system in contact with two heat baths that admits non-equilibrium steady states. In this chapter, we extend the ESE framework to generic overdamped Brownian systems, including those with arbitrarily high dimensional, non-Euclidean configuration spaces. We demonstrate the utility of our framework by numerically finding the ESE forcing for previously unsolved systems. Due to the wide applicability of overdamped Brownian dynamics, we expect our results to prove useful to the many physical contexts where swift, controlled transitions are desirable, such as nanoscale engineering [156, 157], thermodynamic computing [158, 79], and manipulating colloidal systems [159, 160], to name just a few.

6.2 Theory

We consider a particle undergoing Brownian motion in the overdamped limit whose dynamics are governed by the Langevin equation,

$$\gamma \frac{d\mathbf{x}(t)}{dt} = -\nabla V(\mathbf{x}(t); \lambda_i(t)) + \boldsymbol{\eta}(t) + \mathbf{F}_{\text{ext}}(t), \tag{6.2}$$

where $\mathbf{x}$ is the position of the particle, γ is the viscosity, $V(\mathbf{x}; \lambda_i(t))$ is the potential acting on the particle parameterized by control parameters $\lambda_i(t)$, $\boldsymbol{\eta}$ is Gaussian noise with delta function autocorrelation $\langle \eta_i(t)\eta_j(t')\rangle = (2\gamma/\beta)\delta_{ij}\delta(t-t')$, where i, j index Euclidean coordinates and $\mathbf{F}_{\text{ext}}(t)$ is an external force on the particle.

Following standard procedures [55], this leads to a Fokker-Planck equation:

$$\partial_t \rho(\mathbf{x}, t) = \nabla \cdot \left[\left(\frac{\nabla V(\mathbf{x}; \lambda_i(t)) - \mathbf{F}_{\text{ext}}}{\gamma} + \frac{\nabla}{\beta\gamma} \right) \rho(\mathbf{x}, t) \right], \tag{6.3}$$

where $\rho(\mathbf{x}, t)$ is the configuration space probability distribution at a given time. In the absence of an external force, the steady state solution is found by setting the LHS of Eq. (6.3) to zero, yielding the usual Boltzmann distribution, ρ_{eq}.

Now suppose that the control parameters $\lambda_i(t)$ are time-dependent and varied too quickly to assume a quasistatic transition. We seek $\mathbf{F}_{\text{ext}}(t)$ such that $\rho(\mathbf{x}(t), t; \lambda_i(t)) = \rho_{\text{eq}}(\mathbf{x}; \lambda_i(t))$

for all times t. This can only be satisfied if all explicitly time-dependent terms in Eq. (6.3) independently cancel. Defining $\mathbf{P} \equiv \rho_{\text{eq}}\mathbf{F}_{\text{ext}}$, this constraint can be written

$$\nabla \cdot \mathbf{P} = -\gamma \partial_t \rho_{\text{eq}}. \tag{6.4}$$

We now generalize to systems whose configuration space is an arbitrary compact Riemannian manifold M with metric g, and write the vector $\mathbf{P}$ as a differential 1-form $P = P_i \mathrm{d}x^i$. Equation (6.4) then generalizes to

$$\mathrm{d}^\dagger P = -\gamma \partial_t \rho_{\text{eq}}, \tag{6.5}$$

where d is the exterior derivative and $\mathrm{d}^\dagger$ is its Hodge dual, whose action on a k-form is given: $\mathrm{d}^\dagger = (-1)^{n(k-1)+1} \star \mathrm{d} \star$, where $\star$ is the Hodge star operator and n is the dimension of the manifold. We now invoke the Hodge Decomposition, which states that, for any k-form P_k on M, there exists a unique decomposition [161]:

$$P_k = \mathrm{d}A_{k-1} + \mathrm{d}^\dagger B_{k+1} + C_k, \tag{6.6}$$

where A_{k-1} and B_{k+1} are $(k-1)$- and $(k+1)$-forms, respectively, and C_k is a harmonic k-form; *i.e.* $\Delta C_k = 0$, and $\Delta = \mathrm{d}\mathrm{d}^\dagger + \mathrm{d}^\dagger \mathrm{d}$ is the generalized Laplace operator. On a compact Riemannian manifold, harmonic k-forms also satisfy $\mathrm{d}C_k = \mathrm{d}^\dagger C_k = 0$ [162]. Therefore, we may write Eq. (6.4) as

$$\mathrm{d}^\dagger P = \mathrm{d}^\dagger(\mathrm{d}A + \mathrm{d}^\dagger B + C) = \mathrm{d}^\dagger \mathrm{d}A + \mathrm{d}^\dagger \mathrm{d}^\dagger B + \mathrm{d}^\dagger C = \Delta A, \tag{6.7}$$

where A is a 0-form, B is a 2-form, and C is a harmonic 1-form. Eq. (6.5) thus becomes a generalized Poisson's equation:

$$\Delta A = -\gamma \partial_t \rho_{\text{eq}}. \tag{6.8}$$

Coupling this with Eq. (6.6) and taking $B = C = 0$ for simplicity yields our main result:

$$\mathbf{F}_{\text{ext}} = \frac{\mathrm{d}A}{\rho_{\text{eq}}}. \tag{6.9}$$

We now demonstrate the utility of our result by applying it to multiple physically realizable examples.

6.3 Practical examples

Euclidean Configuraton Space

In d-dimensional Euclidean space, the Hodge decomposition trivializes to the Helmholtz decomposition [161]. Our results still hold, though for certain cases the decomposition may no longer be unique. For this space, the generalized Laplace operator is simply the standard

Laplace operator. Note that our choice $B = C = 0$ amounts to a no-curl gauge: $\nabla \times \mathbf{P} = 0$. We may thus define a scalar potential A that satisfies $\nabla A = \mathbf{P}$. This is analogous to standard electrostatics, where A and $\mathbf{P}$ play the roles of the electric potential and field, respectively [163].

Given the general solution to the Laplace operator for Euclidean space, we have, for $d \neq 2$,

$$A(\mathbf{x}) = -\frac{\Gamma(\frac{d-2}{2})}{4\pi^{\frac{d}{2}}} \int d^d\mathbf{x}' \ |\mathbf{x} - \mathbf{x}'|^{2-d}(-\gamma\partial_t\rho_{\text{eq}}(\mathbf{x}')) \tag{6.10}$$

and $\mathbf{F}_{\text{ext}}(\mathbf{x}) = \rho_{\text{eq}}^{-1}\nabla A$. Note that this solution reproduces Eq. (12) of [77] for 1D systems. For the special case of $d = 2$, the potential is given by

$$A(\mathbf{x}) = \frac{1}{2\pi} \int d^2\mathbf{x}' \ \log|\mathbf{x} - \mathbf{x}'|(-\gamma\partial_t\rho_{\text{eq}}(\mathbf{x}')). \tag{6.11}$$

Spherical Configuration Space

We now consider topologically nontrivial configuration spaces. Our first example is an electric dipole with dipole moment $\mathbf{p} = p\hat{\mathbf{p}}$ placed in a time-varying electric field pointed in the z-direction, $\mathbf{E} = E(t)\hat{\mathbf{z}}$, as shown in Fig. 1(a). The potential energy for this system is

$$V(\theta, \phi, t) = -pE(t)\cos(\theta), \tag{6.12}$$

where $\cos\theta = \hat{\mathbf{p}} \cdot \hat{\mathbf{z}}$ and ϕ measures the azimuthal angle about the z-axis. The configuration space of this system is the 2-sphere, $M = S^2$, for which the Laplace operator is

$$\Delta_{S^2} = \frac{1}{\sin\theta}\frac{\partial}{\partial\theta}\left(\sin\theta\frac{\partial}{\partial\theta}\right) + \frac{\partial^2}{\partial\phi^2}. \tag{6.13}$$

To calculate the required ESE force, we find $\rho_{\text{eq}}(t)$, the instantaneous Boltzmann distribution for this system:

$$\rho_{\text{eq}}(t) = \left[\frac{4\pi\sinh(\beta pE(t))}{\beta pE(t)}\right]^{-1} \exp\beta pE(t)\cos\theta, \tag{6.14}$$

such that the governing equation is given by $\Delta_{S^2}A = -\gamma\partial_t\rho_{\text{eq}}$. In the high temperature limit, one may find an explicit expression for A (see Appendix 6.A); however, finding a closed-form expression is, in general, intractable. Instead, we employ a series expansion in the spherical harmonics, $Y_\ell^m(\theta, \phi)$. The spherical harmonics are the eigenfunctions of the spherical Laplace operator, *i.e.* $\Delta_{S^2}Y_\ell^m(\theta, \phi) = -\ell(\ell + 1)Y_\ell^m(\theta, \phi)$, such that if we write $\rho_{\text{eq}} = \sum_{\ell,m} c_{\ell,m}(t)Y_\ell^m(\theta, \phi)$, then by the orthogonality and completeness of the spherical harmonics, we have

$$A = \gamma\sum_{\ell=0}^{\infty}\sum_{m=-\ell}^{\ell}\frac{\partial_t c_{\ell,m}(t)}{\ell(\ell + 1)}Y_\ell^m(\theta, \phi). \tag{6.15}$$

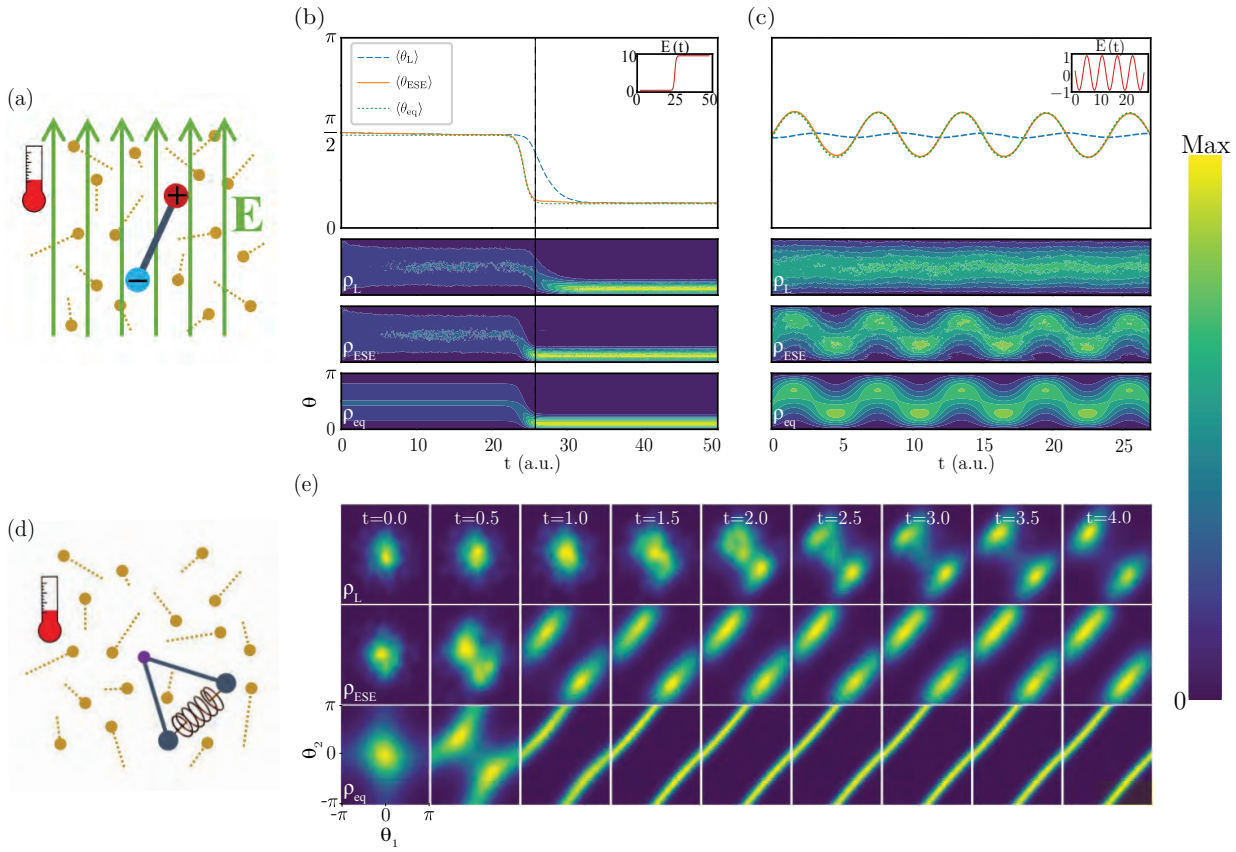


Figure 6.1: **Demonstration of Engineered Swift Equilibration for non-Euclidean configuration space**. **(a)** Schematic diagram of the ensemble considered in subplots **(b)** and **(c)**. An ensemble of electric dipoles are placed in a uniform, time-varying electric field. Due to these constraints, the state of a dipole is specified by a polar coordinate θ and an azimuthal angle ϕ such that the system's configuration space is a (2D) sphere. **(b)** The electric field is varied sigmoidally in time, as shown in the inset. In the top panel, we show the average values of θ over the entire ensemble for a system undergoing Langevin dynamics (dashed blue), ESE dynamics (solid orange), and for a Boltzmann distibution for the given electric field $E(t)$, denoted ρ_{eq} (dotted green). The three lower panels are the corresponding full distributions for θ at all times. **(c)** Same as panel b for the sinusoidally varying electric field shown in the inset. **(d)** Schematic diagram of the ensemble considered in subplot **(e)**. An ensemble of two coupled pendula with time-varying coupling constant. The state of a coupled pendulum is specified by the two angular coordinates of the pendula, $\theta_1, \theta_2 \in [-\pi, \pi)$, such that the full system's configuration space is a torus. **(e)** The probability distributions of an ensemble of coupled pairs of pendula undergoing Langevin dynamics (top) and ESE dynamics (middle) plotted against the instantaneous Boltzmann distribution (bottom) for a coupling constant that changes from zero at small times to a negative value.

Note that $c_{\ell,m}$ may likewise be computed:

$$c_{\ell,m}(t) = \int_\Omega \rho_{\rm eq}(\theta,\phi,t) Y_\ell^{m*}(\theta,\phi) d\Omega. \tag{6.16}$$

Due to the azimuthal symmetry of $\rho_{\rm eq}(\theta,\phi,t)$, only $m=0$ terms will be nonzero, simplifying our analysis. Finally, $\mathbf{F}_{\rm ext}$ is found by taking $\mathbf{P} = \mathrm{d}A \implies \mathbf{F}_{\rm ext} = \rho_{\rm eq}^{-1}(\nabla_{S^2})A$.

We now simulate the system for specified functions $E(t)$. The dynamics of this system are governed by a set of Langevin equations:

$$m(\ddot{\theta} - \sin\theta\cos\theta\dot{\phi}^2) = -\gamma\dot{\theta} - pE\cos\theta + \eta_\theta + F_{{\rm ext},\theta}, \tag{6.17}$$

$$m(\sin\theta\ddot{\phi} + 2\cos\theta\dot{\theta}\dot{\phi}) = -\gamma\sin\theta\dot{\phi} + \eta_\phi + F_{{\rm ext},\phi}. \tag{6.18}$$

Note that, though we do not explicitly enforce the overdamped limit in Eqs. (6.17) and (6.18), we will effectively do so by means of parameter choices in our simulations. For a specified $E(t)$, we numerically solve Eqs. (6.15) and (6.16) to find the ESE force (truncating above $\ell = 5$) and then simulate the Langevin dynamics in both the presence and absence of this force for an "ensemble" of 10^4 dipoles. In units of $\beta = m = p = 1$, we simulate with $\gamma = 20$. Due to the noise terms in Eqs. (6.17) and (6.18), these are stochastic differential equations, which we simulate by means of a first-order Euler-Maruyama algorithm [164] with step size of $dt = 0.01$ time units. Given the promotion of configuration space to a non-Euclidean manifold, the relation for the noise term is modified [165, 166]: $\langle \eta_i(t)\eta_j(t')\rangle = (2\gamma/\beta)g^{ij}\delta(t-t')$, where g^{ij} is the inverse metric of the manifold. For the (unit) sphere, the inverse metric is $g^{\theta\theta} = 1$, $g^{\phi\phi} = 1/\sin\theta$, and all other entries are zero. Therefore, following the standard Euler-Maruyama treatment, we take $\eta_\theta dt = \sqrt{2\gamma dt/\beta}\mathcal{N}(0,1)$ and $\eta_\phi dt = \sqrt{2\gamma dt\csc\theta/\beta}\mathcal{N}(0,1)$, where $\mathcal{N}(0,1)$ is the Normal distribution with zero mean and unit variance. To deal with the spherical-polar coordinate singularities at $\theta = 0$ and $\theta = \pi$, we temporarily rotate to a different local coordinate system and numerically integrate a single time-step whenever $0 < \theta < \pi/10$ or $9\pi/10 < \theta < \pi$ (see Appendix 9.B).

In Fig. 1 we plot both the mean value and the full probability distribution of $\theta(t)$ for both the standard Langevin and ESE dynamics for two representative, temporally-varying electric fields, as described below. Due to the azimuthal symmetry of the problem, the distribution over the azimuthal angle ϕ is not affected by any temporal change in $E(t)$.

In Fig. 1(b), we consider a sigmoidally varying electric field, $E(t) \sim E_0 + (\Delta E)S(t-t_c)$, where

$$S(t) = (1+e^{-t})^{-1} \tag{6.19}$$

is the logistic function, $\Delta E = 10$ is the amplitude of the change of the electric field, and t_c is the transition time. For E_0 small, θ is primarily distributed about $\pi/2$, which corresponds to the equator. We note that for $pE_0 \ll k_BT$, the dipoles have no preferred direction, so they should be uniformly distributed throughout configuration space. However, the distribution appears non-uniform as a function of θ. This is an artifact of our coordinate system: there is more phase space area at $\theta = \pi/2$ (the equator) than elsewhere, such that the probability

as a function of θ should be non-uniform. For $t \gg t_c$, we find that, on average, $\theta < \pi/2$. This is physically sensible: the electric field is strong and directed along the z-axis such that the dipoles will tend to align with it. However, another artifact of our coordinate system is the absence of probability density at the pole at $\theta = 0$. For $t \sim t_c$, in the absence of the ESE force, the system remains out of equilibrium for a finite period of time before eventually relaxing to the new equilibrium. However, when the ESE force is introduced, the system remains close to the equilibrium distribution at all times.

In Fig 1(c), we consider a sinusoidal electric field, $E(t) \sim E\sin(t)$. In this case, we see that the constantly changing field never allows the standard Langevin system to fully equilibrate; instead, the system oscillates with an approximate $\pi/2$ phase-shift at a significantly smaller amplitude. Conversely, the ESE dynamics converge close to the equilibrium distribution at all points in time. For this case, we point out one subtlety: due to the periodicity of the drive, there exists a non-equilibrium periodic steady-state distribution over θ in the absence of ESE forcing, to which the Langevin dynamics converge [167, 168]. However, reaching this steady-state is not the goal of our ESE protocol. Rather, we seek to track the instantaneous Boltzmann distribution for the temporally varying external control parameters at all times, even in this periodic case.

Toroidal configuration space

Next, we consider toroidal configuration space, as exemplified by a system of two pendula, each of mass m and unit length suspended vertically, and coupled to each other with a time-varying coupling constant $\kappa(t)$, as illustrated in Fig. 1(d). The potential may be modeled as

$$V(\theta_1, \theta_2, t) \simeq -(mg\cos\theta_1 + mg\cos\theta_2 - \kappa(t)\cos(\theta_1 - \theta_2)), \tag{6.20}$$

where θ_1 and θ_2 are angles of the respective pendula with respect to the z-axis. Given the periodicity in θ_i, the configuration space of this system is the 2-torus, $M = T^2 = [0, 2\pi] \times [0, 2\pi]$. The Laplace operator for this manifold is

$$\Delta_{T^2} = \frac{\partial^2}{\partial\theta_1^2} + \frac{\partial^2}{\partial\theta_2^2}, \tag{6.21}$$

where one must recall the periodicity of the coordinates: $\theta_i \sim \theta_i + 2\pi n$ for $n \in \mathbb{Z}$. We again employ a series expansion to solve Eq. (6.4). In this case, we carry out a 2D Fourier series. Considering that $\Delta_{T^2} \exp i(m_1\theta_1 + m_2\theta_2) = -(m_1^2 + m_2^2)\exp i(m_1\theta_1 + m_2\theta_2)$, we may write $\rho_{\text{eq}} = \sum_{m_1,m_2} c_{m_1,m_2}(t)\exp i(m_1\theta_1 + m_2\theta_2)$ and deduce that

$$A = \gamma \sum_{m_1,m_2} \frac{\partial_t c_{m_1,m_2}(t)}{m_1^2 + m_2^2} e^{i(m_1\theta_1 + m_2\theta_2)}. \tag{6.22}$$

We again simulate this dynamical system for a given $\kappa(t)$. The governing Langevin equations are now

$$m\ddot{\theta}_{1/2} = -\gamma\dot{\theta}_{1/2} - mg\sin\theta_{1/2} + \kappa(t)\sin(\theta_{1/2} - \theta_{2/1}) + \eta_{\theta_{1/2}} + F_{\text{ext},\theta_{1/2}}. \tag{6.23}$$

As with the last example, the dynamics are not confined to the overdamped limit. For a specified $\kappa(t)$, we numerically solve the ESE force $F_{\text{ext}}(t)$ by means of the Fourier series expansion (truncating above $m_1 = m_2 = 10$) and then simulate the Langevin dynamics in both the presence and absence of this force. In units of $\beta = m = g = 1$, we again simulate for $\gamma = 20$ and employ an Euler-Maruyama algorithm with time step $dt = 0.01$. Conveniently, the noise terms for this system do not have any geometric corrections, such that $\eta_{\theta_1} dt = \eta_{\theta_2} dt = \sqrt{2\gamma dt/\beta}\mathcal{N}(0,1)$. For our simulations, we choose $\kappa(t) \sim -\kappa_0 S(t)$, where $S(t)$ is defined by (6.19) so that the pendula are initially uncoupled but after some critical time t_c they are anti-coupled. In Fig. 1(e), we display the resulting probability distribution for the coordinates (θ_1, θ_2) at several times near t_c. In the absence of the ESE force (top row), equilibration happens over a finite amount of time as the system relaxes to its new anti-coupled distribution. However, when the ESE force is added (second row), the resulting distribution agrees well with the calculated equilibrium distribution $\rho_{\text{eq}}(t)$ corresponding to the control parameter values at each moment in time (bottom row).

6.4 Discussion

In previous studies, the notions of optimality and control often refer to specific protocols designed to minimize excess work or some other performance index when changing between two equilibria or non-equilibrium steady states in finite time [156, 157, 106, 107, 169, 108, 170]. The ESE framework may also be considered a control strategy, though ESE seeks only to minimize time to equilibration throughout the protocol without any constraints or penalties on the work required to do so. Prior work has analyzed the relation between the duration τ of a protocol and the energy dissipated in carrying out a drive, concluding that for a variety of model systems, the energy dissipated is proportional to $1/\tau$ [171, 172, 158, 77, 125]. We may conjecture that the type of ESE protocols we have derived here will behave similarly, with dissipated energy scaling as τ_{relax}/τ, where τ_{relax} is the intrinsic viscous relaxation timescale for the overdamped system in consideration.

In principle, provided a smooth trajectory of control parameters, ESE should allow for arbitrarily rapid equilibrium switching of ensemble distributions. However, the difficulty of realizing the required forces in a laboratory setting would presumably preclude such a situation. In addition, the theory itself breaks down in such a limit due to higher order effects ignored in a basic Langevin treatment, such as a finite characteristic timescale of the noise correlations. Nonetheless, for the range of timescales for which Eq. (9.8) applies, ESE yields a method to achieve controlled, swift equilibration.

Our ESE protocol ensures a high degree of control throughout the drive. Not only do we enforce the mean, or the mean and variance (or any finite combination of moments) of the probability distribution, we dictate the *entire* probability distribution at all times during the protocol. In fact, following [161], if a scalar field integrates to zero over a full compact manifold, it may be written as the divergence of a vector field. Importantly, by integrating

the LHS of Eq. (6.4) over any phase space manifold M, we see that

$$\int_M (-\gamma \partial_t \rho_{\rm eq}) dV = -\gamma \frac{d}{dt} \int_M \rho_{\rm eq} dV = -\gamma \frac{d}{dt}(1) = 0 \tag{6.24}$$

following conservation of probability. We conclude that for any arbitrary time-dependent potential described by some smooth set of coordinates, there will always be a corresponding ESE force that can enforce swift equilibration.

Finally, we note further degrees of freedom in the ESE condition defined by Eq. (6.7): The differential form $d^\dagger P = \Delta A$ allows for an alternative, arbitrary choice of a harmonic 1-form C and a 2-form B by using Eq. (6.6). For a given trajectory specified by $\rho_{\rm eq}(t)$, these choices lead to a class of inequivalent, though perhaps non-conservative [79], driving forces—where now we must use the full form of Eq. (6.6) $\rho_{\rm eq} F = {\rm d}A + {\rm d}^\dagger B + C$—each of which enforces swift equilibration. These additional degrees of freedom, which are inaccessible in low-dimensional Euclidean spaces and therefore have not been observed in past studies, afford greater flexibility in constructing appropriate forces for practical laboratory applications.

6.5 Conclusion

In this chapter, we have successfully extended the ESE protocol to systems with nontrivial configuration space topology. We hope our results will be useful for designing optimal strategies for manipulating a thermalized system of multiple canonical position variables swiftly through controlled parameter changes. Our methods can be used to calculate the necessary auxiliary forces to impose internal equilibrium dynamics in experimental settings, though the derivation we present here is only valid for the overdamped limit. In future work, it will be interesting to generalize our framework to include underdamped systems.

6.A High temperature limit of dipole model

Suppose that we are in the high-temperature regime for the dipole model such that $|pE(t)| \ll k_B T$. In this case we can expand $\exp \beta p E(t)) \approx 1 + \beta p E(t) \cos\theta$ and the partition function as $Z(t) = 4\pi + \mathcal{O}(\beta p E(t))^2$. We then have, to the lowest order, the probability density as

$$\rho(\theta, \phi, t) = \frac{1}{4\pi}(1 + \beta p E(t) \cos\theta) \tag{6.25}$$

Taking the partial time derivative of the above gives us an equation of the form $\Delta_{S^2} A = -(4\pi)^{-1} \gamma \beta p \dot{E} P_1(\cos\theta)$, where $P_1(x) = x$ is the first Legendre polynomial. Using the identity $\Delta_{S^2} P_\ell(cos\theta) = -\ell(\ell+1) P_\ell(cos\theta)$, we immediately have the result

$$A = \frac{1}{8\pi} \gamma \beta p \dot{E} \cos\theta \tag{6.26}$$

Original Coordinates	Transformed Coordinates
(x, y, z)	(z', x', y')
θ	$\arctan\left(\frac{\sqrt{\cos^2\theta' + \sin^2\theta'\sin^2\phi'}}{\sin\theta'\cos\phi'}\right)$
$\arctan\left(\frac{\sqrt{\cos^2\theta + \sin^2\theta\cos^2\phi}}{\sin\theta\sin\phi}\right)$	θ'
$\hat{\theta}$	$\frac{\cos\theta'\sin\phi'}{sqrt\cos^2\theta' + \sin^2\theta'\cos^2\theta'}\hat{\theta}' + \frac{\cos\phi'}{sqrt\cos^2\theta' + \sin^2\theta'\cos^2\theta'}\hat{\phi}'$

Table 6.1: Coordinate transformation used when $0 < \theta < \pi/10$, $9\pi/10 < \theta < \pi$ and is therefore close to coordinate singularities in spherical coordinates.

Note that if the source term $\gamma\partial_t\rho$ contained a constant a $P_0(\cos\theta) = 1$, Poisson's equation would be un-invertible; however, as the source term must integrate to zero, such terms are disallowed.

An interesting note: to first order the requisite force can be applied via a potential that can be practically produced just as a modulation in the original electric field. In particular we have

$$\vec{F} = \frac{dA}{\rho_{\text{eq}}} \approx -\frac{1}{2}\gamma\beta p\dot{E}\sin\theta \tag{6.27}$$

This is enforceable by modulating the applied electric field by $\Delta E_{\text{ESE}}(t) = -\frac{1}{2}\gamma\beta\dot{E}_0$ where E_0 distinguishes the electric field without the additional ESE contribution. If the original electric field were, for example, a sinusoid, this modulation would manifest as an out-of-phase contribution to the original field, resulting at first order in a small phase shift of the total signal.

6.B Simulation details

When numerically integrating (6.17) and (6.18), the ODE becomes stiff and the numerics break down near the coordinate singularities at $\theta = 0, \pi$. Note that this is purely a feature of our local coordinate chart and not of the physics. Therefore, to simulate the system accurately, we must find ways of dealing with these poles. There are a number of schemes, though the conceptually simplest is simply to define a new coordinate chart and transform to this alternative whenever the system is close to a pole in the original coordinates. In this context, we define a primed set of coordinates (θ', ϕ') which are entirely analogous, i.e. a right-handed spherical coordinate system, though whose zenith is now oriented with the original x-axis (the coordinate singularity at $\theta = 0$ now lies on the primed $\hat{y}$-axis). For completeness, we include the transformation in Table 6.1.

Chapter 7

Shortcut engineering active matter: run-and-tumble particles

In this chapter, we demonstrate the successful application of shortcutting techniques to controlling active matter. In particular, we focus on the paradigmatic model of run-and-tumble particles in one dimension. This chapter is adapted from [135] with the permission of all authors.

7.1 Introduction

Over the past several decades, active matter has become a major focus of study in nonequilibrium statistical mechanics. Inspired by interesting features of biological systems, such as self-propulsion [173, 174, 175] and flocking [176, 177], active matter consists of systems in which individual particles are able to dissipate energy from internal or other nonthermal energy reservoirs. Allowing for such internal energy dissipation and entropy production makes such systems inherently out of equilibrium. Active matter displays numerous unique, and at times universal, phenomena, such as pattern formation [178], motility induced phase separation [179, 180, 181], velocity alignment [182], and accumulation at confining walls [183, 184, 185, 186, 187]. Recently, the problem of controlling and manipulating biological as well as synthetic active matter systems has gained significant interest as a means for novel engineering at the nanoscale [188, 189], with numerous potential applications, such active matter engines [190, 191, 192, 193, 194], designed self-assembled structures [195, 196, 197, 198, 199], and programmable active matter devices [200, 201, 202].

As detailed in Ch. 5, significant progress has also been made in the field of shortcut engineering [118, 152, 114, 123, 203, 129, 130, 204, 78, 113]. In particular, for a system whose steady state $\rho_{\rm ss}$ is specified by a set of external control parameters $\mathbf{\Lambda}$, shortcut engineering is a set of approaches to modulate these external controls such that a system in an initial steady state $\rho_0 = \rho_{\rm ss}(\mathbf{\Lambda}_0)$ arrives at a target final steady state $\rho_f = \rho_{\rm ss}(\mathbf{\Lambda}_f)$ in a finite time τ. The protocol duration τ is typically chosen to be shorter than the natural relaxation

timescale of the system τ_r, such that such a protocol *shortcuts* the system's relaxation. These finite-time approaches first gained attention in closed quantum systems, in which such approaches are known as shortcuts to adiabaticity as they shortcut the adiabatic theorem of quantum mechanics [118, 152, 114]. More recently, shortcut engineering has been applied to significantly more complicated systems in both quantum and classical systems, both in the case of deterministic [205, 136] and stochastic dynamics [130, 77, 131, 127, 132, 144, 134], and even to driving rapidly between two nonequilibrium steady states for out-of-equilibrium systems [133, 147] We emphasize that such shortcut protocols typically require the system to be out-of-steady-state with respect to current external controls at intermediate times, but the system arrives at a final steady state corresponding to $\mathbf{\Lambda}(\tau)$ at the end of the protocol, such that after control modulation is concluded, the system remains in this new steady state.

In this chapter, we apply shortcut engineering to the paradigmatic active matter system of run-and-tumble particles (RTPs). An RTP is an overdamped colloidal particle with a given self-propulsion velocity that stochastically and instantaneously redirects to a random direction at a fixed rate, similar to the chemotactic behavior of bacteria [173, 175, 206] Specifically, inspired by recent work on another popular active matter system, active Brownian particles (ABPs) [147], we find a class of shortcut solutions that allow for rapid transitions between two steady-state distributions at different self-propulsion velocities for a system of non-interacting RTPs in a one-dimensional harmonic trap. Our results are experimentally testable with existing techniques [187, 207, 208]. In addition, we derive the optimal protocols that minimize the average external work for such a modulation. Our findings could influence the design of near-term experiments and provide insights needed to faithfully and rapidly control, manipulate, and engineer active systems.

7.2 Run-and-tumble dynamics in 1D

RTP particles undergo dynamics given by

$$\dot{x} = -\mu\partial_x U + v_0\sigma(t) + \eta(t), \tag{7.1}$$

where μ is the particle's mobility coefficient, $U(x)$ is a given confining potential profile, v_0 is the RTP self-propulsion velocity, σ is telegraph noise which assumes the values $\sigma \in \{+1, -1\}$ and transitions in a Poisson process with given average rate $\gamma/2$. Its autocorrelation function is $\langle\sigma(t')\sigma(t)\rangle = e^{-\gamma|t-t'|}$. η is Gaussian white noise due to a thermal heat bath with mean zero and $\langle\eta(t)\eta(t')\rangle = 2D\delta(t-t')$ for diffusion constant D. We specialize to the case of a harmonic trap where $U(x) = \frac{1}{2}kx^2$ such that Eq. (7.1) becomes

$$\dot{x} = -\mu kx + v_0\sigma(t) + \eta(t), \tag{7.2}$$

Following standard methods, we may write an equivalent master equation for the distribution of the particles $P(x,t)$:

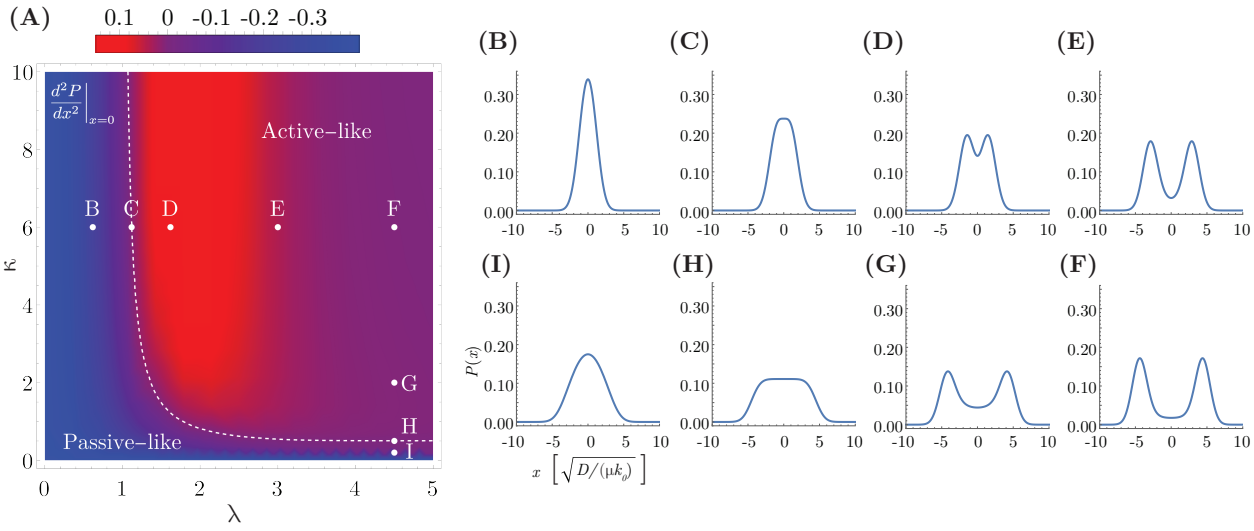


Figure 7.1: **Steady-state distribution of run-and-tumble particles for a variety of parameter values**. **(A)** The second derivative of the steady-state distribution at the trap center as calculated from the first 100 terms of Eq (7.5): a local maximum at the trap center denotes a passive-like state whereas a local minimum denotes an active-like state. The transition between these two regimes is denoted by the dotted line. **(B)-(I)** The steady-state distribution from the first 100 terms in Eq (7.5) for the parameter values denoted in **(A)**. All axes for **(B)-(I)** are the same as denoted in **(I)**. Note that behavior progresses from left to right along both rows, *i.e.* **(B)** and **(I)** are both passive-like, **(C)** and **(H)** are both marginal, and **(D)-(G)** are all active-like.

$$\partial_t P_+ = -\partial_x[(-\mu k x + v_0)P_+] + D\partial_x^2 P_+ - \frac{\gamma}{2}(P_+ - P_-) \tag{7.3a}$$

$$\partial_t P_- = -\partial_x[(-\mu k x - v_0)P_-] + D\partial_x^2 P_- - \frac{\gamma}{2}(P_- - P_+), \tag{7.3b}$$

where $P_+(P_-)$ refers to the probability distribution of the of the right- (left-) moving particles. The final term in each equation refers to the gain and loss between the different particle species whereas the first terms characterize intraspecies time evolution for each particle type.

In steady-state, the distribution must satisfy

$$0 = -\partial_x[(-\mu k x \pm v_0)P_+] + D\partial_x^2 P_+ \pm \frac{\gamma}{2}(P_- - P_+). \tag{7.4}$$

Recent endeavors in finding exact solutions to active matter steady-state distributions [209, 210, 211, 212, 213, 214] have led to the run-and-tumble and distribution in both thermal [215] and athermal ($D = 0$) cases [216]

$$P_{\pm}(x)^* = \sum_{n=0}^{\infty} \left(\frac{v_0}{\sqrt{\mu k D}} \right)^n \frac{1}{2} \sqrt{\frac{\mu k}{2\pi D}} e^{-\frac{\mu k x^2}{2D}} (\pm 1)^n C_n(\frac{\gamma}{\mu k}) He_n \left(\sqrt{\frac{\mu k}{D}} x \right), \tag{7.5}$$

where $C_0(x) \equiv 1$ and

$$C_n(x) = \prod_{j=1}^{n} \frac{1}{j + \frac{1}{2}(1 + (-1)^{n+1})x}, \quad n > 0. \tag{7.6}$$

He_n is the nth Hermite polynomial under the "probabilist's" convention:

$$He_n(x) \equiv e^{x^2/2} \frac{d^n}{dx^n} e^{-x^2/2},$$

and $P_{\text{tot}}(x) = P_+(x) + P_-(x)$. Note that this set of dynamics is characterized by two dimensionless quantities: the dimensionless stiffness $\kappa = \mu k/\gamma$ and the dimensionless velocity $\lambda = v_0/\sqrt{\mu k D}$. κ encodes the competition of the characteristic timescales of particle transmutation $1/\gamma$ and Brownian particle relaxation $1/(\mu k)$. λ, in contrast, represents the competition between thermally driven diffusion and the directed motion due to the active propulsion.

The steady-state behavior of the system is entirely set by these two parameters and one observes both passive-like states, encoded by the particles' tendency to accumulate at the bottom of the potential, and active-like states, encoded by the particles' tendency to accumulate at turning points in the potential. See Fig. 10.1 for a steady-state phase diagram, as measured by the sign of $\partial_x^2 P_{\text{tot}}|_{x=0}$ calculated from the first 100 terms of Eq. (7.5). One can observe that, for $\lambda \to \infty$ (as $D \to 0$), the active-passive transition occurs exactly at $\kappa = 1/2$ whereas higher values of κ are required for smaller λ as the diffusive forces begin to "wash out" the accumulation of particles at the boundaries.

7.3 Shortcut solution

We now wish to implement a shortcut strategy for RTP dynamics. Namely, we assume the distribution is initialized in the steady-state corresponding to the control parameters at time $t = 0$. We wish to carry out some manipulation of the control parameters over some finite time horizon $0 \leq t \leq \tau$ so as to arrive at a final state corresponding to the steady state for the given control parameters at finite time τ. For certain parameter regimes, such a manipulation can result in rapid transitions from one steady state to another over timescales orders of magnitudes shorter than natural relaxation following a control parameter quench. Inspired by a recent work on ABPs [147], we will focus on the case of shortcutting between two different self-propulsion velocities, $v_0(0) = v_{00}, v_0(\tau) = v_{0f}$. We will attempt an inverse engineering approach, choosing an ansatz for the exact evolution of the distribution

and arriving at necessary conditions on controllable external parameters to realize such a distribution. We consider the same ansatz as [147]:

$$P_{\pm}(x,t) = P_{\pm}(x|v_0(t), k_0, D/\alpha(t))^*, \tag{7.7}$$

where $k_0 = k(t=0)$. In particular, if we choose boundary conditions such that

$$\alpha(t=0) = \alpha(t=\tau) = 1,$$

and

$$k(t=0) = k(t=\tau) = k_0,$$

this ansatz allows for a rapid transition between steady states corresponding to different velocities. We highlight that this ansatz is *not* in steady-state for intermediate times, i.e. for $0 < t < \tau$, however, it *is* at $t = 0$ and $t = \tau$ with the boundary conditions specified. We now evaluate Eq. (7.3) for this ansatz. The algebra is somewhat lengthy and we relegate the full calculation to the supplementary material, however, the final necessary constraints on the control parameters are relatively simple:

$$\dot{\alpha} = 2\alpha\mu(k - k_0\alpha), \tag{7.8a}$$

$$\dot{v}_0 = -v_0\mu(k - k_0). \tag{7.8b}$$

Remarkably, this set of control is *identical* to that found in [147] for 2D ABPs. ABPs and RTPs are known to exhibit equivalent hydrodynamics and share many physical properties at a large scales [217, 218], though we emphasize that this shortcut is identical at the single-particle, noninteracting level for different dynamics, equilibrium distributions, and perhaps most surprisingly, dimensionality. This suggests that Eq. (7.8) may prove to be a universal shortcut for both of these systems, or an even broader class of active systems, irrespective of specific model details.

7.4 Explicit protocols

With Eq. (7.8) in hand, we are now able to solve for explicit shortcut protocols for this system. Moreover, given the identical solution to the ABP case, we may map to the solutions already presented [147] We first consider a polynomial solution for α to Eq. (7.8). Considering the four boundary conditions that must be satisfied in addition to the first order differential equation, we require five degrees of freedom and therefore minimally a four degree polynomial (though higher degree inequivalent solutions will likewise produce viable shortcuts). Evaluating Eq. (7.8) for this polymonial ansatz yields

$$\alpha(t) = 1 + \frac{30t^2(t-\tau)^2 \log \frac{v_{00}}{v_{0f}}}{\mu k_0 \tau^5}, \tag{7.9}$$

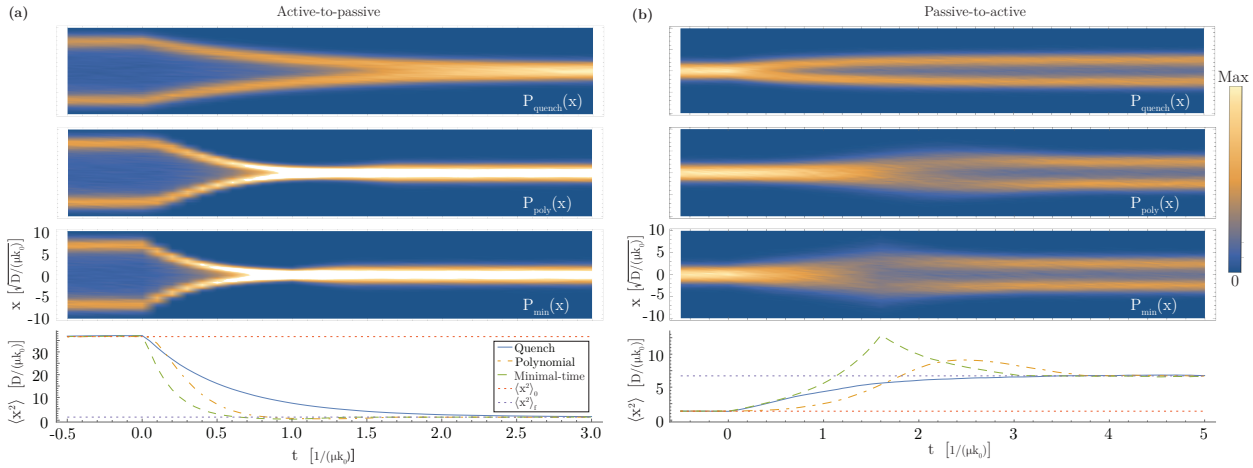


Figure 7.2: **Shortcut protocols can outperform quenched protocols in Langevin dynamics simulations**. (Left) Particle distribution as a function of time from transition onset ($t = 0$) shown for an active-to-passive transition with $\mu k_0 = 1/2$, $\gamma = 1/5$, $d = 1$, $v_{00} = 5$ and $v_{0f} = 1/2$ in simulation units. Rapid parameter quench and resulting relaxation (top), polynomial shortcut with $\tau_{\text{poly}} = 1.71/(\mu k_0)$ (second from top), and minimal-time shortcut with the same minimum and maximum stiffness as the polynomial protocol with $\tau_{\text{min}} \approx 1.311/(\mu k_0)$ (third from top). The polynomial protocol was chosen such that $k(t) > 0$ at all times. Bottom subplot shows the position variance for each of the simulated protocols, quench in solid blue, polynomial in dashed-dotted orange, and minimal-time in dashed green, as well as the theoretical initial, dotted orange, and final, dotted purple, variances (see Appendix 7.A for derivation). Note that both polynomial and minimal-time shortcut protocols converge to the final target distribution significantly faster than quenched relaxation. (Right) Same as left plots but for a passive-to-active transition with $v_{00} = 1/2$ and $v_{0f} = 2$, and we find $\tau_{\text{poly}} = 3.851/(\mu k_0)$ and $\tau_{\text{min}} = 3.041/(\mu k_0)$, again chosen so $k_{\text{poly}}(t) > 0$. Note that for this transition, the minimal-time shortcut protocol marginally outperforms a naive parameter quench, as shown by the slightly more rapid convergence of the dashed green curve relative to the solid blue curve to the final target value in the bottom subplot. Moreover, the polynomial shortcut *underperforms* the naive quench for this transition. Therefore, the active-to-passive shortcut significantly outperforms the natural quenched relaxation, but the passive-to-active shortcut presents a more complicated picture.

where $v_{00}(v_{0f})$ is the initial (final) velocity of the protocol, and τ is the protocol duration. Given α, one can immediately find $k(t)$ and $v_0(t)$ by manipulating Eq. (7.8). However, we note one potential issue with this solution: for $v_{0f} > v_{00}$, that is when the final velocity is greater than the initial, $\alpha(t)$ can, in principle, become zero or even go negative, which, in turn, leads to singularities in $k(t)$ and $v_0(t)$. Evaluating Eq. (7.9), the extrema occur at $t = 0, \tau/2$, and τ. For $v_{0f} > v_{00}$, the minimum of this function occurs at $\tau/2$ which yields a constraint on the minimum protocol duration for such a solution:

$$\alpha(t) > 0 \implies \tau > \frac{15}{8}\frac{\log \frac{v_{00}}{v_{0f}}}{\mu k_0}. \tag{7.10}$$

We remark that the typical timescale for relaxation to equilibrium is given by $\tau_r \sim 1/(\mu k_0)$ such that a polynomial shortcut may not significantly outperform, or may even be slower than, a simple quenched protocol.

In contrast, when $v_{0f} < v_{00}$, there is no such constraint on the minimal time, and, in principle, arbitrarily fast transitions are possible. Such transitions, however, may require physically inaccessible protocols for $k(t)$, such as very strong or even negative stiffness values, but there are no singularities that prevent their mathematical construction.

Given a constrained minimum and maximum value for stiffness, denoted $k_{\min}$ and $k_{\max}$, respectively, a "bang-bang" optimal minimal time protocol was previously constructed in [147]. In particular, in the case of $v_{0f} > v_{00}$ ($v_{0f} < v_{00}$) the protocol consists of spending a certain amount of time t_1 at $k_{\min}$ ($k_{\max}$) before instantaneously transitioning to $k_{\max}$ ($k_{\min}$) for the remainder $\tau_* - t_1$ of the protocol. Again one finds τ_* is larger for $v_{0f} > v_{00}$ than for $v_{0f} < v_{00}$, even for the same values of $k_{\max}$ and $k_{\min}$.

In Fig. 10.2, we have plotted simulations of Langevin dynamics for both active-to-passive (left), $v_{0f} < v_{00}$, and passive-to-active (right), $v_{0f} > v_{00}$ transitions for a quenched transition (top), polynomial shortcut transition (middle), and minimal-time shortcut transition (bottom) for identical maximum and minimum stiffness values as the polynomial protocol. Observe that for passive-to-active transitions, the shortcut protocols are not significantly faster than simple quenched relaxation, though there is a significant speedup for active-to-passive transitions, in principle only limited by the external control.

7.5 Minimal work protocol

We now consider the energetic cost of such shortcuts. The external work of a given shortcut protocol is given by (see Appendix 7.C for a full derivation),

$$\langle W \rangle = \int_0^\tau \int_{-\infty}^{\infty} dx(\partial_t U(x) P(x,t)) = \int_0^\tau \frac{\dot{k}}{2}\left[\frac{D}{\alpha\mu k_0} + \frac{v_0^2}{(\mu k_0)^2 + \mu k_0 \gamma}\right] dt, \tag{7.11}$$

where $v_0(t), k(t)$ and $\alpha(t)$ still must satisfy Eq. (7.8). Defining

$$\Lambda(t) \equiv \int_0^t \alpha(t')dt', \tag{7.12}$$

we can write $\langle W \rangle$ as a local functional:

$$\langle W \rangle = \int_0^\tau \left(\frac{\dddot{\Lambda}}{2\mu\dot{\Lambda}} - \frac{\ddot{\Lambda}^2}{2\mu\dot{\Lambda}^2} + k_0\ddot{\Lambda} \right) \left[\frac{D}{2\mu k_0 \dot{\Lambda}} + \frac{v_{00}^2}{(\mu k_0)^2 + \mu k_0 \gamma)} \frac{1}{\dot{\Lambda}} e^{2\mu k_0 t} e^{-2\Lambda} \right] dt, \tag{7.13}$$

from which one may derive Euler-Lagrange equations to minimize the external work. We relegate the full expression to the supplemental material, but it consists of a nonlinear fourth-order ordinary differential equation in $\Lambda(t)$. Specifying the boundary conditions $\Lambda(0) = 0, \dot{\Lambda}(0) = \dot{\Lambda}(\tau) = 1$, and $\Lambda(\tau) = \tau - 1/(\mu k_0) \log(v_{0f}/v_{00})$ ensures the system begins in the steady state $P(x|v_{00}, k_0, D)$ and ends in $P(x|v_{0f}, k_0, D)$ in total duration τ with minimal external work. We show the required protocols for $k(t)$ and $v_0(t)$ for such a minimal-work protocol in Fig. 10.3 and compare to a minimal-time protocol with identical values of $k_{\min}$ and $k_{\max}$. Observe the discontinuities in k at the start and end of protocol, which have previously been observed in finite-time optimal control problems [156, 104, 100]. Further, this protocol contrasts significantly with the minimal-time protocol, indicating a trade-off between protocol duration and work, a ubiquitous feature of finite-time thermodynamics [219, 220, 221].

7.6 Discussion

By applying the ansantz $P(x,t) = P(x|v_0(t), k_0, D/\alpha(t))$, where $\alpha(0) = \alpha(\tau) = 1$ and $k(0) = k(\tau) = k_0$, we have derived a class of shortcut solutions, Eq. (7.8), that allow for rapid transitions between 1D RTP steady states at the same trap stiffness and temperature and different self-propulsion velocities. Although the limit to $D \to 0$ (athermal limit) is nontrivial, we emphasize that the same shortcut solution works in this case with $\alpha \to 0$ (see Appendix 7.B for derivation). In future work, it will be interesting to consider similar questions for changing trap stiffness or temperature. As a start, although we focused on protocols with D held fixed, one could instead quench D at the end of the protocol to some $D' = D/\alpha(\tau)$, which allows for transitions between different-temperature steady states. We leave the study of shortcut protocols with smoothly-varying temperature for future work.

It is striking that Ref. [147] derived the *identical* shortcut solution as Eq. (7.8) for 2D ABPs in harmonic confinement. RTPs and ABPs are known to share hydrodynamic properties at large length scales, though we emphasize that our work and Ref. [147] focused on *distinct* single-particle distributions in *different* dimensions: it is surprising to us that the shortcut protocols turn out to be identical for these distinct systems. This may point to a universal shortcut protocol applicable to numerous active systems, which could prove useful in engineering active matter. We emphasize that there are very few fully calculated steady-state distributions for active particle systems, such that the typical inverse engineering techniques in shortcut methods will need to be augmented to study general active matter shortcuts.

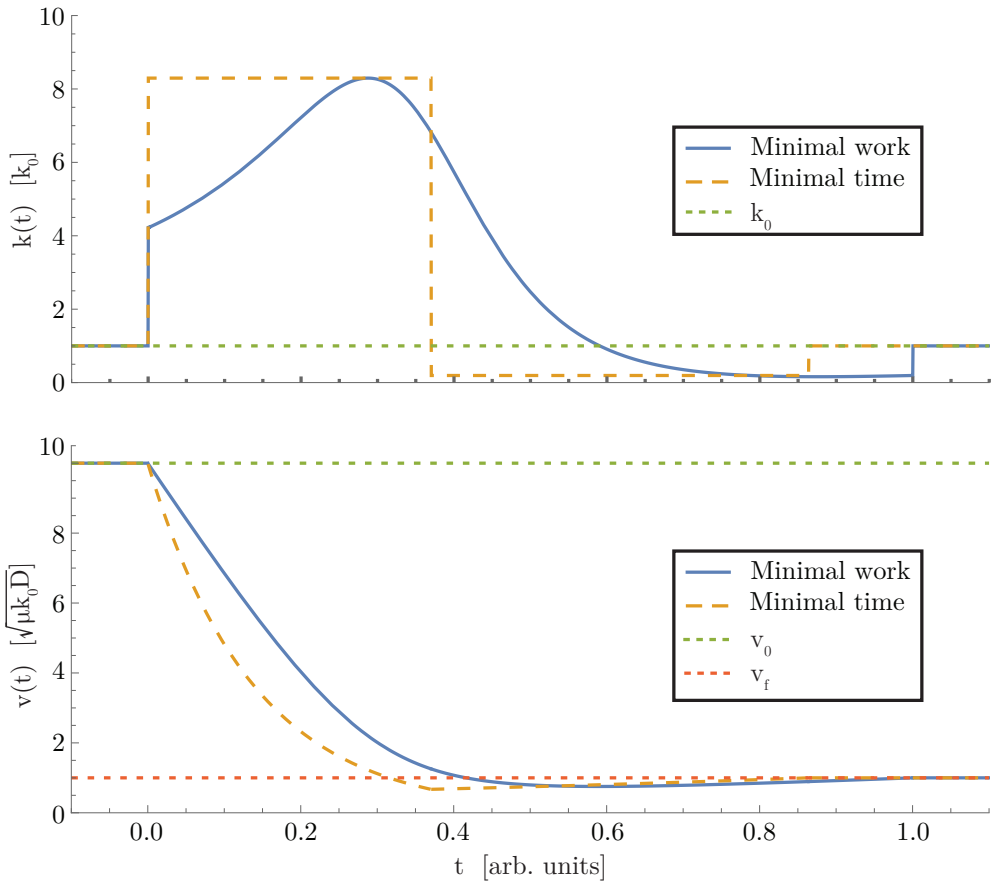


Figure 7.3: **Minimal work (solid blue) and Minimal time (dashed orange) protocols for $k(t)$ and $v_0(t)$.** Maximum and minimum allowed values of stiffness are chosen to be identical and time is measured with respect to duration of minimal-work protocol. We find $\tau_{\text{min-time}} \approx 0.864\tau_{\text{min-work}}$ while $W_{\text{min-time}} \approx 1.571W_{\text{min-work}}$.

Another observation worthy of comment is the tendency of passive-to-active shortcuts to take more time than active-to-passive shortcuts. In fact, if we allow any value for harmonic trap stiffness for intermediate times, including unphysical negative values which have been previously studied in the literature [131], we find that there is no lower time bound whatsoever on active-to-passive transitions. We suggest a simple physical intuition for this asymmetry: in passive-like steady states, both right- and left-moving particles are concentrated at the center of the trap. In contrast, in active-like steady states, right- (left-) moving particles accumulate at the right (left) wall of the trap. Therefore, when trying to transition from an active state to a passive state, one can simply increase the stiffness dramatically to accumulate all particles at the center of the trap before decreasing slightly and allowing the particles to reach their proper steady states. Indeed, we obtained this qualitative strategy quite generally for all explicit protocols we calculated, as shown in Fig 10.3. In contrast, when transitioning from a passive state to an active state, one can only decrease the stiffness to $k = 0$ (at a minimum) and allow the two particle species to reach their final positions by means of their self-propulsion before again raising the stiffness to maintain the trap. This is qualitatively the general protocol we found for optimal passive to active transitions. We emphasize that even if we were to allow k to attain negative values, this may prove detrimental to rapid passive-to-active transitions as a left-moving particles could become initially trapped at the right wall, and vice versa. Conversely, negative values of stiffness allow for arbitrarily rapid active-to-passive transitions.

In this chapter, we calculated the minimal-time and minimal-work protocols when constrained to our shortcut solution Eq. (7.7). More specifically, we focused on the minimal external work protocol: we did not take into account the energy dissipated from the active particles themselves or from other external sources, such as external controls needed to modulate self-propulsion velocities. Including such energetic costs may lead to different optimal protocols. We emphasize that this shortcut, Eq. (7.8), offers a great deal of flexibility given the arbitrary possible choice of α. That said, although this family of solutions does yield full, rapid control of the distribution, it may not contain the absolutely optimal set of controls for a given state-to-state transition. In particular, we calculated the minimal-time and minimal-work protocols connecting two different RTP steady states for a given duration τ when constrained to this specific control strategy. We were able to observe presumably general features, such as work and time trade-offs, but it is a worthwhile question to discover and engineer absolutely optimal protocols for controlling active matter, perhaps through approaches from optimal transport theory [97, 100]. For example, the observed asymmetry in passive-to-active and active-to-passive transitions may be a feature of this specific control protocol, but may not prove to be truly universal. Furthermore, there exists a large literature on optimal control of passive matter in the slowly-varying regime where systems deviate only slightly from reference equilibrium states [106, 107, 169, 222, 76, 223, 110, 111]. Extending these results to active systems could mark a significant advance in engineering active systems.

7.A Derivation

We start with the master equation coupling the right- and left-moving particles due to particle transmutation, Eq. (7.3),

$$\partial_t P_+ = -\partial_x[(-\mu k x + v_0)P_+] + D\partial_x^2 P_+ - \frac{\gamma}{2}(P_+ - P_-) \tag{7.14}$$

$$\partial_t P_- = -\partial_x[(-\mu k x - v_0)P_-] + D\partial_x^2 P_- - \frac{\gamma}{2}(P_- - P_+). \tag{7.15}$$

This has the stationary state solution given by [216]

$$\begin{aligned} P_\pm(x)^* = P_\pm^*(x|v_0,k,D) &= \sum_{n=0}^{\infty} \lambda^n \mathcal{P}_\pm^{(n)} \\ &= \sum_{n=0}^{\infty} \left(\frac{v_0}{\sqrt{\mu k_0 D}}\right)^n \frac{1}{2}\sqrt{\frac{\mu k}{2\pi D}} e^{-\frac{\mu k x^2}{2D}} (\pm 1)^n C_n(\frac{\gamma}{\mu k}) He_n\left(\sqrt{\frac{\mu k}{D}}x\right), \end{aligned} \tag{7.16}$$

where $C_0(x) \equiv 1$ and

$$C_n(x) = \prod_{j=1}^{n} \frac{1}{j + \frac{1}{2}(1+(-1)^{n+1})x}, \qquad n > 0. \tag{7.17}$$

$He_n(x)$ is the nth Hermite polynomial under the "probabilist's convention,"

$$He_n(x) = (-1)^n e^{\frac{x^2}{2}} \frac{d^n}{dx^n} e^{-\frac{x^2}{2}}.$$

We define $\lambda \equiv v_0/\sqrt{\mu k_0 D}$ and

$$\mathcal{P}_\pm^{(n)} \equiv \frac{1}{2}\sqrt{\frac{\mu k}{2\pi D}} e^{-\frac{\mu k x^2}{2D}} (\pm 1)^n C_n(\frac{\gamma}{\mu k}) He_n\left(\sqrt{\frac{\mu k}{D}}x\right).$$

Observe that the coefficients C_n satisfy the recurrence relation

$$C_n(x) = \frac{1}{n + \frac{1}{2}(1+(-1)^{n+1})x} C_{n-1}(x), \tag{7.18}$$

for $n > 0$. We may further define $C_n = 0$ for $n < 0$.

To verify our solution, we evaluate this differential equation for our ansatz:

$$\begin{aligned} P_\pm(x,t) &= P_\pm^*(x|v_0(t),k_0,D/\alpha(t)) \\ &= \sum_{n=0}^{\infty} \left(\frac{\sqrt{\alpha(t)}v_0(t)}{\sqrt{\mu k_0 D}}\right)^n \frac{1}{2}\sqrt{\frac{\alpha(t)\mu k_0}{2\pi D}} e^{-\frac{\alpha(t)\mu k_0 x^2}{2D}} (\pm 1)^n C_n(\frac{\gamma}{\mu k_0}) He_n\left(\sqrt{\frac{\mu k_0 \alpha(t)}{D}}x\right). \end{aligned} \tag{7.19}$$

To aid in our derivation, let us calculate several derivatives that will be helpful later. For clarity, we suppress the arguments of He_n as they will all be of the same form, $\sqrt{\mu k_0 \alpha/D}x$:

$$\partial_t P_\pm = \sum_{n=0}^{\infty} \lambda^n \left[(n+1)\frac{\dot{\alpha}}{2\alpha} + \frac{n\dot{v}_0}{v_0} - \frac{\mu k_0 x^2}{2D}\dot{\alpha} + nx\sqrt{\frac{\alpha\mu k_0}{D}}\frac{He_{n-1}}{He_n}\frac{\dot{\alpha}}{2\alpha} \right] \mathcal{P}^{(n)}, \tag{7.20}$$

$$\partial_x P_\pm = \sum_{n=0}^{\infty} \lambda^n \left[-\frac{\alpha\mu k_0 x}{D} + n\sqrt{\frac{\alpha\mu k_0}{D}}\frac{He_{n-1}}{He_n} \right] \mathcal{P}_\pm^{(n)}, \tag{7.21}$$

$$\begin{aligned} \partial_x^2 P_\pm = \sum_{n=0}^{\infty} \lambda^n \Bigg[&- \frac{\alpha\mu k_0}{D} + \left(\frac{\alpha\mu k_0}{D}\right)^2 x^2 - 2nx\left(\frac{\alpha\mu k_0}{D}\right)^{3/2}\frac{He_{n-1}}{He_n} \\ &+ n(n-1)\frac{\alpha\mu k_0}{D}\frac{He_{n-2}}{He_n} \Bigg] \mathcal{P}_\pm^{(n)}. \end{aligned} \tag{7.22}$$

Using the recursion identity

$$He_{n+1}(y) = yHe_n(y) - nHe_{n-1}(y) \implies He_{n-2}(y) = \frac{yHe_{n-1}(y) - He_n(y)}{n-1}$$

we may simplify further

$$\begin{aligned} &\partial_x^2 P_\pm \sum_{n=0}^{\infty} \lambda^n \left[- \frac{\alpha\mu k_0}{D} + \left(\frac{\alpha\mu k_0}{D}\right)^2 x^2 - 2nx\left(\frac{\alpha\mu k_0}{D}\right)^{3/2}\frac{He_{n-1}}{He_n} + n(n-1)\frac{\alpha\mu k_0}{D}\frac{He_{n-2}}{He_n} \right] \mathcal{P}_\pm^{(n)} \\ &= \sum_{n=0}^{\infty} \lambda^n \Bigg[- \frac{\alpha\mu k_0}{D} + \left(\frac{\alpha\mu k_0}{D}\right)^2 x^2 - 2nx\left(\frac{\alpha\mu k_0}{D}\right)^{3/2}\frac{He_{n-1}}{He_n} \\ &\qquad + nx\left(\frac{\alpha\mu k_0}{D}\right)^{3/2}\frac{He_{n-1}}{He_n} - \frac{n\alpha\mu k_0}{D} \Bigg] \mathcal{P}_\pm^{(n)} \\ &= \sum_{n=0}^{\infty} \lambda^n \left[-(n+1)\frac{\alpha\mu k_0}{D} + \left(\frac{\alpha\mu k_0}{D}\right)^2 x^2 - nx\left(\frac{\alpha\mu k_0}{D}\right)^{3/2}\frac{He_{n-1}}{He_n} \right] \mathcal{P}_\pm^{(n)}. \end{aligned} \tag{7.23}$$

Finally, we calculate

$$\begin{aligned}
v_0 P_\pm &= \sum_{n=0}^{\infty} (\sqrt{\frac{\mu k_0 D}{\alpha}}\lambda)\lambda^n \mathcal{P}_\pm^{(n)} \\
&= \sum_{n=0}^{\infty} \lambda^{n+1}\sqrt{\mu k_0 D}\mathcal{P}_\pm^{(n)} \\
&= \sum_{n=0}^{\infty} \lambda^{n+1}\sqrt{\frac{\mu k_0 D}{\alpha}}\frac{\mathcal{P}_\pm^{(n)}}{\mathcal{P}_\pm^{(n+1)}}\mathcal{P}_\pm^{(n+1)} \\
&= \sum_{n=1}^{\infty} \lambda^{n}(\pm 1)\sqrt{\frac{\mu k_0 D}{\alpha}}\frac{C_{n-1}}{C_n}\frac{He_{n-1}}{He_n}\mathcal{P}_\pm^{(n)} \\
&= \sum_{n=0}^{\infty} \lambda^{n}(\pm 1)\sqrt{\frac{\mu k_0 D}{\alpha}}\frac{C_{n-1}}{C_n}\frac{He_{n-1}}{He_n}\mathcal{P}_\pm^{(n)} \\
&= \sum_{n=0}^{\infty} \lambda^{n}(\pm 1)\sqrt{\frac{\mu k_0 D}{\alpha}}(n + \frac{\gamma}{2\mu k_0}(1+(-1)^{n+1}))\frac{He_{n-1}}{He_n}\mathcal{P}_\pm^{(n)},
\end{aligned} \tag{7.24}$$

such that

$$\begin{aligned}
\pm\partial_x(v_0 P_\pm) &= \sum_{n=0}^{\infty} \lambda^n \sqrt{\frac{\mu k_0 D}{\alpha}}(n + \frac{\gamma}{2\mu k_0}(1+(-1)^{n+1})) \\
&\qquad \times \left[\frac{-\alpha\mu k_0 x}{D}\frac{He_{n-1}}{He_n} + (n-1)\sqrt{\frac{\alpha\mu k_0}{D}}\frac{He_{n-2}}{He_n}\right]\mathcal{P}_\pm^{(n)} \\
&= \sum_{n=0}^{\infty} \lambda^n \sqrt{\frac{\mu k_0 D}{\alpha}}(n + \frac{\gamma}{2\mu k_0}(1+(-1)^{n+1}))\left(-\sqrt{\frac{\alpha\mu k_0}{D}}\right)\mathcal{P}_\pm^{(n)} \\
&= -\sum_{n=0}^{\infty} \lambda^n (n\mu k_0 + \frac{\gamma}{2}(1+(-1)^{n+1}))\mathcal{P}_\pm^{(n)},
\end{aligned} \tag{7.25}$$

where we have made use of the recurrence relation.

Combining Eqs. (7.19), (7.20), (7.21), (7.23), and (7.25), the master equation, Eqs. (7.14)

and (7.15), becomes

$$\begin{aligned}0=\sum_{n=0}^{\infty}\Bigg[&\left((n+1)\frac{\dot\alpha}{2\alpha}+\frac{n\dot v_0}{v_0}-\frac{\mu k_0 x^2}{2D}\dot\alpha+nx\sqrt{\frac{\alpha\mu k_0}{D}}\frac{He_{n-1}}{He_n}\frac{\dot\alpha}{2\alpha}\right)-\mu k\\&-\mu kx\left(-\frac{\alpha\mu k_0 x}{D}+n\sqrt{\frac{\alpha\mu k_0}{D}}\frac{He_{n-1}}{He_n}\right)-(n\mu k_0+\frac{\gamma}{2}(1+(-1)^{n+1}))\\&-D\left(-(n+1)\frac{\alpha\mu k_0}{D}+\left(\frac{\alpha\mu k_0}{D}\right)^2x^2-nx\left(\frac{\alpha\mu k_0}{D}\right)^{3/2}\frac{He_{n-1}}{He_n}\right)\\&+\frac{\gamma}{2}(1+(-1)^{n+1})\Bigg]\lambda^n\mathcal{P}_\pm\\=\sum_{n=0}^{\infty}\Bigg[&\left(\frac{\dot\alpha}{2\alpha}+\alpha\mu k_0-\mu k\right)\left(-\frac{\alpha\mu k_0x^2}{D}+nx\sqrt{\frac{\alpha\mu k_0}{D}}\frac{He_{n-1}}{He_n}+1\right)\\&+n\left(\frac{\dot\alpha}{2\alpha}+\frac{\dot v_0}{v_0}-\mu k_0+\alpha\mu k_0\right)\Bigg]\lambda^n\mathcal{P}_\pm\end{aligned}\tag{7.26}$$

We may satisfy this equation for

$$\frac{\dot\alpha}{2\alpha}+\alpha\mu k_0-\mu k=0,\tag{7.27}$$

$$\frac{\dot\alpha}{2\alpha}+\frac{\dot v_0}{v_0}-\mu k_0+\alpha\mu k_0=0.\tag{7.28}$$

Note that by solving the first, we can further simplify the second:

$$\dot\alpha=2\mu\alpha(k-k_0\alpha),\tag{7.29}$$

$$\dot v_0=-v_0\mu(k-k_0).\tag{7.30}$$

Remarkably, this is precisely the same set of conditions needed for the active Brownian particle shortcut [147].

7.B Athermal Shortcut

For the athermal case, to avoid nuances in taking the limit of $D\to 0$, we can instead work directly with the athermal distribution [215]:

$$P_\pm(x)^*=P_\pm^*(x|v_0,k)=\frac{1}{2}\frac{\mu k\Gamma[\frac{1}{2}(1+\frac{\gamma}{\mu k})]}{\sqrt{\pi}v_0\Gamma[\frac{\gamma}{2\mu k}]}\left(1\pm\frac{\mu kx}{v_0}\right)^{\frac{2\gamma}{\mu k}}\left(1\mp\frac{\mu kx}{v_0}\right)^{\frac{2\gamma}{\mu k}-1}.\tag{7.31}$$

We simply use as an ansatz

$$P_{\pm}(x,t) = P^{*}_{\pm}(x|v_0(t),k_0) = \frac{1}{2}\frac{\mu k \Gamma[\frac{1}{2}(1+\frac{\gamma}{\mu k})]}{\sqrt{\pi}v_0\Gamma[\frac{\gamma}{2\mu k}]}\left(1 \pm \frac{\mu k_0 x}{v_0(t)}\right)^{\frac{2\gamma}{\mu k_0}}\left(1 \mp \frac{\mu k_0 x}{v_0(t)}\right)^{\frac{2\gamma}{\mu k_0}-1}. \quad (7.32)$$

Evaluating these ansätze in Eqs. (7.14) and (7.15), for $D \to 0$ we have, after simplification,

$$\frac{\mu k_0 \Gamma\left[\frac{1}{2}\left(\frac{\gamma}{\mu k_0}+1\right)\right](\dot{v}_0 + v_0\mu(k-k_0))\left(1-\frac{\mu^2 k_0^2 x^2}{v_0^2}\right)^{\frac{\gamma}{2\mu k_0}-1}(\gamma\mu k_0 x^2 - \mu k_0 V_0 x - v_0^2))}{v_0^3\Gamma\left[\frac{\gamma}{2k_0\mu}\right]} = 0, \quad (7.33)$$

$$\frac{\mu k_0 \Gamma\left[\frac{1}{2}\left(\frac{\gamma}{\mu k_0}+1\right)\right](\dot{v}_0 + v_0\mu(k-k_0))\left(1-\frac{\mu^2 k_0^2 x^2}{v_0^2}\right)^{\frac{\gamma}{2\mu k_0}-1}(\gamma\mu k_0 x^2 + \mu k_0 V_0 x - v_0^2)}{v_0^3\Gamma\left[\frac{\gamma}{2k_0\mu}\right]} = 0. \quad (7.34)$$

Both equations may be naturally satisfied by taking

$$\dot{v}_0 = -v_0\mu(k-k_0), \quad (7.35)$$

which is precisely Eq. (7.30), or the shortcut upon taking $\alpha \to 0$.

7.C Average external work

We now calculate the average work done externally in this protocol. We emphasize that we focus only on the work due to manipulating the potential: there may also be some energy cost in changing v_0 (not to mention the housekeeping heat to maintain the system's activity), but herein we focus only on the potential work. Therefore,

$$\begin{aligned}\langle W\rangle &= \int_0^{t_f} dt \int dx\ P(x,t)\partial_t U(x,t) \\ &= \int_0^{t_f} \frac{\dot{k}}{2}\int dx\ x^2 \sum_{n=0}^{\infty}\left(\frac{\sqrt{\alpha(t)}v_0(t)}{\sqrt{\mu k_0 D}}\right)^{2n}\sqrt{\frac{\alpha(t)\mu k_0}{2\pi D}} \\ &\qquad \times e^{-\frac{\alpha(t)\mu k_0 x^2}{2D}} C_{2n}(\frac{\gamma}{\mu k_0}) He_n\left(\sqrt{\frac{\mu k_0 \alpha(t)}{D}}x\right).\end{aligned} \quad (7.36)$$

Let us focus on the spatial integral

$$\begin{aligned}\int dx\ x^2 e^{-\frac{\alpha(t)\mu k_0 x^2}{2D}} He_{2n}\left(\sqrt{\frac{\mu k_0 \alpha(t)}{D}}x\right) &= \left(\frac{D}{\mu k}\right)^{3/2}\int dy\ y^2 e^{-y^2/2} He_{2n}(y)\\ &= \left(\frac{D}{\alpha(t)\mu k_0}\right)^{3/2}\int dy\ y^2 \frac{d^{2n}}{dy^{2n}} e^{-y^2/2}\\ &= \sqrt{2\pi}\left(\frac{D}{\alpha(t)\mu k_0}\right)^{3/2}(\delta_{n,0}+2\delta_{n,1}).\end{aligned}$$

Accordingly, the work performed during the protocol is

$$\begin{aligned}\langle W\rangle &= \int_0^{t_f} dt\ \frac{\dot{k}}{2}\sum_{n=0}^{\infty}\left(\frac{\sqrt{\alpha(t)}v_0(t)}{\sqrt{\mu k_0 D}}\right)^{2n}\sqrt{\frac{\alpha(t)\mu k_0}{2\pi D}}C_{2n}(\frac{\gamma}{\mu k_0})\sqrt{2\pi}\left(\frac{D}{\alpha(t)\mu k_0}\right)^{3/2}(\delta_{n,0}+2\delta_{n,1})\\ &= \int_0^{t_f}\ \frac{\dot{k}}{2}\left[\frac{D}{\alpha\mu k_0}+\frac{v_0^2}{(\mu k_0)^2+\mu k_0\gamma}\right]dt.\end{aligned} \tag{7.37}$$

From Eqs. (7.29) and (7.30), we have

$$v_0(t) = v_{00}e^{-\mu\int_0^t(k-k_0)dt},$$

where v_{00} is the initial velocity. We can also rearrange:

$$k = \frac{\dot{\alpha}}{2\mu\alpha}+k_0\alpha \implies \dot{k} = \frac{\ddot{\alpha}}{2\mu\alpha}-\frac{\dot{\alpha}^2}{2\mu\alpha^2}+k_0\dot{\alpha},$$

such that

$$v_0(t) = v_{00}e^{-\int_0^t[\frac{\dot{\alpha}}{2\alpha}+\mu k_0(\alpha(t')-1)]dt'} = \frac{v_{00}}{\sqrt{\alpha}}e^{\mu k_0 t}e^{-\mu k_0\int_0^t\alpha(t')dt'}.$$

Finally, defining

$$\Lambda(t) = \int_0^t \alpha(t')dt', \tag{7.38}$$

we can rewrite $\langle W\rangle$ as a local functional in Λ,

$$\langle W\rangle = \int_0^{t_f}\left(\frac{\dddot{\Lambda}}{2\mu\dot{\Lambda}}-\frac{\ddot{\Lambda}^2}{2\mu\dot{\Lambda}^2}+k_0\ddot{\Lambda}\right)\left[\frac{D}{2\mu k_0\dot{\Lambda}}+\frac{v_{00}^2}{(\mu k_0)^2+\mu k_0\gamma)}\frac{1}{\dot{\Lambda}}e^{2\mu k_0 t}e^{-2\Lambda}\right]dt, \tag{7.39}$$

such that we may derive the Euler-Lagrange equation for $\Lambda(t)$:

$$
\begin{aligned}
0 =& D\left(6\ddot{\Lambda}^3 + \dddot{\Lambda}\dot{\Lambda}^2 - 6\dddot{\Lambda}\dot{\Lambda}\ddot{\Lambda}\right) \\
&+ \frac{2v_{00}^2 e^{2\mu k_0(s-\Lambda)}}{\gamma + \mu k_0}\left(8(\mu k_0)^3\dot{\Lambda}^6 - 20(\mu k_0)^3\dot{\Lambda}^5 + 16(\mu k_0)^3\dot{\Lambda}^4\right) \\
&+ \frac{2v_{00}^2 e^{2\mu k_0(s-\Lambda)}}{\gamma + \mu k_0}\left(-4\mu k_0\dot{\Lambda}^3\left((\mu k_0)^2 + 3\mu k_0\ddot{\Lambda} + \dddot{\Lambda}\right) - 3\dot{\Lambda}\ddot{\Lambda}\left(3\mu k_0\ddot{\Lambda} + 2\dddot{\Lambda}\right) + 6\ddot{\Lambda}^3\right) \\
&+ \frac{2v_{00}^2 e^{2\mu k_0(s-\Lambda)}}{\gamma + \mu k_0}\left(\dot{\Lambda}^2\left(8(\mu k_0)^2\ddot{\Lambda} + 4\mu k_0\dddot{\Lambda} + 6\mu k_0\ddot{\Lambda}^2 + \dddot{\Lambda}\right)\right).
\end{aligned}
\tag{7.40}
$$

Solving this Euler-Lagrange equation will lead to extremal work protocols, such as the minimal protocol constructed.

Part III

Thermodynamic geometry and optimal control

Chapter 8

Thermodynamic geometry

8.1 Early geometric approaches

Geometry and statistical mechanics have long been connected fields. Both symplectic geometry and contact geometry as distinct mathematical fields derive from Gibbsian statistical mechanics [224, 225, 226]. However, the term *Thermodynamic geometry* refers specifically to a class of interconnected approaches using differential geometry to describe thermodynamic systems. The field was first introduced by Frank Weinhold [227, 228, 229, 230, 231] and significantly advanced by George Ruppeiner [232, 233, 234, 235, 236]. Weinhold considered classical thermodynamic systems described by their internal energy as a function of extensive thermodynamic variables, $U(S, V, N, \cdots)$. For systems in equilibrium, this is a well-defined smooth function. Weinhold was then able to demonstrate that the laws of thermodynamics were compatible with the construction of a Riemannian metric of the form $g^W_{ij} = \partial_i \partial_j U(S, \{N\})$ where ∂_i denotes a derivative with respect to the ith indexed extensive parameter and $\{N\}$ is the set of all extensive parameters excluding S and U itself. That is, Weinhold established a geometric approach to thermodynamics.

A few years later, by following a similar construction with a slightly modified metric $g^R_{ij} = \partial_i \partial_j S(U, \{N\})$, Ruppeiner not only demonstrated the existence of an *a priori* distinct geometric description of thermodynamics, he developed a novel interpretative and predictive aspect to the theory. Ruppeiner studied the curvature induced by this metric and demonstrated connections to thermodynamic fluctuation theory [234]. He has also argued that, quite generally for thermodynamic systems, the sign of the scalar curvature of this thermodynamic manifold corresponds to the interactions present in the system: negative curvature corresponds to primarily attractive interactions, positive curvature to primarily repulsive [235]. Ruppeiner's approach spurred significant independent development, with particular application to black hole thermodynamics [237, 238].

Finally, Schögl introduced a different form of thermodynamic geometry for *intensive* control parameters, such as temperature and chemical potential, in 1985 [239]. Although all of these approaches may seem distinct, the early thermodynamic geometries were all

based on equilibrium macroscopic thermodynamics and essentially demonstrate calculations carried out in different ensembles, thereby effectively yielding identical results [240].

8.2 Thermodynamic length and dissipation

In [241], Peter Salamon and Michael Berry gave a new interpretation to the meaning of this thermodynamic geometric space. In particular, working in *endoreversible* thermodynamics, Salamon and Berry recognized that the thermodynamic geometric length, $\mathcal{L}$, between two states in this space was a measure of the minimum dissipation required to transform between them in finite time [242]. Endoreversible thermodynamics is a near-equilibrium formalism in which the system and surroundings are considered weakly coupled, such that they are both independently in equilibrium, though they may not be in mutual equilibrium with each other. This approach is accurate when systems are driven slowly and weakly from some reference equilibrium state, as was relevant to Salamon and Berry's calculation. Assuming the transformation is carried out adiabatically, i.e. slowly, they showed that to leading order in the driving rates,

$$\mathcal{D} \geq \frac{\mathcal{L}^2}{\tau}, \tag{8.1}$$

where $\mathcal{D}$ is the dissipation and τ is the protocol duration. This therefore immediately connected the thermodynamic length, a quantity calculable purely from equilibrium thermodynamics, to the dissipation, a feature explicitly of the nonequilibrium theory.

Crooks extended this result to the case of small, fluctuating stochastic systems in [240]. Importantly, all the thermodynamic geometries discussed above deal with systems in terms of macroscopic parameters which may not be well-defined for the noisy dynamics of mesoscale systems. Following the formalism of stochastic thermodynamics, Crooks arrived at a proper definition for thermodynamic length for such mesoscale systems that maintained the connection to dissipation [240].

8.3 Geometric optimal control

In a foundational work, Sivak and Crooks utilized the known connections between thermodynamic length and minimal dissipation [106] to arrive at an approach for finding optimal protocols to manipulate thermodynamic systems, whether at the macro- or meso-scale. In particular, Sivak and Crooks considered the problem of parametric optimal control in the slow driving limit. For a Hamiltonian $H(\mathbf{x}; \mathbf{\Lambda})$ indexed by control parameters $\{\mathbf{\Lambda}\}$, Sivak and Crooks demonstrated that, to leading order in the driving rates, the dissipation is given by [106]

$$\mathcal{D} = \int dt \sum_{\mu,\nu} \dot{\mathbf{\Lambda}}^{\mu}(t) g_{\mu\nu}(\mathbf{\Lambda}(t)) \dot{\mathbf{\Lambda}}^{\nu}(t), \tag{8.2}$$

where $g_{\mu\nu}$ is the thermodynamic metric relevant to the problem, and $\mathbf{\Lambda}^{\mu}$ is a vector of all control variables. Focusing on classical stochastic systems, they derived the expression for $g_{\mu\nu}$ through dynamic linear response theory:

$$g_{\mu\nu}(\mathbf{\Lambda}) = \frac{1}{k_B T} \int_0^{\infty} dt \, \langle \delta X_{\mu}(t) \delta X_{\nu}(0) \rangle_{\mathbf{\Lambda}} \,, \tag{8.3}$$

where $\langle \cdot \rangle_{\mathbf{\Lambda}}$ denotes an equilibrium average carried out at fixed $\mathbf{\Lambda}$. Importantly, this makes the expression for the dissipation, Eq. (8.2) time-local and based solely on equilibrium time-correlations, making the calculation of the thermodynamic metric analytically tractable in certain simple cases [107, 158, 108, 87, 109] and amenable to sampling in more complex cases [222, 243].

Importantly, Sivak and Crooks also demonstrated, much like Weinhold, Ruppeiner, Salamon, and Berry, that the laws of thermodynamics mandate that the matrix $g_{\mu\nu}$ satisfy the requirements to be a (pseudo)metric. Therefore, upon deriving the metric, the problem can be divorced from thermodynamical details and reframed entirely as a problem in geometry: deriving minimally dissipative finite-time thermodynamical protocols now corresponds to constructing shortest-length smooth curves in a Riemannian manifold. This problem has been studied extensively in the literature of Geometric Optimal Control [244]. At a base level, given some set of paths in the space of control parameters one must follow, the Sivak-Crooks formalism yields the proper time-parametrization to minimize dissipation. If one has even more control, i..e the ability to choose the shape of the path in the first place, one could derive the control geodesics, that is the shortest-distance paths between two points in the thermodynamic manifold, such that the protocol minimizes dissipation for any smooth path connecting the two endpoints of the control curve. Other problems can also be of interest for different optimization functions: for example, in studying engines, geometric approaches using this formalism instead looked at optimal cycles for maximum efficiency or maximum power. A fuller presentation of maximally efficiency engines will be given in Chapter 10.

Thermodynamic geometry as applied for optimal control has been extended broadly beyond its original focus in open classical systems. Initially, extensions were made to include temperature-varying protocols [107] and simple quantum protocols [87], though recently a wide array of successful applications in quantum systems have been derived [88, 245], with particular focus on engines [223, 246]. Very recently, thermodynamic geometry and geometric optimal control have led to novel methods of studying chemical reaction networks [247], complex many-body systems [248], and even intrinsically nonequilibrium systems, such as active matter [101]. In the rest of this Part, we will detail applications of thermodynamic geometry to engines, with particular focus on applications to classical harmonic oscillators, though many of our results are more general.

Chapter 9

Optimal finite-time Brownian Carnot Engine

In this chapter, we apply thermodynamic geometry to optimize the Brownian Carnot cycle, an experimentally tractable heat engine at the nanoscale [249]. This exercise is both pedagogical in recognizing the application of thermodynamic geometry to heat engine optimization, but we also gain key insights through this study that may be applied more broadly. This chapter is adapted from [110] with the permission of all authors.

9.1 Introduction

Since the turn of the millennium, our understanding of nonequilibrium processes has improved dramatically [46, 53, 50, 54, 250, 251, 45]. Over the past decade in particular, powerful techniques for controlling colloidal mesoscopic systems have facilitated experimental realizations of finite-time thermodynamic cycles [252, 160, 249, 253, 254, 159]. A major step forward was achieved by the construction of a mesoscopic Stirling cycle with a harmonically trapped particle suspended in a temperature-controlled, laser heated fluid [160]. Another significant advance was achieved by placing an electrically charged colloidal particle in an electrostatic field with tunable noise in order to mimic a thermal bath with a continuously varying temperature [249]. By following alternating adiabatic (constant Shannon entropy) and isothermal strokes, these authors produced a mesoscopic colloidal Carnot cycle.

However, although a large class of control protocols, including those used in this experiment, reproduce the standard Carnot cycle when performed quasistatically, the choice of a specific temporal parametrization significantly impacts the thermodynamic performance of the engine when operated in finite time. In this chapter, we connect the versatile thermodynamic geometry approach with the colloidal harmonic oscillator used previously [160, 249] and calculate explicit optimal protocols for this important model system. We find improvements in the efficiency, output power, and dissipated energy in steady-state operation

for a wide variety of cycle durations. Our results may find use in practical development of mesoscale engines.

9.2 Thermodynamic geometry

Thermodynamic length was originally introduced as a notion of metric distance between equilibrium states of a physical system [227, 232, 241, 255, 239, 240]. Since their introduction, thermodynamic length and similar geometric approaches have found wide-ranging applications in various contexts [234], with recent success in optimal control of nonequilibrium systems [106, 107, 256, 169, 108, 87, 222, 257, 243, 223, 245, 258]. We will follow the treatment introduced in a recent pioneering study [76] that successfully applied a geometric approach to closed thermodynamic cycles. In particular, we consider a thermodynamic system with two control parameters, $\mathbf{\Lambda} = (T, \lambda)$, operated cyclically, where T is the time-varying temperature of an external bath and λ represents a mechanically varied parameter. The work, W, and effective energy intake from the heat source [76], U, are given

$$W = -\oint dt \left\langle \frac{\partial H_\lambda}{\partial \lambda_t} \right\rangle \dot{\lambda}_t, \qquad U = \oint dt \, \langle \log \rho_t \rangle \, \dot{T}_t, \tag{9.1}$$

where H_λ is the system Hamiltonian for a given value of λ, ρ is the phase space density, t subscripts denote values at a given time t, and brackets denote ensemble averages, i.e. phase space integrals against ρ for a given t.

This expression for the work is fairly standard, but the quantity U above may be less familiar (U *does not* represent the internal energy of the system). For any quasistatic, reversible process, a change in the entropy of a system must coincide with an exchange of heat with an external bath by the amount given by the expression for U. For systems driven out of equilibrium, the entropy can increase even in the absence of heat exchange, as is the case during a free expansion, for example. This quantity, which upon performing integration by parts converts to $\oint T dS$ in steady-state driving, where S is the system entropy, then includes contributions at each moment from both the actual amount of heat exchanged with the environment plus the amount of heat that would result in the extra increase in S during a corresponding reversible process at temperature T.

Thus, the energy irreversibly dissipated over the course of a full cycle, A, (alternatively known as the dissipated availability or work) can be written

$$A = U - W \geq 0, \tag{9.2}$$

where the inequality arises from the second law. The equality is saturated only for quasistatic driving in which case the phase space density assumes a Boltzmann form at all times:

$$\rho_{\mathbf{\Lambda}} = e^{-\beta(H_\lambda - F_{\mathbf{\Lambda}})}, \tag{9.3}$$

where $F_{\mathbf{\Lambda}}$ is the free energy for a given λ and T and $\beta \equiv (k_B T)^{-1}$.

Following [106, 107, 76], we consider the system to be operating in the slow-driving regime wherein temporal variations of control parameters are assumed slow relative to the relaxation timescale of the system. Standard dynamic linear response then gives the dissipated energy to lowest order in $\dot{\mathbf{\Lambda}}$

$$A \approx \oint dt\ \dot{\mathbf{\Lambda}} \cdot \mathbf{g} \cdot \dot{\mathbf{\Lambda}}, \tag{9.4}$$

where $\mathbf{g}$ is defined as the inverse diffusion tensor, given by equilibrium time-correlation functions

$$g_{ij}(t) = \beta(t) \int_0^\infty dt' \left\langle \delta X_i(0) \delta X_j(t') \right\rangle_{\mathbf{\Lambda}(t')}. \tag{9.5}$$

Here $X_i(t)$ is the time-dependent thermodynamic force conjugate to control variable i: $X_T = -\log \rho_{\mathbf{\Lambda}}$ and $X_\lambda = -\partial H_\lambda / \partial \lambda_t$ and $\delta X = X - \langle X \rangle$. The tensor $\mathbf{g}$ is symmetric by construction and can be shown to be positive-semidefinite [107, 76] as a consequence of the second law. Because it satisfies these conditions, one can interpret $\mathbf{g}$ as a metric tensor, introducing a well-defined notion of geometric distance on cycles in control parameter space. Non-cyclical paths can yield a negative dissipated energy, suggesting that entropy production may be a more appropriate quantity to study when considering such processes [107, 259]. For an arbitrary closed path $\boldsymbol{\phi}$ through control space, we may define the corresponding thermodynamic length $\mathcal{L}_{\boldsymbol{\phi}}$ as

$$\mathcal{L}_{\boldsymbol{\phi}} = \int \sqrt{d\boldsymbol{\phi} \cdot \mathbf{g} \cdot d\boldsymbol{\phi}}, \tag{9.6}$$

which is independent of parametrization. Beyond the thermodynamic length, a different geometric quantity, the thermodynamic divergence, may be understood as the thermodynamic cost in dissipated energy of a physical operation. The divergence is defined as

$$\mathcal{D}_{\boldsymbol{\phi}} = \tau \int_0^\tau dt\ \dot{\boldsymbol{\phi}} \cdot \mathbf{g} \cdot \dot{\boldsymbol{\phi}}, \tag{9.7}$$

where now $\boldsymbol{\phi}$ is explicitly parametrized by a time-varying protocol with $t \in [0, \tau]$ and the divergence depends on this parametrization. By comparing Eqs. (9.4) and (9.7), we see that the thermodynamic divergence precisely matches the dissipated energy of a protocol scaled by the protocol duration. Paths and parametrizations that minimize the thermodynamic divergence are therefore minimally dissipative and thermodynamically optimal in that sense. Between any two points, such paths are known as geodesics. Moreover, for any given path in control space that is not a geodesic, there still exists an optimal parametrization that minimizes the divergence, and therefore the dissipated energy, for a fixed protocol duration. Explicitly, comparing Eqs. (9.6) and (9.7), the Cauchy-Schwarz inequality implies $A = \mathcal{D}/\tau \geq \mathcal{L}^2/\tau$. This bound is saturated only for optimal driving protocols where control parameters are changed in such a way that the quantity $\dot{\boldsymbol{\phi}} \cdot \mathbf{g} \cdot \dot{\boldsymbol{\phi}}$, which we identity as the instantaneous dissipated power, $\mathcal{P}_{\text{diss}}$, is constant over the full protocol duration [106].

9.3 Brownian working substance

The parametric harmonic oscillator is often used as the paradigmatic model of colloidal thermodynamic systems and has been successfully applied as the working substance in physical realizations of mesoscopic heat engines [160, 249]. This model system consists of a particle of mass m in a harmonic trap with time dependent stiffness $k(t)$ in contact with a heat bath at temperature $T(t)$, evolving under Langevin dynamics

$$m\ddot{z} = -\zeta\dot{z} - k(t)z + \eta(t), \tag{9.8}$$

where z is the position of the particle, ζ is the friction coefficient, and $\eta(t)$ is Gaussian white noise satisfying

$$\langle \eta(t)\eta(t')\rangle = 2\zeta k_B T\delta(t-t'), \tag{9.9}$$

ensuring that the dynamics satisfy detailed balance. With these two control variables, the thermodynamic forces can be expressed as

$$\mathbf{X} = \left(\tfrac{1}{2T}(p^2/m + kz^2) + \tfrac{1}{T}\log\left(2\pi\sqrt{\tfrac{mT^2}{k}}\right),\quad -1/2z^2\right), \tag{9.10}$$

where p is the momentum of the particle. Following methods similar to [107], we arrive at our first major result, the full metric tensor for this thermodynamic space (see Appendix 9.A for a detailed derivation):

$$g_{ij} = \beta\int_0^\infty dt\,\langle \delta X_i(t)\delta X_j(0)\rangle = \frac{mk_B}{4\zeta}\begin{pmatrix} \frac{1}{T}\left(4+\frac{\zeta^2}{km}\right) & -\frac{1}{k}\left(2+\frac{\zeta^2}{km}\right) \\ -\frac{1}{k}\left(2+\frac{\zeta^2}{km}\right) & \frac{T}{k^2}\left(1+\frac{\zeta^2}{km}\right)\end{pmatrix}_{ij}. \tag{9.11}$$

9.4 Optimal Brownian Carnot engine

The Carnot engine is a four-stroke engine consisting of alternating isothermal steps in contact with a heat bath of either a hot temperature T_h or a cold temperature $T_c < T_h$ and adiabatic steps during which no heat is exchanged with a bath. Consistent with the second law, all engines acting reversibly between two heat baths at these temperatures cannot have a lower thermodynamic efficiency than the Carnot engine, with Carnot thermodynamic efficiency given by $\eta_C = 1-T_c/T_h$. However, the classical Carnot engine operates quasistatically and therefore performs only a finite amount of work over an arbitrarily long cycle period, thus delivering no power. Accordingly, finite-time, nonzero-power thermodynamics of this engine have been a topic of significant interest [260, 261, 157, 262, 52, 263, 264, 265, 219, 266, 220, 267, 268, 223, 269, 270].

Recently, a laser trapped colloidal particle in contact with a time-varying (effective) heat bath was used to experimentally produce a Carnot engine with the Brownian working substance described in the previous section. Isothermal expansion and compression arise from

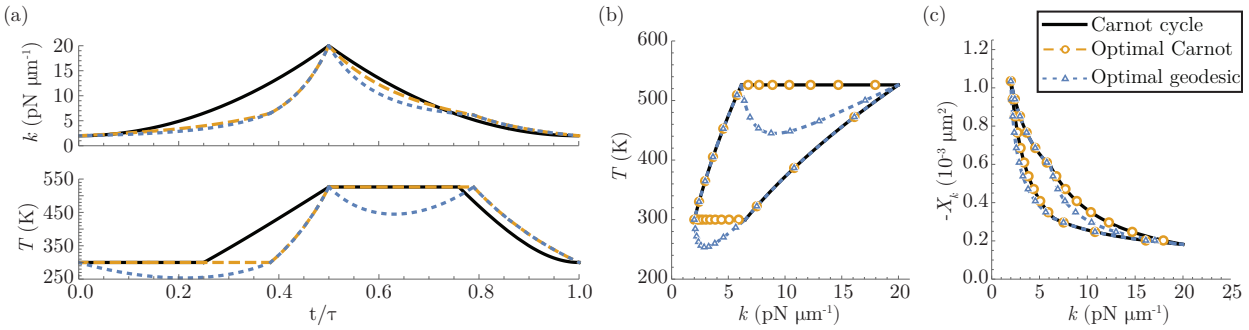


Figure 9.1: **Shape and temporal parametrization of a previously tested Brownian Carnot cycle, the optimized Brownian Carnot cycle, and an optimal geodesic cycle matched to the Carnot cycle**. **(a)** The stiffness (top) and temperature (bottom) for three heat engines as a function of time: an experimentally tested Brownian Carnot cycle [249] (solid black), the optimally parametrized Brownian Carnot cycle (dashed orange), and the optimal cycle employing geodesics between adjacent pairs of corners of the previous Carnot cycles (dotted blue). Horizontal axes are shared between subplots. **(b)** The functional form in control parameter space of the Carnot cycle (solid black) and the optimal geodesic cycle (dotted blue). Orange circles (blue triangles) denote points along the optimal Carnot (geodesic) cycle parametrization at 25 equal duration intervals in time. **(c)** Same as in **(b)** for the Clausius diagram of stiffness k against its conjugate thermodynamic force in the quasistatic limit $-X_k = x^2/2 = k_B T/2k$.

changes in $k(t)$ for a fixed temperature T. Adiabatic paths were achieved by holding fixed T^2/k, an adiabatic invariant for this system, which maintains a constant value of Shannon entropy [271]. A portrait of the Carnot cycle in (T, k) space is plotted in Fig. 9.1(b).

Considering the metric given in Eq. (9.11), we now construct the optimal parametrization for the Carnot engine. For isothermal steps, the dissipated power can be obtained by setting $\dot{T} = 0$ in the integrand of Eq. (9.4), which gives

$$\mathcal{P}_{\text{diss,iso}} = \frac{m k_B T}{4\zeta} \frac{\dot{k}^2}{k^2} \left(1 + \frac{\zeta^2}{km}\right). \tag{9.12}$$

The optimal trajectory in k is then found through the corresponding Euler-Lagrange equation

$$\left(2\zeta + \frac{2mk}{\zeta}\right) \ddot{k} - \left(\frac{3\zeta}{k} + \frac{2m}{\zeta}\right) \dot{k}^2 = 0, \tag{9.13}$$

which can be solved numerically for given initial and final values of k. The total thermodynamic cost of such an isothermal step is given by the integral of Eq. (9.12) for the solution k^*_{iso} of Eq. (9.13) over the duration of the protocol.

For adiabatic steps, the key constraint is that $\alpha \equiv T^2/k$ be held fixed. Under this

constraint, the dissipated power is given by

$$\mathcal{P}_{\text{diss}} = \frac{k_B \zeta \alpha \dot{T}^2}{4T^3}, \tag{9.14}$$

leading to the Euler-Lagrange equation,

$$\ddot{T} = \frac{3\dot{T}^2}{2T}, \tag{9.15}$$

which is analytically solvable. For a generic adiabatic protocol of duration τ that transitions from initial stiffness k_i and temperature $T_i \equiv \sqrt{\alpha k_i}$ at time $t = 0$ to a final stiffness k_f and temperature $T_f \equiv \sqrt{\alpha k_f}$ at time $t = \tau$, the protocol is

$$T^*_{\text{adiab}}(t) = \frac{T_i T_f \tau^2}{(\sqrt{T_f}\tau + (\sqrt{T_i} - \sqrt{T_f})t)^2}, \tag{9.16}$$

$$k^*_{\text{adiab}}(t) = T^*_{\text{adiab}}(t)^2/\alpha, \tag{9.17}$$

leading to a (constant) energetic cost of

$$\mathcal{P}^*_{\text{diss,adiab}} = \frac{k_B \zeta \alpha (\sqrt{T_f} - \sqrt{T_i})^2}{T_i T_f \tau^2}. \tag{9.18}$$

The total Carnot cycle consists of alternating isothermal and adiabatic processes connecting four points in (T, k) space. Following [249], we order the four strokes as: 1) isothermal compression at T_c, 2) adiabatic compression between T_c and T_h, 3) isothermal expansion at T_h, and 4) adiabatic expansion between T_h and T_c. In order to allocate the optimal amount of time to each stroke of the cycle, we note that for any optimally-parametrized process $\boldsymbol{\phi}^*$, the dissipated energy is given $A_{\boldsymbol{\phi}^*} = \mathcal{D}_{\boldsymbol{\phi}^*}/\tau = \mathcal{L}^2_{\boldsymbol{\phi}^*}/\tau$, such that $\mathcal{P}_{\text{diss},\boldsymbol{\phi}^*} = \mathcal{L}^2_{\boldsymbol{\phi}^*}/\tau^2$. This must be true of both the full cycle and each optimized stroke, such that $\mathcal{L}_i^2/\tau_i^2 = \mathcal{L}_{\text{tot}}^2/\tau^2 \implies \mathcal{L}_i/\tau_i = \mathcal{L}_{\text{tot}}/\tau \implies \tau_i = \tau \mathcal{L}_i/\mathcal{L}_{\text{tot}}$ where τ_i and $\mathcal{L}_i$ are the duration and thermodynamic length, respectively, of the ith stroke ($\sum_i \tau_i = \tau$).

Optimal geodesic engine. The Carnot engine is significant in reversible thermodynamics as the paradigmatic model of a heat engine with maximal efficiency under various conditions, such as for specified hot and cold heat baths and considering only inward heat flows when assessing the thermodynamic cost. As discussed previously, its path in control space follows a prescribed shape set by the well-known quasistatic cycle. However, in this geometric framework, there is (at least) one well-defined minimal dissipation path connecting any two points in control space: a geodesic. Given the existence of geodesic protocols that are less dissipative than the corresponding strokes of the Carnot cycle, we next construct an engine consisting only of geodesics that connect adjacent pairs of the four corners of the Carnot cycle. The shape of such an engine is depicted in Fig. 9.1(b). The two adiabatic strokes are in fact exactly geodesic and are unchanged for this cycle, though the geodesic

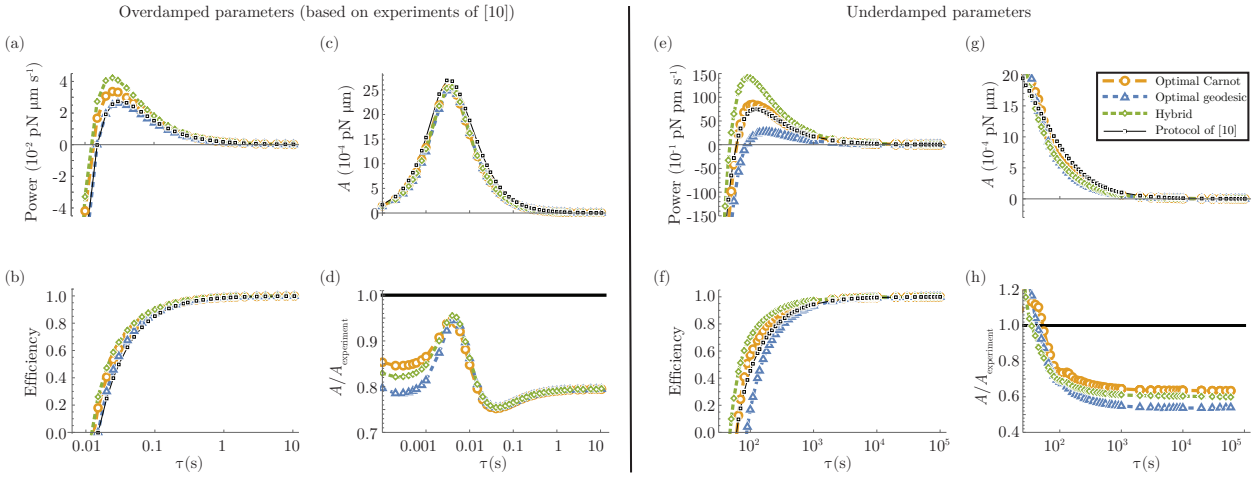


Figure 9.2: **Performance of various engines considered in the main text as a function of protocol duration τ.** We numerically simulate the system under cyclic operation of the control parameters for protocol duration τ and plot the performance of each engine after reaching steady state. In all plots, results of simulations of an engine following the experimental protocol used in [249] are shown with black squares and a straight black linear interpolation, the optimal Carnot cycle with orange circles and dashed orange linear interpolation, the optimal geodesic cycle with blue triangles and blue dotted linear interpolation, and a hybrid cycle consisting of the optimized Carnot cycle with the cold isothermal compression step replaced by the corresponding geodesic path with green diamonds and dashed linear interpolation. **(a)** Average power. **(b)** Average efficiency. **(c)** Average dissipated energy. **(d)** Dissipated energy scaled relative to that of experimental protocol. Material parameters, i.e. m, ζ, T_c, T_h and k, are chosen based on those used in the experiment of [249]. Observe the dissipation is minimized for the geodesic engine, though this engine is less efficient and less powerful than the optimized Carnot and hybrid engines; the hybrid engine is both most efficient and powerful for all protocol durations considered. **(e)**-**(h)** Same as **(a)**-**(d)** for different material parameters for which the contrasting performance between different cycles is clearer (see Appendix 9.B for details of material parameter values). Horizontal axes of **(a)**,**(c)**,**(e)**, and **(g)** are the same as each subfigure below them, **(b)**,**(d)**,**(f)**, and **(h)**, respectively.

paths corresponding to the isothermal strokes now involve variations in temperature. Individual strokes again may be pieced together according each stroke a duration proportional to its thermodynamic length as required for optimally-parametrized processes, leading to the parametrization of the cycle depicted in Fig. 9.1(a).

9.5 Engine performance

We now calculate the performance of the various engines described in the previous section and compare them against a previously studied experimental cycle [249], which we use as a benchmark. To mimic the experiment, we pin the four corners of the Carnot cycle at $(T_0, k_0) = (300\text{ K}, 2\text{ pN }\mu\text{m}^{-1})$, $(T_1, k_1) = (300\text{ K}, 6.5\text{ pN }\mu\text{m}^{-1})$, $(T_2, k_2) = (600\sqrt{10/13}$ K, 20 pN $\mu\text{m}^{-1})$, $(T_3, k_3) = (600\sqrt{10/13}\text{ K}, 80/13\text{ pN }\mu\text{m}^{-1})$, and $(T(\tau), k(\tau)) = (T_0, k_0)$. Following standard methods starting from Eq. (9.8), we can derive an equivalent Fokker-Planck equation for the evolution of the probability density over phase space. Integrating across various covariances (see Appendix 9.B), we arrive at the coupled differential equations governing the evolution of $\langle z^2\rangle$, $\langle pz\rangle$, and $\langle p^2\rangle$:

$$\frac{d}{dt}\langle z^2\rangle = \frac{2}{m}\langle pz\rangle\,, \tag{9.19}$$

$$\frac{d}{dt}\langle pz\rangle = \frac{\langle p\rangle^2}{m} - k\langle z^2\rangle - \frac{\zeta}{m}\langle pz\rangle\,, \tag{9.20}$$

$$\frac{d}{dt}\langle p^2\rangle = -2k\langle pz\rangle - 2\frac{\zeta}{m}\langle p^2\rangle + 2\zeta k_B T. \tag{9.21}$$

Given that our model system only encounters a harmonic potential, if we assume the system starts in a Gaussian form, it will remain Gaussian for the duration of the protocol, such that these covariances encode the *entire* phase space distribution of the Brownian oscillator. Therefore, numerically solving these equations for given control parameters $k(t)$ and $T(t)$ and allowing the system to come to its steady state, we are able to fully simulate the system and evaluate various performance metrics of the engine. We use *simulations* of the experimental protocol of [249] as a benchmark. We do this rather than use the actual experimental results to allow for the evaluation of a greater range of protocol durations and for more detailed (simulated) data than was experimentally measured. We validate our numerical simulations by direct comparison to the experiment in Appendix 9.D.

In Fig. 9.2(a), we plot the power output $P = W/\tau$ as a function of cycle duration τ. As expected, for small times W is negative such that no work is extracted from the cycle and the power is large in magnitude and negative for each of the engines, resulting in a maximum positive value for the power at a finite value of cycle duration. We observe a noticeable benefit to the use of the optimized Carnot engine, though the optimal geodesic engine actually leads to a *reduction* in power.

To better understand this, we plot the dissipated energy A for these protocols in Fig. 9.2(c)-(d). We note a >20% decrease in the dissipated work per cycle for both the optimal Carnot

engine as well as the geodesic engine compared to the previously tested experimental protocol. For these experimental parameters, the thermodynamic length of the optimal Carnot cycle is only 0.0003% greater than that of the geodesic cycle, such that its benefit is difficult to observe in these figures. We therefore also simulate for a different set of material values where the benefits are clearer, now demonstrating a $\sim$50% decrease in dissipated work for the optimal geodesic engine; these results are plotted in Fig. 9.2(e)-(h). This second set of material parameters corresponds to using a ball of millimeter radius and density comparable to gold, which may not be achievable with current experimental technology but serves to illustrate the differences between the various cycles in a significantly more underdamped regime. see Appendix 9.B for further simulation details. We can compute the efficiency of all of these engines, displayed in Fig. 9.2(b) and (f) as a function of cycle duration. Here we define efficiency not as the ratio of work output to heat input, but as the ratio of work output to total effective thermal energy uptake [76]:

$$\eta = \frac{W}{U} \approx 1 - \frac{A}{\mathcal{W}}, \tag{9.22}$$

where $\mathcal{W}$ is the net work extracted from a quasistatic cycle with $\rho_t = \rho_{\mathbf{\Lambda}}$ at all time; Eq. (10.1) holds to lowest nontrivial order in driving rates. As stated previously, this definition is more appropriate for engines of time-variable heat baths and has a universal maximum value of one for any reversible engine. As expected, we observe that both optimized protocols yield a superior efficiency relative to the experimental protocol in the long time limit, as well as for earlier times in most cases. Interestingly, the optimal Carnot cycle is more efficient than the optimal geodesic cycle. This surprising result, along with the comparable result found for the powers, may be understood by recognizing that the cost function for this optimization scheme is only the availability A, and indeed we see the geodesic cycle produces the smallest total availability. In fact, for slowly driven cycles, the optimal geodesic cycle yields the minimum possible value of A for any cycle passing through the four corners of the Carnot cycle in a given time. However, the efficiency and power depend not only on the dissipated energy but also on the total possible energy accessible to the engine in the most ideal conditions, namely $\mathcal{W}$. This therefore introduces a further figure of merit of an engine: for slowly driven systems, the most efficient engine will minimize the ratio $A/\mathcal{W}$. Thus, although the (optimal) Carnot engine produces a larger dissipated energy, it is more efficient.

In fact, given that $\mathcal{W}$ is a monotonic function of the area enclosed by the cycle plotted in Fig. 9.1(b), the geodesic corresponding to the hot isothermal expansion acts to decrease the value of $\mathcal{W}$ as it bows downward into the the cycle, whereas the equivalent for cold isothermal compression acts to increase $\mathcal{W}$. This intuition suggests that we form a more efficient cycle than any considered above by starting with the optimized Carnot cycle and replacing only the cold isothermal compression with the corresponding geodesic path. We plot the shape of this cycle in comparison to others we consider in Fig. 9.3. Indeed, of all the cycles we considered, this hybrid cycle produces the most efficient engine in terms of both $A/\mathcal{W}$ and power (Fig. 9.2). see Appendix 9.D for further comparisons of all simulated cycles

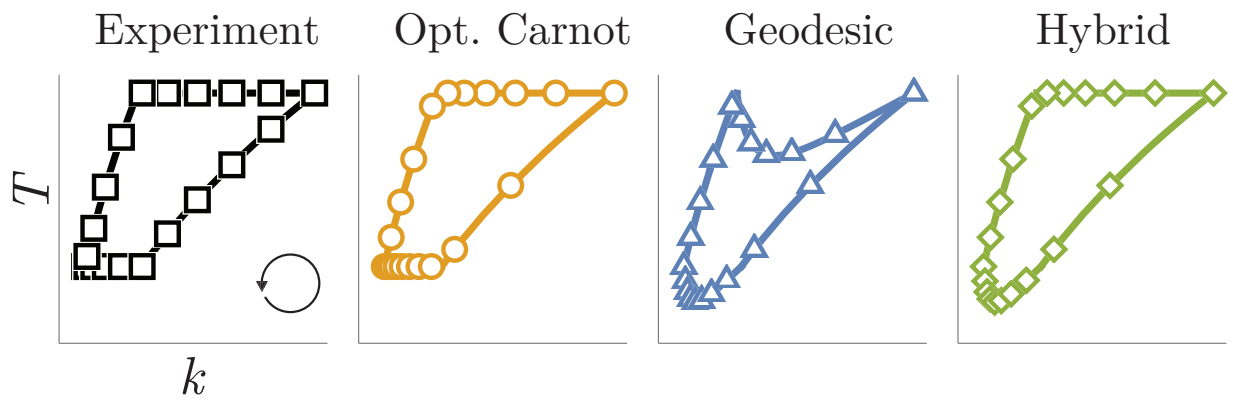


Figure 9.3: **The thermodynamic cycles and parametrizations considered**. Closed curves represent the bath temperature (T) vs. trap stiffness (k) for each engine. Markers are placed at 20 points along each cycle separated by equal time intervals. Colors and marker shapes correspond to the conventions in previous figures.

to the experimental results of [249]. All of the optimized cycles statistically significantly outperform the experimentally measured Carnot cycle.

9.6 Discussion

Here we have considered the optimal temporal parametrization for the Brownian Carnot cycle, and we have also derived two new finite-time thermodynamic cycles that incorporate geodesics connecting consecutive pairs of corners of the Carnot cycle. We have demonstrated that each of these three new engines is less-dissipative than the experimentally tested temporal parametrization of the Brownian Carnot cycle [249], with our hybrid engine being the most efficient among those studied. A clear next step would be to carry out a similar procedure for other thermodynamic engines and refrigerators, such as those corresponding to the Stirling and Otto cycles.

Although the treatment of thermodynamic length is highly accurate for slowly driven cycles (see Appendix 9.C), contributions from higher order corrections have been reported in the literature [272] and have been used, for example, to give stronger bounds on free energy estimates of thermodynamic processes [273]. Likewise, lessons from studies of finite-time processes that shortcut relaxation timescales could further facilitate the development of optimal cyclic engines [156, 130, 205, 77, 136, 131, 78, 132, 133, 144, 134]; such questions have been studied for overdamped dynamics [274, 275]

Finally, although we were able to construct a novel and minimally-dissipative cycle connecting each of the four pairs of adjacent corners of the Carnot cycle with geodesics, it was *less* efficient than the corresponding Carnot cycle. Recognizing that we could simultaneously

reduce the availability A and increase the work W by incorporating a geodesic path in place of the cold isothermal compression while retaining the other three strokes of the optimized Carnot cycle, we obtained our hybrid cycle, which is the most efficient of the engines we considered. We found this more efficient cycle by assembling strokes that were obtained by minimizing only dissipation, but it may be possible to derive maximally efficient cycles more directly. Importantly, for slow driving, the form of efficiency we considered here (Eq. 10.1) is a purely geometric quantity, such that its optimization suggests a new design principle for the *shape* of a cycle, beyond just its optimal temporal parametrization or introducing geodesics between pairs of points. We will pursue this further in future work.

9.7 Conclusion

In this Chapter, we have characterized the thermodynamic geometry of the colloidal harmonic oscillator system and used these results to derive explicit protocols for optimal Carnot-like cycles. Using similar methods, one could construct optimal parametrizations and introduce geodesics to minimize dissipation for any chosen cycle of the model working system studied. Future work may be directed towards higher order corrections to our results, application of our results to the study of further cycles, and the development of fundamentally new and more efficient nonequilibrium thermodynamic cycles. We hope our results will facilitate the design and construction of optimal thermal machines at the mesoscale.

9.A Thermodynamic metric for the parametric harmonic oscillator

Here, we will derive the thermodynamic metric given in Eq. (9.11). Significant methods in our treatment were previously developed in [106, 107], and we will follow a similar derivation. First, we recapitulate the definition

$$g_{ij} = \beta \int_0^\infty \langle \delta X_i(t) \delta X_j(0) \rangle \,, \tag{9.23}$$

where $\delta X_i \equiv X_i - \langle X_i \rangle$, $\beta \equiv (k_B T)^{-1}$ is inverse temperature, and brackets denote an ensemble average over an initial equilibrium distribution and thermal noise. Following Eq. (9.10), these thermodynamic forces take the form

$$\mathbf{X} = \left(\tfrac{1}{2T}(p^2/m + kz^2) + \tfrac{1}{T} \log \left(2\pi \sqrt{\tfrac{mT^2}{k}} \right), \quad -1/2z^2 \right). \tag{9.24}$$

where z is the particle's position, m is mass, k is the stiffness constant, and T is the temperature of the heat bath. In order to calculate the metric, therefore, we need to calculate various two-point correlation functions, which are dynamical quantities for fixed external

parameters. In particular, we will be interested in z and $p \equiv m\dot{z}(t)$ for a particle whose dynamics are given by Eq. (9.8) at fixed values of k and T, reproduced here

$$m\ddot{z} + kz + \zeta\dot{z} = F(t). \tag{9.25}$$

Given that this is a second order linear differential equation, we may write its solution as the sum of homogeneous, $z^{(h)}$, and particular, $z^{(p)}$, solutions, $z = z^{(h)} + z^{(p)}$, where all dependence on initial conditions is carried in $z^{(h)}$ and all dependence on the random thermal forcing $F(t)$ is carried in $z^{(p)}$. Following this reasoning and assuming $F(t)$ is a zero-mean Gaussian white noise process, it is a simple exercise to show that in general $\langle \delta X_i(t)\delta X_j(0)\rangle = \langle \delta X_i^{(h)}(t)\delta X_j(0)\rangle$ for any thermodynamic force X. Therefore, we need only calculate the homogeneous solution to the differential equation, and thus set $F = 0$.

First, let us consider the case $\zeta^2 \neq 4km$, such that Eq. (9.25) with $F = 0$ is easily solved to give

$$z_h(t) = \frac{p(0) + m\Lambda_- z(0)}{m(\Lambda_- - \Lambda_+)} e^{-\Lambda_+ t} + \frac{p(0) + m\Lambda_+ z(0)}{m(\Lambda_+ - \Lambda_-)} e^{-\Lambda_- t} \tag{9.26}$$

for given initial conditions $z(0)$ and $p(0)$ and

$$\Gamma_\pm \equiv \frac{\zeta}{2m} \pm \frac{1}{2}\sqrt{\left(\frac{\zeta}{2}\right)^2 - \frac{4k}{m}}. \tag{9.27}$$

$p(t)$ is then given by $m\dot{z}$. Assuming the system is initially Boltzmann distributed with $\rho_{\text{Boltzmann}}(z,p) \propto \exp[-\beta(p^2/2m + kz^2/2)]$, equilibrium correlation functions can then be written as follows:

$$\langle z(0)^2\rangle = \frac{k_B T}{k} \tag{9.28a}$$

$$\langle p(0)^2\rangle = m k_B T \tag{9.28b}$$

$$\langle z(0)^4\rangle = 3\left(\frac{k_B T}{k}\right)^2 \tag{9.28c}$$

$$\langle z(0)^2 p(0)^2\rangle = \langle z(0)^2\rangle \langle p(0)^2\rangle = (k_B T)^2 \frac{m}{k} \tag{9.28d}$$

$$\langle p(0)^4\rangle = 3\left(m k_B T\right)^2, \tag{9.28e}$$

and we find the following averages

$$\begin{aligned}\langle \delta z_h(t)^2 \delta z(0)^2\rangle &= \langle (z_h(t)^2 - \langle z(0)^2\rangle)(z(0)^2 - \langle z(0)^2\rangle)\rangle \\ &= 2\left(\frac{k_B T}{k(\Lambda_+ - \Lambda_-)}\right)^2 (\Lambda_- e^{-\Lambda_+ t} - \Lambda_+ e^{-\Lambda_- t})^2\end{aligned} \tag{9.29a}$$

$$\begin{aligned}\langle \delta p_h(t)^2 \delta z(0)^2\rangle &= \langle (p_h(t)^2 - \langle p(0)^2\rangle)(z(0)^2 - \langle z(0)^2\rangle)\rangle \\ &= 2\left(\frac{m k_B T \Lambda_+ \Lambda_-}{k(\Lambda_+ - \Lambda_-)}\right)^2 (e^{-\Lambda_+ t} - e^{-\Lambda_- t})^2\end{aligned} \tag{9.29b}$$

$$\begin{aligned}\langle \delta z_h(t)^2 \delta p(0)^2 \rangle &= \langle (z_h(t)^2 - \langle z(0)^2 \rangle)(p(0)^2 - \langle p(0)^2 \rangle) \rangle \\ &= 2\left(\frac{mk_BT}{\Lambda_+ - \Lambda_-}\right)^2 (e^{-\Lambda_+ t} - e^{-\Lambda_- t})^2 \end{aligned} \tag{9.29c}$$

$$\begin{aligned}\langle \delta p_h(t)^2 \delta p(0)^2 \rangle &= \langle (p_h(t)^2 - \langle p(0)^2 \rangle)(p(0)^2 - \langle p(0)^2 \rangle) \rangle \\ &= 2\left(\frac{mk_BT}{\Lambda_+ - \Lambda_-}\right)^2 (\Lambda_- e^{-\Lambda_- t} - \Lambda_+ e^{-\Lambda_+ t})^2 \end{aligned} \tag{9.29d}$$

which, upon integration yield

$$\int_0^\infty dt\, \langle \delta z_h(t)^2 \delta z(0)^2 \rangle = \frac{m(k_BT)^2}{k^2\zeta}\left(1 + \frac{\zeta^2}{km}\right) \tag{9.30a}$$

$$\int_0^\infty dt\, \langle \delta p_h(t)^2 \delta z(0)^2 \rangle = \int_0^\infty dt\, \langle \delta z_h(t)^2 \delta p(0)^2 \rangle = \frac{(mk_BT)^2}{k\zeta} \tag{9.30b}$$

$$\int_0^\infty dt\, \langle \delta p_h(t)^2 \delta p(0)^2 \rangle = \frac{m^3(k_BT)^2}{\zeta}, \tag{9.30c}$$

$$\tag{9.30d}$$

which we can now use to calculate the thermodynamic metric. Before doing so, we must also consider the unique case of critical damping for which $\zeta^2 = 4mk \implies \Lambda_+ = \Lambda_-$ and the dynamics yield an entirely different homogeneous solution:

$$z_{h,\text{crit}}(t) = e^{-\sqrt{\frac{k}{m}}t}\left[y(0) + \left(z(0)\sqrt{\frac{k}{m}} + \frac{z(0)}{m}\right)t\right]. \tag{9.31}$$

Carrying out the same procedure yields

$$\langle \delta z_{h,\text{crit}}(t)^2 \delta z(0)^2 \rangle = \frac{2}{m}\left(\frac{k_BT}{k}\right)^2 (m + 2\sqrt{km}t + kt^2)e^{-2\sqrt{\frac{k}{m}}t} \tag{9.32a}$$

$$\langle \delta p_{h,\text{crit}}(t)^2 \delta z(0)^2 \rangle = \langle \delta z_{h,\text{crit}}(t)^2 \delta p(0)^2 \rangle = 2(k_BT)^2 t^2 e^{-2\sqrt{\frac{k}{m}}t} \tag{9.32b}$$

$$\langle \delta p_{h,\text{crit}}(t)^2 \delta p(0)^2 \rangle = 2m(k_BT)^2(m - 2\sqrt{km}t + kt^2)e^{-2\sqrt{\frac{k}{m}}t}, \tag{9.32c}$$

and

$$\int_0^\infty dt\, \langle \delta z_h(t)^2 \delta z(0)^2 \rangle = \frac{5(k_BT)^2\sqrt{km}}{2k^3} = \frac{m(k_BT)^2}{k^2\zeta}\left(1 + \frac{\zeta^2}{km}\right) \tag{9.33a}$$

$$\int_0^\infty dt\, \langle \delta p_h(t)^2 \delta z(0)^2 \rangle = \int_0^\infty dt\, \langle \delta z_h(t)^2 \delta p(0)^2 \rangle = \frac{m(k_BT)^2\sqrt{km}}{2k^2} = \frac{(mk_BT)^2}{k\zeta} \tag{9.33b}$$

$$\int_0^\infty dt\, \langle \delta p_h(t)^2 \delta p(0)^2 \rangle = \frac{(k_BT)^2 m^2\sqrt{km}}{2k} = \frac{m^3(k_BT)^2}{\zeta}, \tag{9.33c}$$

$$\tag{9.33d}$$

such that, ultimately, regardless of the value of k, we arrive at the same time correlation functions. We must calculate correlations between various pairs of the conjugate forces

$$\delta\mathbf{X} = \begin{pmatrix} \frac{1}{2T}(\delta p^2/m + k\delta z^2) & -\frac{1}{2}\delta z^2 \end{pmatrix}.$$

Combining Eqs (9.23),(9.30), and (9.33), we finally have

$$g_{ij} = \begin{pmatrix} g_{TT} & g_{T\lambda} \\ g_{\lambda T} & g_{\lambda\lambda} \end{pmatrix}_{ij} = \frac{mk_B}{4\zeta} \begin{pmatrix} \frac{1}{T}\left(4 + \frac{\zeta^2}{km}\right) & -\frac{1}{k}\left(2 + \frac{\zeta^2}{km}\right) \\ -\frac{1}{k}\left(2 + \frac{\zeta^2}{km}\right) & \frac{T}{k^2}\left(1 + \frac{\zeta^2}{km}\right) \end{pmatrix}_{ij}, \tag{9.34}$$

reproducing Eq. (9.11).

9.B Fokker-Planck dynamics of the harmonic oscillator and simulations

Here we present a derivation of the system of equations used to simulate the harmonic oscillator and we provide some details of those simulations. Following standard methods [55], we may translate the Langevin equation given in Eq. (9.25) into a Fokker-Planck equation over the particle's distribution in phase space:

$$\frac{\partial\rho}{\partial t} + \frac{p}{m}\frac{\partial\rho}{\partial z} - kz\frac{\partial\rho}{\partial p} - \frac{\zeta}{m}\frac{\partial(p\rho)}{\partial p} - \frac{\zeta}{\beta}\frac{\partial^2\rho}{\partial p^2} = 0. \tag{9.35}$$

Integrating across various dynamical variables leads to evoluation equations for the covariances. Explicitly, let us first integrate against z^2. All terms that do not involve derivatives with respect to z trivially die as ρ is normalized and therefore must be zero at the (infinite) boundaries. This then leaves

$$\left(\frac{\partial\rho}{\partial t} + \frac{p}{m}\frac{\partial\rho}{\partial z}\right) z^2 \implies \frac{d}{dt}\langle z^2\rangle = -\frac{1}{m}\int dzdp\; pz^2\frac{\partial\rho}{\partial z} = \frac{2}{m}\int dzdppz\rho = \frac{2}{m}\langle pz\rangle,$$

where we have integrated by parts in the intermediate steps. Similar arguments lead to the rest of the coupled system in Eqs. (9.19)-(9.21).

We reiterate here that, for the dynamics considered, if the system is initially Gaussian distributed, it will remain so for all times, such that knowledge of these covariances specifies the entire phase space distribution:

$$\rho_{\text{Gaussian}} = \frac{1}{2\pi\sqrt{\langle p^2\rangle\langle z^2\rangle - \langle pz\rangle^2}}\exp\left[-\frac{\langle p^2\rangle z^2 + \langle z^2\rangle p^2 - 2\langle pz\rangle pz}{2(\langle p^2\rangle\langle z^2\rangle - \langle pz\rangle^2)}\right],$$

from which one may derive the free energy, entropy, and all other thermodynamic quantities of interest. As a result, with these three covariances alone, we can faithfully study the system well outside of the linear response regime.

Simulations are then done by numerically integrating Eqs. (9.19)-(9.21) for a given set of parameter values. In particular, we first fix m and ζ and then repeatedly integrate Eqs. (9.19)-(9.21), where $k(t)$ and $T(t)$ are cyclically varied with a set time period τ according to the protocol in question (e.g., according to the optimal Carnot engine or the geodesic engine) until the engine arrives at a steady state. For protocols with very small values of τ, reaching the steady state may take a significant number of cycles, whereas for large values where the cycle is near-equilibrium, steady state cyclic operation can be accomplished after only a handful of cycles. All thermodynamic quantities are then calculated under steady state operation, again by means of numerical integration. All integrations are carried by the NIntegrate function of Wolfram Mathematica 12. See Table 9.1 for details of the parameter values used to generate Fig. 9.2.

Parameter	Fig. 2(a)-(d)	Fig. 2(e)-(h)
m	0.545 pg	80.9 mg
ζ	7.51 μg s^{-1}	15.0 mg s^{-1}
T_0	300 K	300 K
T_1	300 K	300 K
T_2	526.235 K	526.235 K
T_3	526.235 K	526.235 K
k_0	2.00 mg s^{-2}	6.40 mg s^{-2}
k_1	6.50 mg s^{-2}	20.8 mg s^{-2}
k_2	20.0 mg s^{-2}	64.0 mg s^{-2}
k_3	6.15 mg s^{-2}	19.6 mg s^{-2}

Table 9.1: **Parameter values used to generate Fig. 9.2**.

For Fig. 9.2(a)-(d), we use parameter values consistent with a spherical polystyrene bead of 1 micron diameter. The value of ζ is chosen to be consistent with the bead suspended in water at 300K and undergoing Stokes flow. We note that viscosity itself is a temperature dependent quantity, though we leave the consideration of these small corrections to future work. For Fig. 9.2(e)-(h) in contrast, we consider a denser and larger bead, such that the thermodynamic costs of the resulting protocols are more easily distinguished.

9.C Numerical validation of slow-driving approximation

In this section, we expand on the definition of the slow-driving approximation and compare the results of this approximation to the numerical results from simulation. In essence,

the crux of this regime is that all driving timescales, given by $\boldsymbol{\tau}_{D,i} \sim |\Lambda_i/\dot{\Lambda}_i|$, occur slower than all relaxation timescales for the system in question. Under this assumption and following standard linear response theory [106] or alternatively a derivative truncation approximation [107] leads to the definition of the thermodynamic metric tensor given by Eq. (9.5).

For the model system in question, there are two relaxation timescales relevant to driving: the inertial, underdamped timescale $\tau_u = m/\zeta$ and the overdamped timescale $\tau_o = \zeta/k$. For driving that occurs significantly slower than this timescale, the assumptions underpinning thermodynamic geometry become more accurate and so too should its predictions. However, τ_o itself depends on the current value of the control parameter k, as does the characteristic maximum driving timescale τ_D, set by the maximum value of $\{|\Lambda_i/\dot{\Lambda}_i|\}$. Therefore, for protocols that occur over a variety of values of k and T, thermodynamic geometric increasingly becomes accurate for $\tau_u/\tau_D, \tau_o/\tau_D \ll 1$ at all times over the full protocol. This is especially true of steady-state engines for which accumulated distances from equilibrium compile over time. To this end, we define the dimensionless quantities

$$A = \frac{1}{\tau}\oint_0^\tau \frac{\tau_u}{\tau_D(t)}dt, \quad B = \frac{1}{\tau}\oint_0^\tau \frac{\tau_o(t)}{\tau_D(t)}dt \tag{9.36}$$

where τ again represents the protocol duration of a full cycle, and A and B serve as time averages of the ratios of the time scales. As before, thermodynamic geometry will prove more accurate for $A, B \ll 1$. Finally, defining the fractional time $s \equiv t/\tau$ and the non-dimensionalized driving timescale $\tilde{\tau}_D(s) \equiv \tau_D(s\tau)/\tau$, we have

$$A = \frac{1}{\tau}\oint_0^\tau \frac{\tau_u}{\tau_D(t)}dt = \frac{\oint_0^1 \frac{\tau_u}{\tilde{\tau}_D(s)}}{\tau} \equiv \frac{\tau_A}{\tau}, \quad B = \frac{1}{\tau}\oint_0^\tau \frac{\tau_o(t)}{\tau_D(t)}dt = \frac{\oint_0^1 \frac{\tau_o(s\tau)}{\tilde{\tau}_D(s)}}{\tau} \equiv \frac{\tau_B}{\tau},$$

where we define

$$\tau_A \equiv \oint_0^1 \frac{\tau_u}{\tilde{\tau}_D(s)}, \quad \tau_B \equiv \oint_0^1 \frac{\tau_o(s\tau)}{\tilde{\tau}_D(s)} \tag{9.37}$$

both of which are timescales independent of τ such that for $\tau_A, \tau_B \ll \tau$, thermodynamic geometry is a good approximation. We can now calculate τ_A and τ_B for all protocols considered, which we show in Table 9.2:

With these results in hand, we now plot the numerical simulation results of dissipated energy and power as a function of protocol duration on the same axes as the linear response result (in red upside down triangles). Each subplot contains the simulation results for a single quantity for a single protocol (e.g. the Hybrid protocol is in green diamonds on the third row) and is plotted against the linear response prediction for the corresponding protocol: importantly, although all linear response predictions are shown with identical red triangles, the linear response prediction in each subplot is the one specifically matched to the numerical protocol shown in the same subplot (i.e. they are *not* all the same). The two left columns correspond to similar material parameters as [249] and Fig. 9.2(a)-(d) and the two right columns correspond to the same as Fig. 9.2(e)-(h). The vertical dotted lines are the maximum of τ_A, τ_B for each plot. For $\tau \gg \tau_A, \tau_B$ indeed we see excellent agreement with the

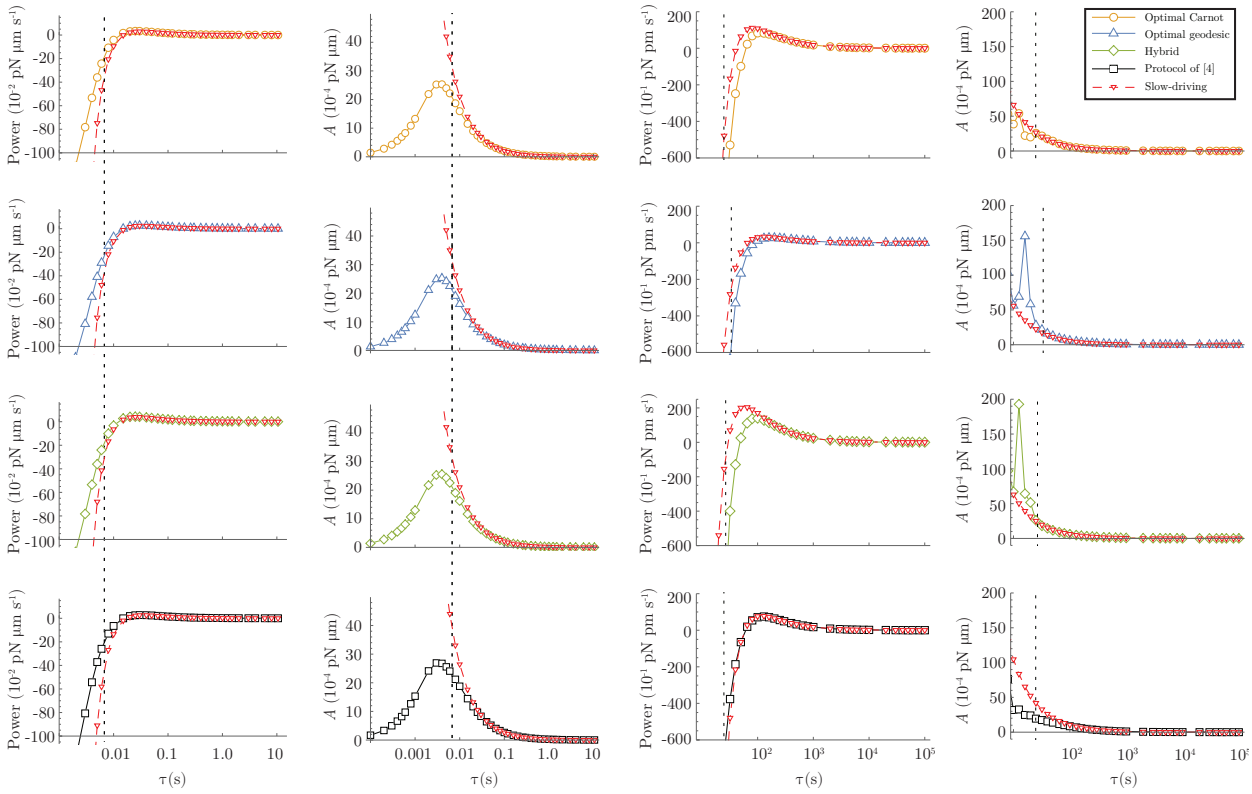


Figure 9.4: **Comparison of full numerical results to linear response**. Power and dissipated availibility A as a function of protocol duration for optimal Carnot (orange circles), geodesic (blue triangles), hybrid (green diamonds), and simulations of the experimental protocol used in [249] (black squares), compared against the calculated linear response result for each (red down triangles). The linear response result is calculated for each protocol specifically. Dashed lines represent the larger of $\tau_{A/B}$ and therefore the timescale at which linear response is expected to start to be predictive. The left two columns are for overdamped parameters, same as Fig. 9.2(a)-(d), and the right two columns are for underdamped parameters, same as Fig. 9.2(e)-(h), see Table 9.1 for specific material values. All subplots in the same column share horizontal axes.

Protocol	Parameters of Fig. 2(a)-(d)		Parameters of Fig. 2(e)-(h)	
	τ_A (s)	τ_B (s)	τ_A (s)	τ_B (s)
Optimal Carnot	3.33755×10^{-7}	0.00676226	24.8006	4.22641
Optimal geodesic	3.33755×10^{-7}	0.00676226	33.6818	6.52093
Hybrid	3.33755×10^{-7}	0.00676226	26.6871	5.12534
Protocol of [249]	3.33755×10^{-7}	0.00676226	24.8006	4.22641

Table 9.2: Timescales τ_A and τ_B at which slow-driving and thermodynamic geometry becomes a valid approximation. The larger of $\tau_{A/B}$ is shown in dotted lines in Fig. 9.4

linear response predictions and often even relatively good agreement for $\tau \gtrsim \tau_A, \tau_B$, showing the significant predictive power for this theory over a wide range of protocol durations and further justifying its popularity as one perturbative approach to finite-time thermodynamics.

9.D Comparison of simulated results to experiment

We previously showed the results of simulations for cycles operating in steady state for the colloidal parametric harmonic oscillator system studied previously in experiment [249, 252], and used simulations of the Carnot cycle protocol studied in [249] as a benchmark. To validate these simulations, here we compare directly with the experiment itself. In Fig. 9.5(a)-(b), we display the stochastic efficiency and power as a function of protocol duration for experimental data provided by the authors of [249] plotted against the numerical simulation meant to replicate this experiment. We find good agreement throughout the experimental regime tested but now with further quantitative predictions beyond this regime. In addition, in Fig. 9.5(c)-(d), we plot the same thermodynamic quantities but now for the experimental results plotted against all the all numerically simulated cycles again using similar material parameters to those used experimentally. We now see that the optimized Carnot and hybrid engines outperform not only the averages of the experimental results but also the uncertainties for a large range of protocol durations, further bolstering our results.

It bears mentioning that the stochastic efficiency is a further different definition of efficiency, introduced in [249]. To reiterate, the efficiency we consider, which we will term "irreversible efficiency" to avoid confusion, is defined as $\eta \equiv W/U \leq 1$ where W is output work and U is input thermal energy, which has an upper bound of unity saturated for *any* reversible cycle. The standard "textbook" definition of efficiency, which we term "thermodynamic efficiency" η_{th} is given by the ratio of W/Q_+ where Q_+ is the rectified heat flow into the system over the full cycle (i.e. only heat flow in is counted). For the quasistatic Carnot cycle, the thermodynamic efficiency is by definition W/Q_H where Q_H is the heat flow into the system from the hot reservoir as all other strokes are either adiabatic, $Q = 0$, or have a

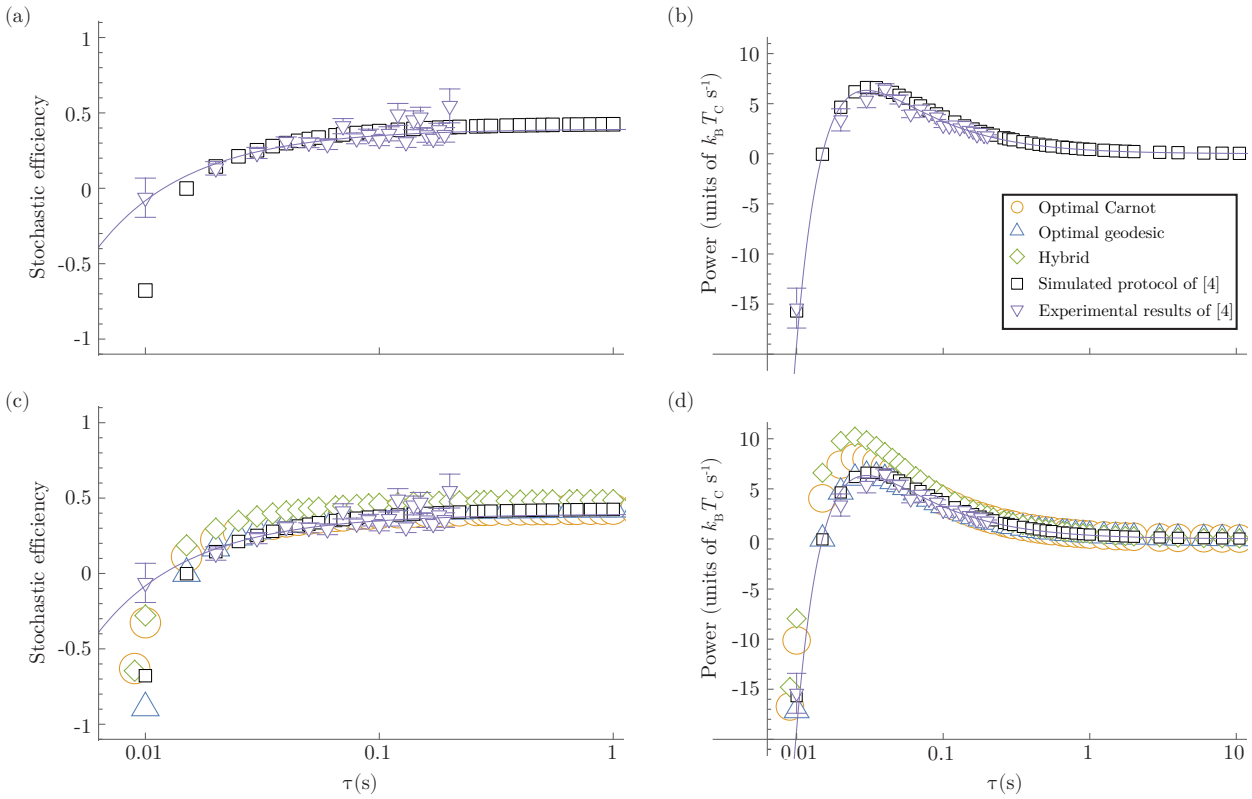


Figure 9.5: **Comparison of simulated results to experiment**. **(a)** Stochastic efficiency and **(b)** power as a function of protocol duration for simulations of the experiment in [249] (black squares) compared against experimental data provided from the authors of [249] (purple down triangles). Error bars are the standard error of this data and the purple line is a best-fit (cf. Fig. 2b of [249]). **(c)** and **(d)** same as **(a)** and **(b)**, respectively, but now with optimal Carnot (orange circles), geodesic (blue triangles), hybrid (green diamonds) for same material parameters also shown. Horizontal axes of (a) and (b) are the same as (c) and **(d)**, respectively.

heat flow purely out of the system. However, for finite-time Carnot engines, this is not necessarily true, such that [249] defines the "stochastic efficiency" as $\eta_s = W/(Q_1^{\text{adia}} + Q_H + Q_2^{\text{adia}})$, where $Q_{1/2}^{\text{adia}}$ are total (non-rectified) heat flow during the adiabatic strokes. They show that this definition of efficiency converges faster to the quasistatic value of η_{th} as a function of protocol duration and so study it in their experiment. This quantity is what is plotted in Fig. 9.5(a),(c).

Chapter 10

A geometric bound on the efficiency of irreversible thermodynamic cycles

In this chapter, we use the lens of thermodynamic geometry and the insights gained from Chapter 7 to explore the full space of thermodynamic cycles with continuously-varying bath temperature in search of optimally shaped cycles acting in the slow-driving regime. We apply classical isoperimetric inequalities to derive a universal geometric bound on the efficiency of any irreversible thermodynamic cycle and explicitly construct efficient heat engines operating in finite time that nearly saturate this bound for a specific model system. This chapter is adapted from [111] with the permission of all authors.

10.1 Introduction

Over the past several decades, stochastic thermodynamics has dramatically improved our understanding of nonequilibrium statistical physics [46, 53, 50, 54, 250, 251, 45]. A major focus of study in this area has been the performance of engines operating in finite time, where both power and dissipation are finite, often with an emphasis on engines operating at maximal power [260, 261, 157, 262, 52, 265, 219, 266, 267, 268, 223, 269, 270, 276, 110, 277, 246]. A recurring theme has been the interplay, and often incompatibility, among high efficiency, high output power, and low dissipation [265, 266, 223, 110]. To that end, we recently characterized optimal protocols for the finite-time operation of a Brownian Carnot engine [110], a colloidal system introduced in [249], finding minimally dissipative cycles often came at the expense of reduced power and efficiency.

In this work, we study the implications of this interplay from a geometric perspective and arrive at a universal bound on the efficiency of heat engines operating in finite time. We also numerically construct optimal cycles that nearly saturate the bound, and we characterize its tightness for a specific model system and compare them to a variety of non-optimal cycles. We find that even natural extensions of well-known quasi-static cycles (e.g. Carnot engines) to finite-time cycles perform far less efficiently than the optimal cycles, demonstrating the

utility of our result.

10.2 Efficiency of irreversible engines

Following [76], we use a definition of efficiency that directly captures the irreversibility of a thermodynamic cycle. Specifically, for a generic thermodynamic engine operated by cyclically varying the temperature T of a heat bath in contact with the system and some volume-like mechanical control variable λ, the (average) efficiency is defined as

$$\eta \equiv \frac{W}{U} = \frac{\oint X_\lambda d\lambda}{-\oint X_T dT}, \tag{10.1}$$

where X_ν is the thermodynamic force conjugate to the control variable $\nu \in \{T, \lambda\}$, defined as

$$X_\lambda \equiv -\left\langle \frac{\partial H_{\mathbf{\Lambda}}}{\partial \lambda} \right\rangle, \tag{10.2}$$

$$X_T = S \equiv -\left\langle \log \rho_t \right\rangle, \tag{10.3}$$

where $H_{\mathbf{\Lambda}}$ is the Hamiltonian of the (working) system for a fixed set $\mathbf{\Lambda} = (T, \lambda)$, S is the system entropy, ρ_t is the phase space distribution of the system at time t, and brackets denote ensemble averages. Note that U here does not represent the internal energy, but can be thought of as the uptake of thermal energy from the heat source, or the amount of energy that is available for work production under a given temperature profile [76]. This efficiency is well-defined for any engine with positive work output, $W > 0$. Following the first law of thermodynamics and appealing to the cyclic operation of the engine, the efficiency may be rewritten as

$$\eta = \frac{\oint X_\lambda d\lambda}{-\oint S dT} = \frac{\oint X_\lambda d\lambda}{\oint X_\lambda d\lambda + \oint T d\Sigma} \leq 1, \tag{10.4}$$

where $d\Sigma \equiv dS - dQ/T$ is the total infinitesimal entropy production in the universe. Here, Q is the heat exchange into the system from the reservoir at a temperature T. Following the second law, $d\Sigma \geq 0$ such that the inequality follows directly and the unity bound can only be saturated for quasistatic, reversible engines. This definition of efficiency has gained traction in the study of finite-time heat engines [276, 278, 110], and a comparable definition is standard for monothermal cycles, e.g. in active matter or chemical transduction contexts [279, 192, 191, 280].

Now, let us consider a finite-time operation such that $\Sigma > 0$ and the system is driven with finite driving rates $\dot{\mathbf{\Lambda}}$. The thermodynamic forces may be expanded as

$$X_\mu = \mathcal{X}_\mu - g_{\mu\nu}\dot{\Lambda}_\nu, \tag{10.5}$$

where summation over repeated indices is implied. Here, $\mathcal{X}_\mu$ is the quasistatic value of X for a given set $\mathbf{\Lambda}$ and, following the standard linear response framework, $g_{\mu\nu}$ is given by a

correlation function

$$g_{\mu\nu} = \beta \int_0^\infty dt \, \langle \delta X_\mu(t) \delta X_\nu(0) \rangle_{\mathbf{\Lambda}} \, . \tag{10.6}$$

Using this expansion, the efficiency can be written

$$\eta = \frac{\oint X_\lambda d\lambda}{-\oint X_T dT} \approx \frac{\oint (\mathcal{X}_\lambda - g_{\lambda\nu}\dot{\Lambda}_\nu) d\lambda}{-\oint (\mathcal{X}_T - g_{T\nu}\dot{\Lambda}_\nu) dT} \approx 1 - \frac{\oint dt \dot{\Lambda}_\mu g_{\mu\nu} \dot{\Lambda}_\nu}{\oint \mathcal{X}_\lambda d\lambda} = 1 - \frac{A}{\mathcal{W}}, \tag{10.7}$$

where A is the dissipated work (or alternatively called the dissipated availibility) through one cycle and $\mathcal{W}$ is the work output for quasistatic driving. Following [227, 232, 241, 255, 239, 234, 240, 106], we see that the thermodynamic control space is imbued with a geometric structure by reinterpreting $g_{\mu\nu}$ as a metric tensor. Geometric approaches such as this have greatly facilitated the development of optimal protocols for nonequilibrium systems [240, 106, 107, 158, 169, 87, 108, 222, 245, 273]. With these definitions, the dissipated work satisfies

$$\tau A \equiv \tau \oint dt \dot{\Lambda}_\mu g_{\mu\nu} \dot{\Lambda}_\nu \geq \left(\oint dt \sqrt{\dot{\Lambda}_\mu g_{\mu\nu} \dot{\Lambda}_\nu} \right)^2 \equiv \mathcal{L}^2, \tag{10.8}$$

where τ is the cycle duration and $\mathcal{L}$ is the *thermodynamic length* of the protocol as defined by the metric. Optimal driving then yields [76]

$$\eta \leq \eta^* = 1 - \frac{\mathcal{L}^2}{\mathcal{W}\tau}, \tag{10.9}$$

which gives the optimal geometric efficiency η^* for any closed curve in thermodynamic control space.

The bound, Eq. (10.9), applies to any generic closed curve, yielding the best possible efficiency for an optimal temporal parametrization for a given path. We now seek to go further and find cycles that are maximally efficient over the space of all possible closed paths in thermodynamic control space. Fixing the protocol duration and given Eq. (10.9), to leading order in $1/\tau$, we must therefore find the curve that minimizes the quantity $\mathcal{L}^2/\mathcal{W}$.

10.3 Isoperimetric bound on efficiency

We now note an important feature of $\mathcal{W}$. It is well known from standard thermodynamics that the quasistatic work is simply given by the area contained within the curve of the (quasistatic) cycle in $\lambda - \mathcal{X}_\lambda$ space, which we will henceforth refer to as Clausius space in reference to the Clausius curve. We will refer to the inner region of this curve as $\mathcal{C}$ and the boundary (the Clausius curve) as $\partial\mathcal{C}$. By means of an appropriate change of coordinates, the metric $g_{\mu\nu}$ may be transformed for this space, yielding a metric $g^{\mathcal{C}}_{\mu\nu}$ such that the thermodynamic

length is given

$$\begin{aligned}\mathcal{L} &= \oint_{\partial\mathcal{C}} \sqrt{\begin{pmatrix} dT \\ d\lambda \end{pmatrix}_\mu g_{\mu\nu} \begin{pmatrix} dT \\ d\lambda \end{pmatrix}_\nu} \\ &= \oint_{\partial\mathcal{C}} \sqrt{\begin{pmatrix} d\mathcal{X}_\lambda \\ d\lambda \end{pmatrix}_\mu g^{\mathcal{C}}_{\mu\nu} \begin{pmatrix} d\mathcal{X}_\lambda \\ d\lambda \end{pmatrix}_\nu},\end{aligned} \tag{10.10}$$

and the quasistatic work is

$$\mathcal{W} = \iint_{\mathcal{C}} d\lambda d\mathcal{X}_\lambda = \oint_{\partial\mathcal{C}} \mathcal{X}_\lambda d\lambda. \tag{10.11}$$

We define one final quantity of interest: the thermodynamic area, defined as the integral over of the region with the proper thermodynamic geometric measure:

$$\mathcal{A} = \iint_{\mathcal{C}} \sqrt{g^{\mathcal{C}}} d\lambda d\mathcal{X}_\lambda, \tag{10.12}$$

where $g^{\mathcal{C}} \equiv \det g^{\mathcal{C}}_{\mu\nu}$. The physical interpretation of this quantity may not be as clear as that of thermodynamic length, though we will use it as a key ingredient. Notably, dating to antiquity [281, 282], bounds exist relating the perimeter $\mathscr{L}(D)$ and area $\mathscr{A}(D)$ of a region D, known as *isoperimetric inequalities*. In general, for a simply-connected two-dimensional region, one has two inequalities [282]

$$\mathscr{L}^2 \geq 4\pi\mathscr{A} - 2\left[\iint_D K^+\right]\mathscr{A}, \tag{10.13}$$

$$\mathscr{L}^2 \geq 4\pi\mathscr{A} - \left[\sup_D K\right]\mathscr{A}^2. \tag{10.14}$$

where K is the Gaussian curvature of the underlying space and $K^+(p) \equiv \max(K(p), 0)$ for a point $p \in D$. As a simple example, we remind the reader of the case of Euclidean space where $K = K^+ = 0$ and both inequalities yield $\mathscr{L}^2 \geq 4\pi\mathscr{A}$, which is saturated only for the optimal shape of a circle. Similar isoperimetrically optimal shapes exist for other manifolds [282]. Importantly, whenever the curvature is everywhere nonpositive, Eq. (10.13) yields the familiar Euclidean bound, though it is only tight for special spaces, such as when $K = 0$.

In the context of thermodynamic geometry, the bound readily applies, where now we consider the thermodynamic length of a closed curve and the thermodynamic area of the enclosed region. That is

$$\mathcal{L}^2 \geq 4\pi\mathcal{A} - 2\left[\iint_{\mathcal{C}} K^+\right]\mathcal{A}, \tag{10.15}$$

$$\mathcal{L}^2 \geq 4\pi\mathcal{A} - \left[\sup_{\mathcal{C}} K\right]\mathcal{A}^2. \tag{10.16}$$

Henceforth, we will focus on the case when $K \leq 0$ and will relegate the more general case to Appendix 10.A. In this case, we may assume $\mathcal{L}^2 \geq 4\pi\mathcal{A}$. Therefore,

$$\frac{\mathcal{L}^2}{\mathcal{W}} = \frac{\mathcal{L}^2}{\mathcal{W}}\frac{\mathcal{A}}{\mathcal{A}} = \frac{\mathcal{L}^2}{\mathcal{A}}\frac{\mathcal{A}}{\mathcal{W}} \geq 4\pi\frac{\mathcal{A}}{\mathcal{W}} = 4\pi\overline{\sqrt{g^{\mathcal{C}}}}, \tag{10.17}$$

where the overline indicates an area average value. Given this bound, we may now write for the efficiency a universal bound

$$\eta \leq 1 - \frac{\mathcal{L}^2}{\mathcal{W}\tau} \leq 1 - \frac{4\pi\overline{\sqrt{g^{\mathcal{C}}}}}{\tau}. \tag{10.18}$$

This bound, which we will refer to as an isoperimentric bound on efficiency, is our first major result and presents a fundamentally new and purely geometric bound on the efficiency of nonequilibrium engines. Also, whereas the previous bound, Eq. 10.9 was directly applicable to the optimized parametrization of a specific predetermined cycle, this bound places constraints on the optimal *shape* of a cycle and can only be approached for geometrically optimized cycle shapes. This therefore introduces a new optimization principle wherein optimally efficient cycles must minimize the average value of $\sqrt{g^{\mathcal{C}}}$ over the region they enclose in Clausius space. In a pioneering study, a similar bound was recently recovered for the specific case of the Brownian gyrator [278], though we highlight that Eq. (10.18) applies generically.

10.4 Construction of optimal cycles.

Given this isoperimetric bound, we now seek to construct optimal cycles that (nearly) saturate it. This is done by finding shapes that minimize the ratio $\mathcal{L}^2/\mathcal{A}$. Inspired by previous literature [282], we will use a variational principle. Namely, we seek to maximize $\mathcal{A}$ while holding $\mathcal{L}^2$ fixed; we do so by means of a Lagrange multiplier. The relevant functional takes the form

$$\mathcal{F} = \oint dt \left(\sqrt{g^{\mathcal{C}}} X_\lambda \dot{\lambda} - \xi \begin{pmatrix} \dot{X}_\lambda \\ \dot{\lambda} \end{pmatrix}_\mu g^{\mathcal{C}}_{\mu\nu} \begin{pmatrix} \dot{X}_\lambda \\ \dot{\lambda} \end{pmatrix}_\nu \right), \tag{10.19}$$

where ξ serves as a Lagrange multiplier enforcing a fixed dissipation for shapes that maximize the corresponding area [1]. Optimization is found through solving the resulting Euler-Lagrange equations for $X_\lambda(t)$ and $\lambda(t)$ under a cyclic constraint.

10.5 Parametric harmonic oscillator

We will now illustrate the utility of this result by studying the parametric harmonic oscillator. This important model system consists of a particle of mass m trapped in a

[1] The dissipation $\oint (dX_\lambda, d\lambda) \cdot \mathbf{g} \cdot (dX_\lambda, d\lambda)$ is geometrically denoted the energy of the curve and optimization with respect to its value held fixed still optimizes the ratio $\mathcal{L}^2/\mathcal{A}$ while simultaneously outputting an optimal, arclength parametrization of the resultant curve.

harmonic potential with variable stiffness $V(x) = 1/2k(t)x^2$ in contact with a heat bath of variable temperature $T(t)$ and subject to viscous damping ζ. This system has been studied extensively [156, 160, 107, 271, 249, 159, 283, 110], and its geometry has been well characterized — the metric is

$$g_{\mu\nu} = \frac{mk_B}{4\zeta} \begin{pmatrix} \frac{1}{T}\left(4 + \frac{(\zeta)^2}{km}\right) & -\frac{1}{k}\left(2 + \frac{(\zeta)^2}{km}\right) \\ -\frac{1}{k}\left(2 + \frac{(\zeta)^2}{km}\right) & \frac{T}{k^2}\left(1 + \frac{(\zeta)^2}{km}\right) \end{pmatrix}_{\mu\nu}.$$

In this case, the mechanical control variable is k and the corresponding force is $X_k = -1/2\,\langle x^2 \rangle$. In the quasistatic limit, we have $\mathcal{X}_k = -k_B T/2k$ by the equipartition theorem. Therefore, under the change of variables $(T, k) \to (\tilde{P}, \tilde{V}) \equiv (\mathcal{X}_k, k)$, we find

$$g^{\mathcal{C}}_{\mu\nu} = -\begin{pmatrix} \frac{\zeta}{2\tilde{P}} + \frac{2m\tilde{V}}{\zeta\tilde{P}} & \frac{m}{\zeta} \\ \frac{m}{\zeta} & \frac{m\tilde{P}}{2\zeta\tilde{V}} \end{pmatrix},$$

where we use $\tilde{P}$ and $\tilde{V}$ to suggestively map to pseudo-pressure and pseudo-volume in Clausius space and recapture the usual identity $d\mathcal{W} = \tilde{P}d\tilde{V}$. We find $g^{\mathcal{C}} = m/(4\tilde{V})$ and the Gaussian curvature $K = 1/(\zeta\tilde{P}) \leq 0$ as $\tilde{P} \leq 0$ such that Eq. (10.18) applies. As a result, we have

$$\eta \leq 1 - \frac{2\pi\sqrt{\frac{m}{\tilde{V}}}}{\tau}$$

for any possible thermodynamic cycle.

We now seek to characterize the optimal cycles for this model system. Following Eq. (10.19), we consider the functional

$$\mathcal{F} = \oint dt \left[\sqrt{g^{\mathcal{C}}}\tilde{P}\dot{\tilde{V}} + \xi \begin{pmatrix} \dot{\tilde{P}} \\ \dot{\tilde{V}} \end{pmatrix} \begin{pmatrix} \frac{\zeta}{2\tilde{P}} + \frac{2m\tilde{V}}{\zeta\tilde{P}} & \frac{m}{\zeta} \\ \frac{m}{\zeta} & \frac{m\tilde{P}}{2\zeta\tilde{V}} \end{pmatrix} \begin{pmatrix} \dot{\tilde{P}} \\ \dot{\tilde{V}} \end{pmatrix} \right]. \tag{10.20}$$

The Euler-Lagrange equations are then found by varying with respect to $\tilde{P}$ and $\tilde{V}$ (see Appendix 10.B). To our knowledge, the resulting Euler-Lagrange equations are analytically intractable, so we turn to numerics. For simplicity, we generate cycles from a given set of initial conditions, $\tilde{P}(0), \tilde{V}(0), \dot{\tilde{P}}(0)$, and $\dot{\tilde{V}}(0)$, and a given value of the Lagrange multiplier ξ. If we concern ourselves only with the shape of the curve rather than its particular parameterization, we could instead parameterize $\tilde{P}$ as a function of $\tilde{V}$, such that one of these initial condition degrees of freedom is redundant. Thus, optimal shapes are specified by a four-parameter family determined by $\tilde{P}(t = 0), \tilde{V}(t = 0), d\tilde{P}/d\tilde{V}(t = 0)$ and ξ.

Generically, it is unclear whether these conditions will be sufficient to specify a smooth closed curve [281, 282, 284]. In general, the isoperimetrically optimal curves will consist of stable smooth curves that have constant geodesic curvature at (nearly) all points [281, 282, 284]. In our case, the numerical solutions yield curves of constant geodesic curvature

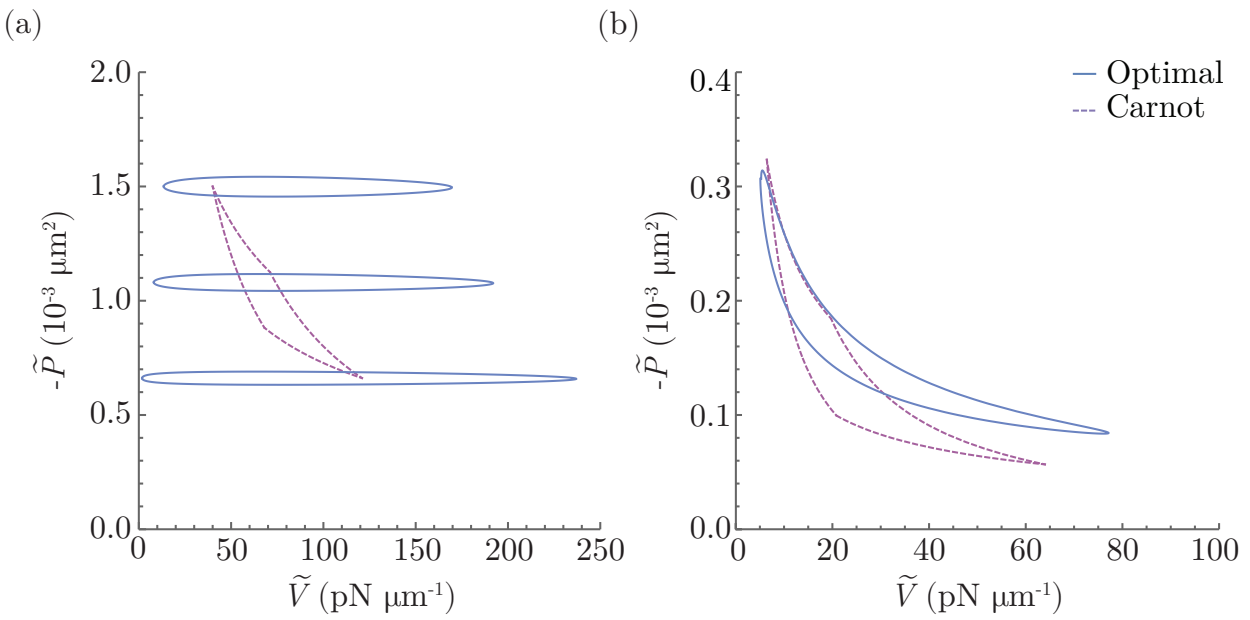


Figure 10.1: **Comparison of Brownian Carnot cycle and optimal isoperimetric cycle**. **(a)** A Brownian Carnot cycle (dashed purple) and three isoperimetrically optimal cycles (blue) with identical values of $\mathcal{W}$ and $\sqrt{g^{\mathcal{C}}}$ using mass and damping values from [249]. The optimal cycles have a $55\times$ increase in performance relative to the Carnot cycle. **(b)** Same as (a), but in a more underdamped regime.

that are typically non-closed but instead consist of "near-miss" cycloids (Appendix 10.B), which has been observed previously while seeking optimal cycles [283]. However, as we are interested only in cyclic engines, we will construct cycles that traverse a single optimal period by truncating the curve when it is at the nearest point on the curve whose tangent curve is parallel to the original tangent curve. We then connect these two points by a straight line, thus closing the cycle. For small cycles, the resulting kink is imperceptible whereas it becomes more noticeable for larger cycles, as can be seen in Figs. 10.1 and 10.2. Similarly, the efficiencies are impacted more significantly for larger deviations from smooth curves. Truly optimal curves would consist of fully smooth closed curves of constant geodesic curvature, which may only be realizable in specific regions of the Clausius space. By choosing to work with specific initial conditions, we allow for the construction of near optimal cycles at all points of Clausius space at the cost of having to introduce small, finite sections of non-optimality. As we will see, these "optimal" cycles still prove remarkably close to saturating the bound and strongly outperform all other cycles we consider.

For example, consider the Brownian Carnot cycle, whose shape is given in Fig. 10.1. Setting $\zeta = 7.51\ \mu\text{g s}^{-1}$ and $m = 0.545$ pg (based on experimental parameters used in [249]),

and choosing the extremal values of $\tilde{P}$ and $\tilde{V}$ shown, Eq. (10.17) implies that its greatest possible efficiency is

$$(1-\eta)\tau = \frac{\mathcal{L}^2}{\mathcal{W}} = 9.58 \times 10^{-4}\ \text{s} \gg 1.76 \times 10^{-5}\ \text{s} = \frac{4\pi\mathcal{A}}{\mathcal{W}},$$

demonstrating that the performance of the Carnot cycle is a factor of 55 times larger than the optimal value for these parameter settings. In contrast, by constructing a series of (nearly) optimally-shaped cycles with identical values of $\mathcal{W}$ and $\overline{\sqrt{g^{\mathcal{C}}}}$, we instead find the bound is approached to within three-hundredths of one percent. The shapes of these cycles are displayed in Fig. 10.1(a).

We next consider a slightly underdamped parameter regime, setting $m = 80.9$ mg and $\zeta = 15.0\ \text{mg}\,\text{s}^{-1}$. In this regime, various Carnot engine cycles (for given limits on hot and cold bath temperature) perform somewhat better, but they still do not come close to saturating it. Intriguingly, in contrast to the previous regime, optimally constructed shapes now appear much closer to Carnot-like cycles than those previously constructed, as in Fig 10.1(b). Now, we find that optimal engines seemingly remain close to adiabats for a significant duration of the cycle, albeit with a rapid (and smooth) turnaround at corners. This is replicated for other choices of maximal temperature and stiffness as shown in Fig. 10.1(b). We also show optimal cycles for a variety of values of m/ζ in Appendix 10.B.

We can further evaluate our bound by comparing it to generic cycles in Clausius space. In particular, in Fig. 10.3, we plot the value of $\overline{\sqrt{g^{\mathcal{C}}}}$ against $\mathcal{L}^2/\mathcal{W}$ for 15000 randomly constructed cycles, as well as 1000 randomly selected Carnot, Stirling, Otto, and hybrid Carnot/geodesic (introduced in [110]) cycles (see Appendix 10.C for a review of these various cycles and Appendix 10.D for details of how Fig. 3 is constructed). We also plot 500 optimally constructed cycles. As is easily observed, the optimal cycles nearly saturate the bound for a large parameter regime of $\overline{\sqrt{g^{\mathcal{C}}}}$ whereas other cycles are far less efficient. The data are surprisingly structured: for a fixed shape, we find $\mathcal{L}^2/\mathcal{W} \sim \left(\overline{\sqrt{g^{\mathcal{C}}}}\right)^2$, an interesting empirical finding. Cycles that saturate the bound must therefore *not* maintain the same cyclical shape for different average values of $\sqrt{g^{\mathcal{C}}}$, but instead change so as to remain optimal, as was shown in Fig. 10.2.

10.6 Discussion

In this work, we have applied the classical isoperimetric inequalities to thermodynamic spaces, yielding a novel universal bound on the efficiency of any closed thermodynamic cycle for a generic system. We have then constructed optimal cycles that nearly saturate this bound for the specific model system of the parametric harmonic oscillator. Importantly, this bound, although not always tight, nevertheless strongly constrains the efficiency of thermodynamic cycles and introduces new design principles for the design of efficient finite-time heat engines. We emphasize that all results are independent of temporal parametrization and depend only on the shape of cycles.

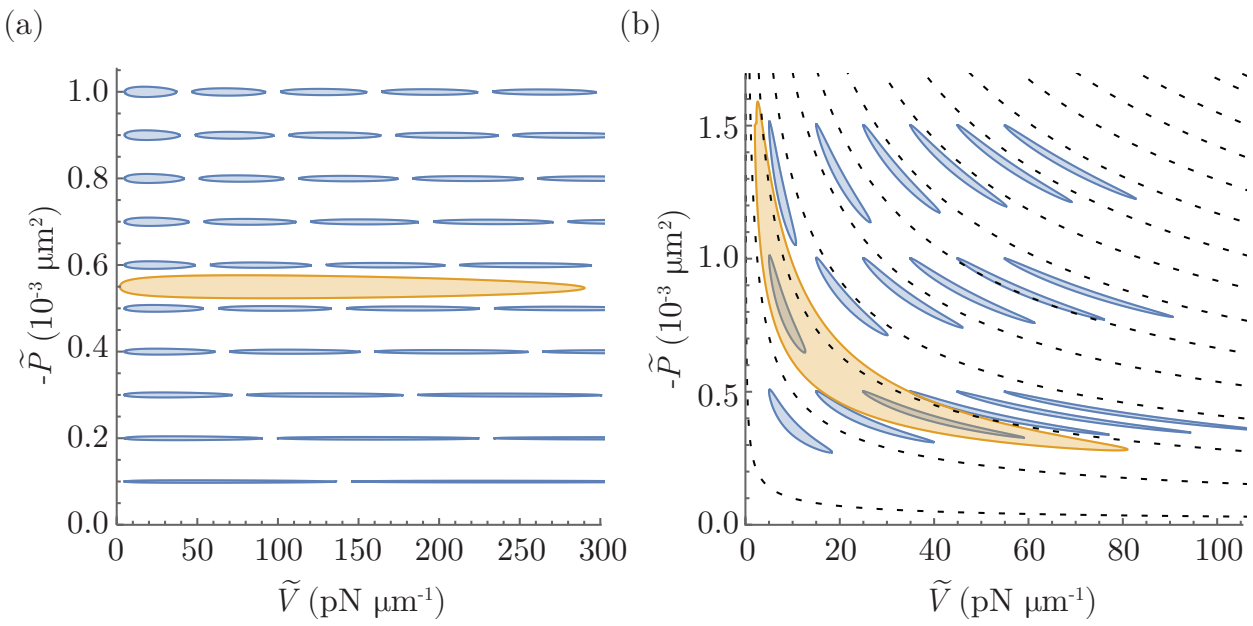


Figure 10.2: **Examples of numerically constructed optimal isoperimetric cycles (a)** Optimally constructed cycles with quasistatic output work of 6 pN μm (blue) and 120 pN μm (orange) for experimental parameters used in [249]. **(b)** Same as (a) for underdamped parameters; adiabats shown in dotted lines.

This derivation ultimately arises from thermodynamic geometry, which is a perturbative solution to first order in response theory. Our bound is therefore only approximate in nature and does not technically constrain the efficiency of engines acting beyond slow-driving. However, it is unlikely such engines would prove less dissipative and more efficient than their slower-driven counterparts, such that one would expect the bound to still apply, but not be as tight. A more interesting question is whether there are higher order or even nonperturbative bounds that constrain the efficiency of all finite time cycles. Such bounds have been found for the fluctuations of the more traditional definition of efficiency about its mean [285, 258, 286]. Similarly, one should ask if the efficiency of optimal engines in our framework would still outperform others, such as the Carnot or Stirling engine, even when far away from linear response where our results are not guaranteed to apply. We leave the detailed study of the question to future work, but there does exist anecdotal evidence that engines designed in linear response prove more efficient, even when operating far-from-equilibrium [76, 110].

Also, although the main focus of this work was in optimizing the average efficiency of thermodynamic cycles, given that our optimal cycles were designed to be minimally dissipative for a fixed thermodynamic area, they should also have a high output power, though they may not be *optimally* powerful cycles. A recurring theme in the literature is the set of tradeoffs between high output power, high efficiency, low dissipation, and minimal fluctua-

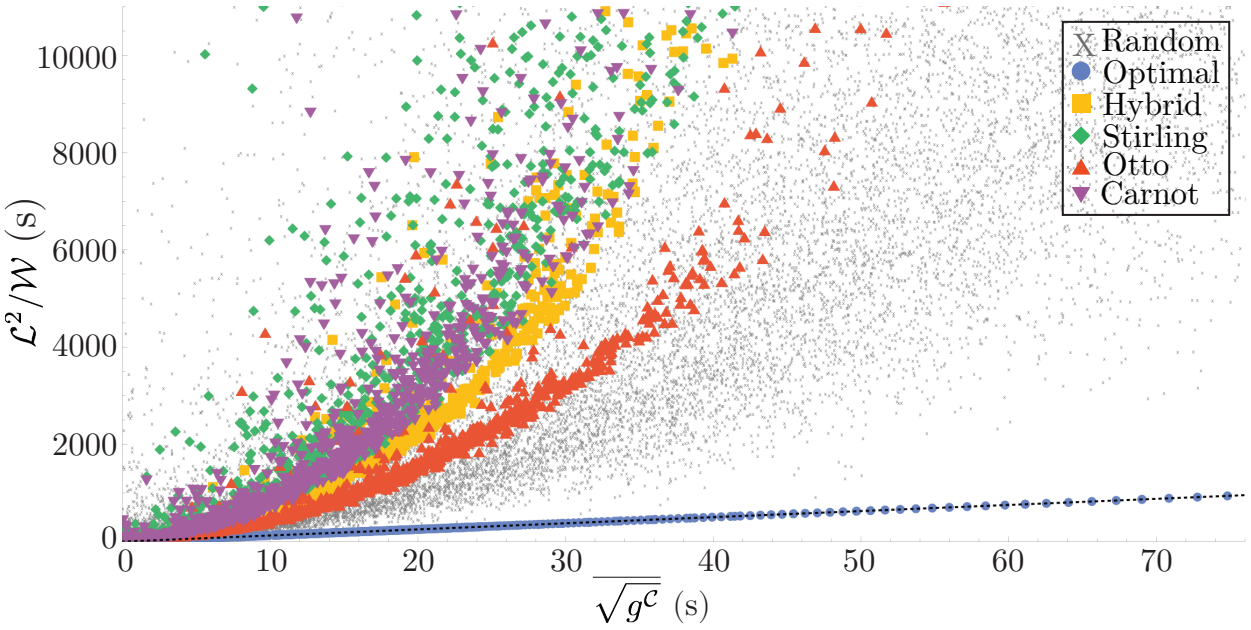


Figure 10.3: **Optimally constructed cycles strongly outperform Carnot and all other cycles tested**. Optimal (blue circles), Hybrid (orange squares), Stirling (green diamonds), Otto (red upwards triangle), Carnot (purple downwards triangle), and randomly constructed (gray X's) plotted against the bound Eq. (10.17) (black dotted line).

tions about the means of stochastic thermodynamic quantities [268, 220, 245, 76, 270, 246, 277, 286]. Studying this interplay further and designing optimal cycles achieving different objectives is of interest for future work. Similarly, we focused on the problem of finding optimal, unconstrained cycles in thermodynamic space, such that control parameters, the temperature of the heat bath and mechanical controls, are allowed to vary continuously in time. Although this regime has been studied extensively [265, 76, 276, 110, 277] and is experimentally accessible [249], it is a distinct and worthwhile question to address the problem of constructing optimal, finite-time engines under other more constrained control settings where such smooth variations may not be possible.

In addition and more generally, isoperimetric inequalities have been a significant direction of study in mathematics, and we expect them to have important implications in thermodynamic geometry. We are encouraged by their recent application to the Brownian gyrator [278] and adiabatic thermal engines operating between two heat baths [246], but we anticipate there remains a great deal to be learned by their application in various thermodynamic settings. In particular, whereas ultimately our bound relied on the introduction of thermodynamic area, isoperimetric inequalities for manifolds with density [287, 288, 289] (see Appendix 10.E) could lead to further strict bounds on dissipation directly given a work output.

Finally, although our main focus here was on classical thermal systems, thermodynamic geometry is equally applicable to quantum settings and this bound likewise should constrain the efficiency of quantum heat engines, a major focus of current research [290, 291, 292, 245, 223, 270].

10.7 Conclusion

Here, we have used classical geometric results in concert with geometric approaches to thermodynamics to place a bound on the efficiency of any irreversible heat engine and study it in the specific case of the parametric harmonic oscillator. This bound applies irrespective of the system details or dynamics and it suggests new design principles for construction of efficient engines at microscopic scales.

10.A Isoperimetric bound on efficiency for arbitrary thermodynamic manifolds

In the case when the curvature K of the thermodynamic manifold $\mathcal{M}$ is of arbitrary and not necessarily constant sign, we must start with Eqs. (10.15) and (10.16):

$$\mathcal{L}^2 \geq 4\pi\mathcal{A} - 2\left[\iint_{\mathcal{C}} K^+\right]\mathcal{A}, \tag{10.21}$$

$$\mathcal{L}^2 \geq 4\pi\mathcal{A} - \left[\sup_{\mathcal{C}} K\right]\mathcal{A}^2. \tag{10.22}$$

We no longer assume $K \leq 0$ such that we work with these equations directly. Following directly the same method as above, we have

$$\frac{\mathcal{L}^2}{\mathcal{W}} \geq 2\left(2\pi - \left[\iint_{\mathcal{C}} K^+\right]\right)\frac{\mathcal{A}}{\mathcal{W}} = 2\left(2\pi - \left[\iint_{\mathcal{C}} K^+\right]\right)\overline{\sqrt{g^{\mathcal{C}}}}, \tag{10.23}$$

$$\frac{\mathcal{L}^2}{\mathcal{W}} \geq \left(4\pi - \left[\sup_{\mathcal{C}} K\right]\mathcal{A}\right)\frac{\mathcal{A}}{\mathcal{W}} = \left(4\pi - \left[\sup_{\mathcal{C}} K\right]\mathcal{A}\right)\overline{\sqrt{g^{\mathcal{C}}}}. \tag{10.24}$$

In both cases, we see that there is an effective correction to the bound in the chapter. For $K > 0$, Eqs. (10.23) and (10.24) must be used in place of the bound given in the text. Importantly, for sufficiently large (positive) K and/or $\mathcal{A}$, these bounds actually may yield $\mathcal{L}^2/\mathcal{W} \geq 0$, such that they provide no useful information. For $K \leq 0$, as before we still have $\mathcal{L}^2/\mathcal{W} \geq 4\pi\overline{\sqrt{g^{\mathcal{C}}}}$, though Eq. (10.24) gives further refinements and places stricter bounds (Eq. (10.23) degenerates to the simpler bound for $K \leq 0$). For the interested reader, we recommend the extensive review given by [282] and references therein, specifically in §4, for a review of these forms of the classical isoperimetric inequalities, their geometric interpretation and implications, and their limitations.

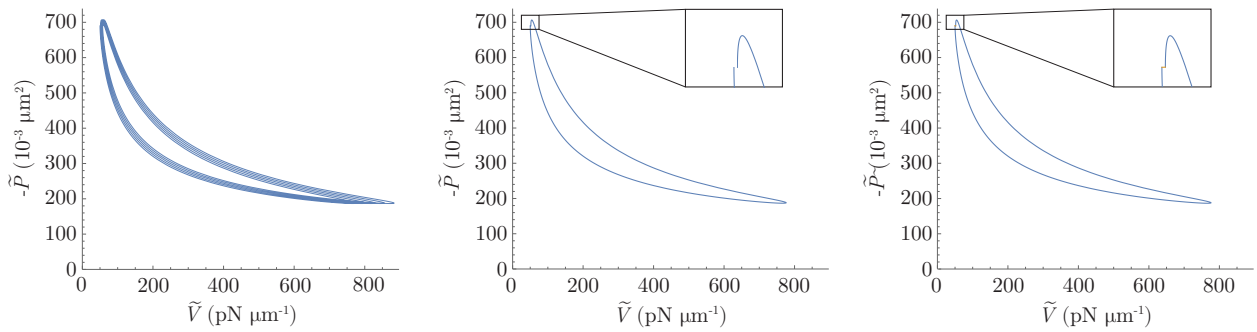


Figure 10.4: **Characteristic example of optimal cycle construction**. Left panel: A candidate non-closed curve that solves Eqs. (10.26) and (10.27) for given initial conditions integrated over a set time domain. Middle panel: The candidate curve is truncated at the closest point tangent to the initial condition after a single "period." A magnified section of the curve at this truncation point is shown in the inset demonstrating the non-closed nature of the curve. Left Panel: A cycle is formed by closing the curve with a straight line path (shown in orange).

10.B Isoperimetrically optimal Brownian protocols

We previously stated an isoperimetric bound and then found protocols that (nearly) saturated it for the specific case of the parametric harmonic oscillator in a variable heat bath. Here, we give a fuller account of our methods and demonstrate additional optimal protocols. In particular, starting with Eq. (10.20), we consider the following functional:

$$\mathcal{F} = \oint dt \left[\sqrt{g^{\mathcal{C}}} \tilde{P} \dot{\tilde{V}} + \xi \begin{pmatrix} \dot{\tilde{P}} \\ \dot{\tilde{V}} \end{pmatrix} \begin{pmatrix} \frac{\zeta}{2\tilde{P}} + \frac{2m\tilde{V}}{\zeta \tilde{P}} & \frac{m}{\zeta} \\ \frac{m}{\zeta} & \frac{m\tilde{P}}{2\zeta\tilde{V}} \end{pmatrix} \begin{pmatrix} \dot{\tilde{P}} \\ \dot{\tilde{V}} \end{pmatrix} \right]. \tag{10.25}$$

Standard arguments tell us setting the first variation of this functional to zero yields a constant geodesic curvature [281, 282]. Explicitly, this constraint yields the Euler-Lagrange equations (in $\tilde{P}$ and $\tilde{V}$ variables):

$$\xi\tilde{P}\left[m\tilde{P}\left(\dot{\tilde{V}}^2 - 4\tilde{V}\ddot{\tilde{V}}\right) - 2\tilde{V}\ddot{\tilde{P}}\left(\zeta^2 + 4m\tilde{V}\right)\right] + \xi\tilde{V}\dot{\tilde{P}}^2\left(\zeta^2 + 4m\tilde{V}\right) + \zeta\tilde{P}^2\sqrt{m\tilde{V}}\dot{\tilde{V}} = 8\xi m\tilde{P}\tilde{V}\dot{\tilde{P}}\dot{\tilde{V}}, \tag{10.26}$$

$$\tilde{P}\left[\dot{\tilde{P}}\left(2\xi m\tilde{V}\dot{\tilde{V}} + \zeta\sqrt{m\tilde{V}^3}\right) + 4\xi m\tilde{V}^2\ddot{\tilde{P}}\right] = \xi m\left[4\tilde{V}^2\dot{\tilde{P}}^2 + \tilde{P}^2\left(\dot{\tilde{V}}^2 - 2\tilde{V}\ddot{\tilde{V}}\right)\right]. \tag{10.27}$$

Solving these equations therefore yields curves that have constant geodesic curvature and are therefore candidates to be isoperimetrically optimal. Over a given domain, the *isoperimetric profile* gives the (perhaps degenerate set of) minimizer(s) of perimeter for a

fixed area, and can be shown to be closed and smooth; furthermore, given certain demands on connectedness and compactness of a domain [282], it can be shown to exist. Nevertheless, its existence is not equivalent to its construction, and finding exactly isoperimetrically optimal shapes is a significant undertaking in the mathematics literature, especially for surfaces of non-constant, non-symmetric curvature.

To avoid this significant difficulty, we bypass the problem of finding exactly closed curves of constant geodesic curvature and instead simply look for closed, not-necessarily-smooth curves that maintain constant curvature everywhere excluding small regions. Finding such cycles is a far simpler task and they still perform optimally relative to the bound, Eq. (10.17). In particular, Starting with Eqs. (10.26) and (10.27), we numerically integrate for the given set of initial conditions of $\tilde{P}(0), \tilde{V}(0), \dot{\tilde{P}}(0)$, and $\dot{\tilde{V}}(0)$, and a given value of ξ. As noted previously, if we are only interested in the resultant curve rather than its particular parameterization, we could instead parameterize $\tilde{P}$ as a function of $\tilde{V}$, such that one of these initial condition degrees of freedom is redundant so optimal shapes under this construction are specified by a four-parameter family. Like the variational optimal isoperimentric construction of a circle, the Lagrange multiplier ξ enforcing constant curve energy $\oint dt(\dot{\tilde{P}}, \dot{\tilde{V}}) \cdot \mathbf{g} \cdot (\dot{\tilde{P}}, \dot{\tilde{V}})$ correlates to a diameter-like quantity that specifies the size of the resultant cycle.

Generically, and typically, the cycles we find are not closed and instead result in cycloids in space. However, seeing as we are interested only in closed cycles for engine operation, we find the first point on the curve whose tangent vector is tangent to that initial condition, empirically these tend to be quite close, and connect them by a straight line. A characteristic example of this process is demonstrated in Fig. 10.4 for a specific choice of initial conditions. Generally speaking, this small correction to close the cycle amounts to an added value of thermodynamic length that is significantly shorter than that of the rest of the cycle (and therefore energetically cheap relative to the total cycle), but we still do recognize the lack of true optimality of these cycles. Nevertheless, compared to the bound, they perform quite well, as can be seen in Fig. 10.3. Empirically, we find these cycles can approach the bound to within tens of thousandths of a percent and are never more than a handful of percentages above it for the parameter values we explore.

In Fig. 10.5, we plot such isoperimetrically optimized curves for a variety of values of m and ζ, which impact the metric and curvature of the underlying manifold, $K = 1/(\zeta\tilde{P})$. The curves themselves can further be understood by studying the metric

$$g^{\mathcal{C}}_{\mu\nu} = -\begin{pmatrix} \frac{\zeta}{2\tilde{P}} + \frac{2m\tilde{V}}{\zeta\tilde{P}} & \frac{m}{\zeta} \\ \frac{m}{\zeta} & \frac{m\tilde{P}}{2\zeta\tilde{V}} \end{pmatrix},$$

where the ratio of various terms, including the fixed ratio m/ζ set by material parameters, show the competition between various directions of minimal length. Considering these ratios (which *do* have dimensions) can give intuition into why a cycle might favor being heavily horizontal, as in Fig. 10.1 and Figs 10.5(a)-(d) of this supplement. In all plots, blue cycles enclose an quasistatic work (given by their enclosed Euclidean area in these units) of 6 pN

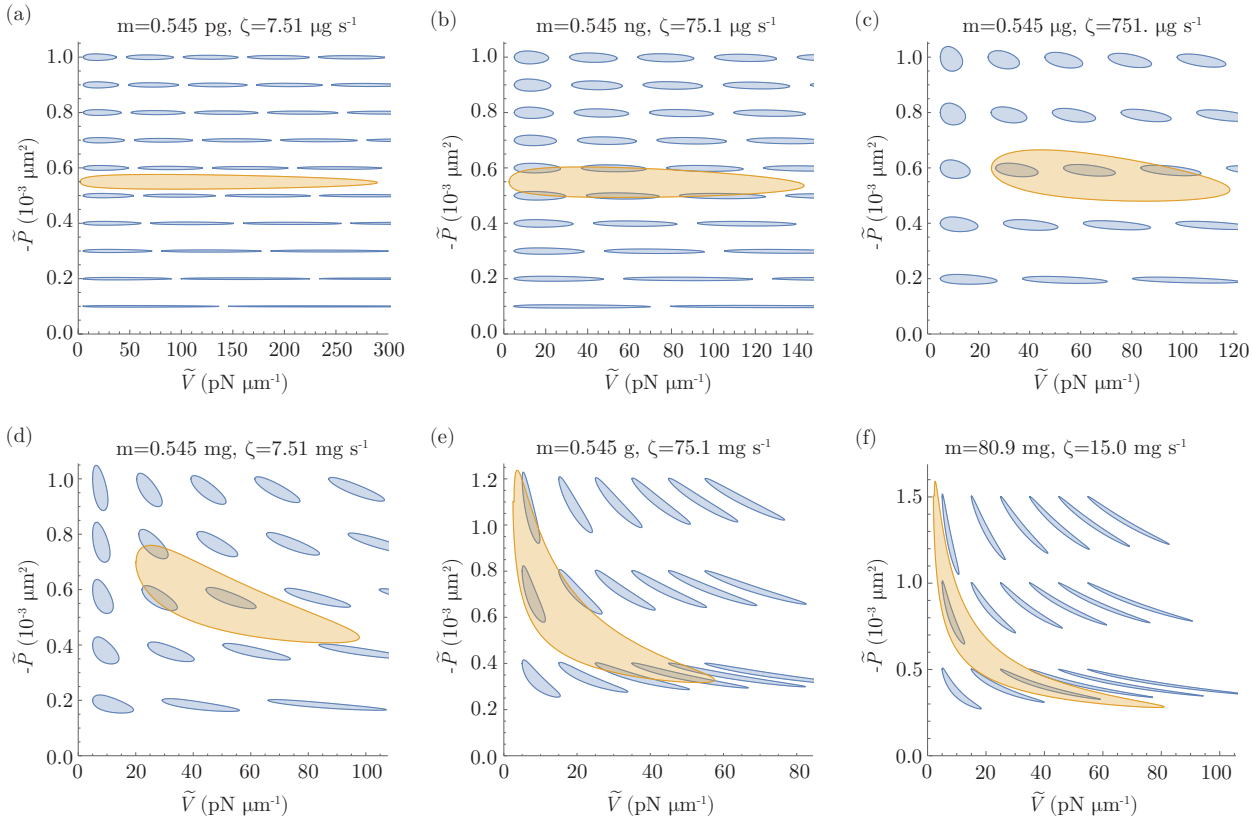


Figure 10.5: **Plots of optimally constructed cycles for a variety of material parameters and in a variety of regions of Clausius space**. The specific values of m and ζ relevant to each plot are displayed above them. All smaller blue plots contain the same Euclidean area (and therefore quasistatic work) of 6 pN μm and the larger orange plots contain 120 pN μm. Note, **(a)** and **(f)** are reproduced from Fig. 10.2**(a)** and **(b)**, respectively, to be compared with cycles for other choices of m and ζ.

μm and orange cycles enclose 120 pN μm, such that we can observe the resultant cycles over multiple scales.

We observe that for smaller values of m/ζ, the cycles are overwhelmingly horizontal (in the plotted units). As noted previously, evaluating sample values of the metric for this case, this makes sense as the cost to change horizontally is far cheaper than to change vertically. As m/ζ increases, however, the optimal curves become more curved and seemingly follow more or less along adiabats. In a previous work, we showed adiabats of this model are exactly geodesic [110], so this empirical finding makes intuitive sense as these are the least costly means of connecting any given points in Clausius space. More generally, characterizing the full set of optimal curves of this model as a function of m and ζ is a difficult but worthwhile analytical and numerical task which we will leave to future work.

10.C Classical Brownian protocols

In Fig. 10.3, we compared the optimally constructed curves detailed previously to a variety of cycles. Here, we review notable classical thermodynamic processes and cycles and how they are manifested in Brownian colloidal systems, following [160, 271, 249, 159].

Thermodynamic Processes

Isothermal Processes

For Brownian systems, isothermal processes retain their usual meaning in that temperature is maintained throughout the process. However, given the stochastic and nonequilibrium nature of the working system, a notion of temperature may be ill-defined for the system itself and so the bath temperature T is maintained while other control variables are allowed to vary, specifically the trap stiffness k for the working substance considered.

In Clausius space, we have $\tilde{V} \equiv k$ and $\tilde{P} \equiv -k_B T/(2k)$ such that $\tilde{P}\tilde{V} = -k_B T/2$ and the equation of state of this system mirrors a (virtual) ideal gas with $N = -1/2$, and an isothermal process thus corresponds to

$$T = \text{const.} \iff (\tilde{P}\tilde{V})_{\text{isothermal}} = \text{const.} \tag{10.28}$$

as in the case of an ideal gas.

Adiabatic Processes

In classical thermodynamics, an adiabatic process is one that occurs with no heat exchange, and is therefore exactly isentropic for reversible processes. Although these use interchangeably, there can be irreversible adiabatic processes that are therefore *not* isentropic. In the Brownian context, adiabatic processes are defined as those that maintain the system entropy were the process occurring quasistatically.

In the case of the parametric harmonic oscillator, the Boltzmann distribution of states is given

$$\rho_{\text{Boltzmann}} = \frac{1}{Z} e^{-\beta(\frac{p^2}{2m} + \frac{1}{2}kx^2)}, \tag{10.29}$$

where $\beta \equiv (k_B T)^{-1}$ is the inverse temperature, p is the particle momentum, x is the particle position, and the partition function is given

$$Z = 2\pi k_B T \sqrt{\frac{m}{k}}. \tag{10.30}$$

The Helmholtz free energy is thus

$$F = -k_B T \log Z = -k_B T \log \left(2\pi k_B T \sqrt{\frac{m}{k}} \right), \tag{10.31}$$

such that, finally, the equilibrium system entropy for fixed k and T is

$$S = -\frac{\partial F}{\partial T} = k_B \left[1 + \log \left(2\pi k_B T \sqrt{\frac{m}{k}} \right) \right]. \tag{10.32}$$

Therefore, a Brownian adiabatic process is defined:

$$S = \text{const.} \iff \left(\frac{T^2}{k} \right)_{\text{adiabitc}} = \text{const.} \iff \left(\tilde{P} \tilde{V}^{1/2} \right)_{\text{adiabatic}} = \text{const.} \tag{10.33}$$

Note for overdamped Brownian systems, although the definition of adiabatic processes remains the same, the system's inertial degrees of freedom are ignored such that S becomes a function of T/k directly and adiabatic processes are those that maintain this ratio. To avoid confusion, these processes are instead typically denoted as pseudo-adiabatic [271].

Isochoric Processes

Like isothermal processes, isochoric processes retain their standard definition in that the main control variable is maintained. In control space, this manifests as $k = \text{const.}$ such that

$$(k)_{\text{isochoric}} = \text{const.} \iff (\tilde{V})_{\text{isochoric}} = \text{const.} \tag{10.34}$$

Geodesic Processes

Geodesics are the shortest paths connecting two given points on a manifold and generalize straight-line paths to non-Euclidean spaces (e.g. great circles are the geodesics on the surface of a sphere). Recently, geodesics have been suggested as a means to construct thermodynamic processes [107, 110]. Specifically, the geodesics of the thermodynamic manifold connecting two given points in control space are calculated and the resulting path in control space is followed as the process. Given their definition, these processes correspond to those of shortest thermodynamic length between any two points in control space and are therefore the least dissipative between those two points. Generically, such paths must be found numerically, as is the case for this model system [110].

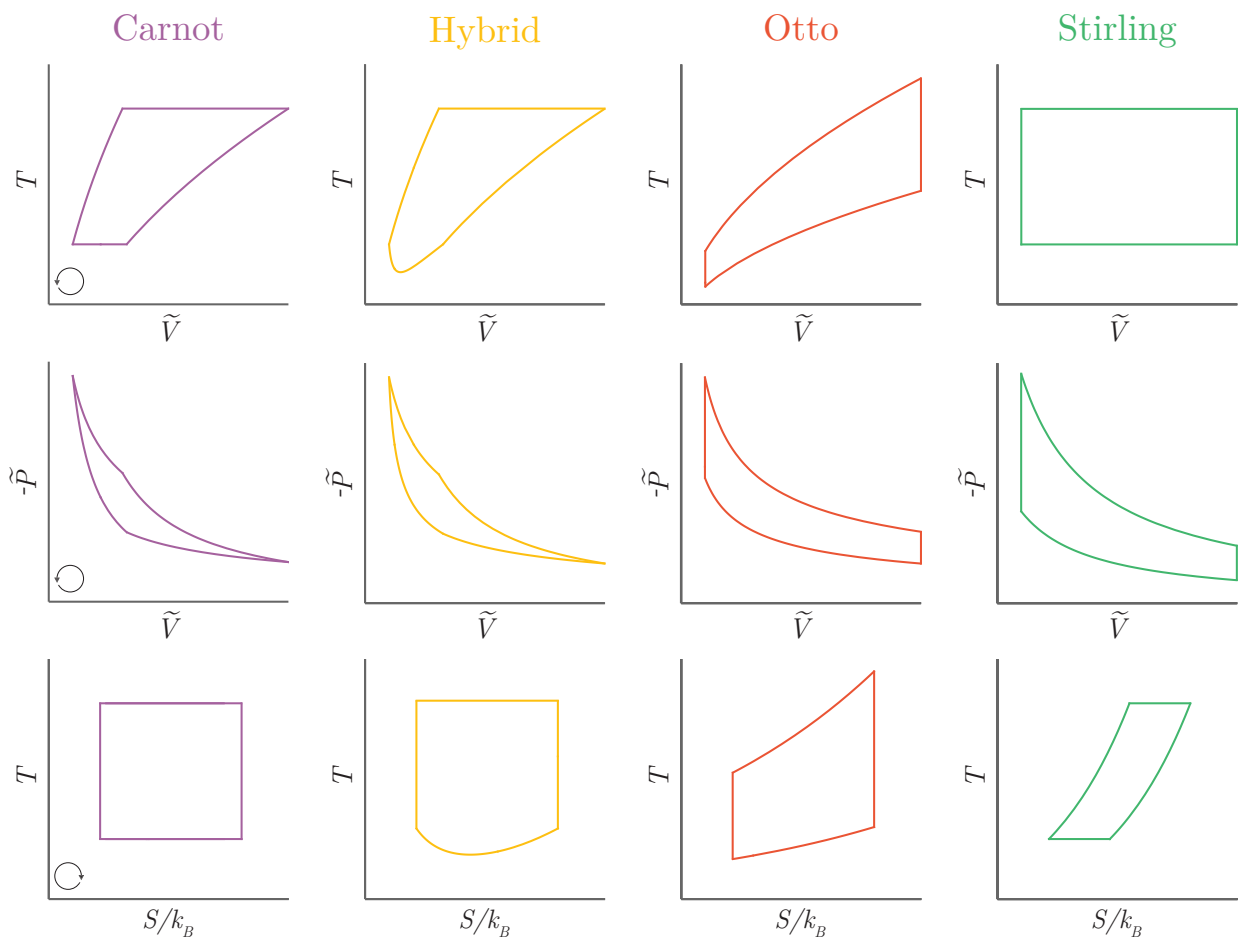


Figure 10.6: **Quasistatic profiles of classical thermodynamic cycles in various spaces**. Carnot cycle (far left, purple), Hybrid cycle (middle left, yellow), Otto cycle (middle right, red), and Stirling cycle (far right, green) shown in control ($T - \tilde{V}$) space, Clausius ($\tilde{P}-\tilde{V}$) space and $T-S$ space. Arrows in Carnot cycle profiles denote orientation for positive work output: the same orientations produce positive work output for all other cycles.

Thermodynamic Cycles

Brownian Carnot cycle

Following the usual definition of the Carnot cycle, a Brownian Carnot cycle consists of alternating isothermal and adiabatic strokes. A schematic quasistatic profile in control space, Clausius space and $T - S$ space are shown on the far left of Fig. 10.6 in purple.

Brownian Hybrid cycle

Hybrid cycles were introduced in [110] and consist of a Carnot cycle with slight modification. Namely, heat is extracted from a high temperature bath by means of an isothermal stroke and connected to a low temperature bath by means of adiabatic strokes. However, in lieu of an exhaust isothermal stroke at a low temperature bath, these two corners of the usual Carnot cycle are connected by means of a geodesic stroke, such that the cycle is a hybrid between a Carnot cycle and a geodesic cycle lending the cycle its name. This geodesic stroke is, by definition, less dissipative than the corresponding isothermal stroke connecting these two corners, though proves to provide more output work. As a result, the Hybrid cycle is less dissipative, more efficient, and more powerful for a given cycle duration than its corresponding Carnot cycle. A schematic quasistatic profile in control space, Clausius space and $T-S$ space are shown on the middle left of Fig. 10.6 in yellow.

Brownian Otto cycle

Following the usual definition of the Otto cycle, a Brownian Otto cycle consists of alternating isochoric and adiabatic strokes. A schematic quasistatic profile in control space, Clausius space and $T-S$ space are shown on the middle right of Fig. 10.6 in red.

Brownian Stirling cycle

Following the usual definition of a Stirling cycle, a Brownian Stirling cycle consists of alternating isothermal and isochoric strokes. A schematic quasistatic profile in control space, Clausius space and $T-S$ space are shown on the far right of Fig. 10.6 in green.

10.D Construction of Fig. 10.3

In this section, we give further details on how Fig. 10.3 is constructed. First, we detail the construction of the "named" cycles. For each named cycle, we randomly selected the corners of the cycle in Clausius space to construct the sufficient number of cycles. In the case of the Carnot cycle, this amounted to randomly selecting the maximum and minimum temperature and entropy; for the Stirling, temperature and volume; for the Otto, volume and entropy; and for the Hybrid, the same corners were considered as a randomly constructed Carnot. To plot over a sufficient region of space, these cycles were sampled such that a significant number would appear for a wide range of $\overline{\sqrt{g^{\mathcal{C}}}}$, amounting to a wide range of average values for $1/\sqrt{\tilde{V}}$.

For the randomly constructed cycles, denoted by the gray X's in the figure, cycles are specified by $-\tilde{P}(t) = f_1(\sin(x)) + f_2(\cos(x))$ and $\tilde{V}(t) = f_3(\sin(x)) + f_4(\cos(x))$ where the functions are of the form $f_i(x) = c_{i0} + c_{i1}x + c_{i3}x^3 + c_{i5}x^5$ with random coefficients c_{ij}, and where x is evaluated over the full period $[0, 2\pi]$. Given that thermodynamic space for this model system is only well-defined for $\tilde{V} > 0$ and $\tilde{P} < 0$, there are nevertheless constraints on

c_{ij} such that f_i are all positive. First, we choose $c_{10} + c_{20}$ a randomly selected positive number over a uniform distribution whereas $c_{30} + c_{40}$ is selected from a Pareto distribution with minimum value 0.02 and shape parameter 0.5 such that again cycles are sampled from a large range of of average values for $1/\sqrt{\tilde{V}}$ (roughly uniform over the range $[0, 100]$). From there $c_{i1} \sim \mathcal{U}_{[-c_{i0}/2, c_{i0}/2]}$, $c_{i3} \sim \mathcal{U}_{[-(c_{i0}/2-|c_{i1}|),(c_{i0}/2-|c_{i1}|)]}$, and $c_{i5} \sim \mathcal{U}_{[-(c_{i0}/2-|c_{i1}|-|c_{i3}|),(c_{i0}/2-|c_{i1}-|c_{i3})|]}$ where $\mathcal{U}_{[a,b]}$ is the continuous uniform distribution over the range $[a, b]$. By these selections, all f_i are guaranteed positive functions such that the cycles are well-defined, randomly constructed, smooth and closed thermodynamic cycles that sample a large region of Clausius space. Altogether, 30000 such cycles were constructed, though a significant number have values of $\mathcal{L}^2/\mathcal{W}$ that are outside the plotted range of Fig. 10.3.

Finally, the optimally constructed cycles were selected by choosing 500 sets of values for $\tilde{P}(0), \tilde{V}(0), \dot{\tilde{P}}(0), \dot{\tilde{V}}(0)$, and ξ and solving Eqs. (10.26) and (10.27) numerically. Values were sampled over a large range of average values of $1/\sqrt{\tilde{V}}$ to demonstrate their performance against the bound over a wide region of Clausius space.

For all such constructed cycles, the thermodynamic lengths, areas, and quasistatic work values (i.e. Euclidean areas) are calculated (these are all purely geometric quantities), and used to construct the figure.

10.E Isoperimetric inequalities with density

Manifolds with density have become of interest recently in the mathematics literature [287]. These mathematical structures, which we will denote as $\mathcal{M}_\psi$ consist of a base manifold $\mathcal{M}_0$ with usual definitions of volume $\mathscr{V}$ and area $\mathscr{A}$ (or area and length in the case of two dimensions) but further equipped with a defined set of densities $\{\psi\}$ such that the volume $\mathscr{V}_\psi$ and area $\mathscr{A}_\psi$ become

$$d\mathscr{V} = \psi_{\mathscr{V}} d\mathscr{V}_0,$$
$$d\mathscr{A} = \psi_{\mathscr{A}} d\mathscr{A}_0.$$

Generalizing various results, notably isoperimetric inequalities, for standard manifolds to manifolds with density has been on ongoing endeavor with success for certain specific cases, most notably the Gauss space: Euclidean space with a normalized Gaussian density centered at the origin for both area and volume.

Of interest to us is the recognition that, in Clausius space, $d\mathcal{W} = d\mathcal{X}_\lambda d\lambda$ whereas $d\mathcal{A} = \sqrt{g^{\mathcal{C}}} d\mathcal{X}_\lambda d\lambda$. Previously, we leveraged the ratio of these two quantities to place on bound on $\mathcal{L}^2/\mathcal{W}$. However, recognizing

$$d\mathcal{W} = \frac{1}{\sqrt{g^{\mathcal{C}}}} d\mathcal{A}, \tag{10.35}$$

suggests that if we consider the manifold with density consisting of

1. A base manifold of Clausius space

2. A trivial (i.e. unit) length density

3. An area density consisting of $1/\sqrt{g^{\mathcal{C}}}$

Then finding isoperimetric inequalities and isoperimetric curves on this manifold with density would yield general bounds on $\mathcal{L}^2/\mathcal{W}$ and, in turn, efficiency. Solving such a problem generally, or even in a specific case, is a highly nontrivial task; nevertheless, the significant impact such results would have merits their investigation.

Part IV

Bringing the slow up to speed: connecting thermodynamic geometry and shortcut engineering

Chapter 11

The equilibrium manifold: bridging thermodynamic and shortcut geometries

In this chapter, after introducing some necessary mathematical preliminaries, we demonstrate a geometric approach to optimal thermal shortcutted protocols, thereby allowing similar methods as used in Part III but now for shortcut engineering. We then demonstrate that, although derived independently, the shortcut and thermodynamic geometries are in fact identical, thereby linking optimal shortcut engineering with thermodynamic geometry and tying together the two main themes of this thesis. The development is heavily inspired by the works [77, 80], and especially by the very recent work of Zhong and DeWeese [99]. In this chapter, we review the results of these foundational works before applying them and demonstrating a deep unification of thermodynamic geometry and shortcut engineering.

11.1 Kolmogorov operators

Before delving into the main focus of this chapter, we review the Kolmogorov operators. We follow the treatment given in [92]. We start by considering a generic diffusion process, written as a stochastic differential equation,

$$d\mathbf{X}_t = \mathbf{b}(X_t, t)dt + \boldsymbol{\sigma}(X_t, t) \cdot d\mathbf{W}_t, \tag{11.1}$$

for a random variable $\mathbf{X}_t$, where $\mathbf{b}(X, t)$ is the drift, $\boldsymbol{\sigma}(X, t)$ is the diffusion, and W_t is a Wiener process. Let us consider an arbitrary function of the X, $f(X)$, where we assume that $f(X)$ and all of its first and second derivatives are continuous and bounded. Let us define

$$u(y, s) \equiv \mathbb{E}[f(X_t)|X_s = y], \tag{11.2}$$

where $\mathbb{E}[\cdot]$ denotes an expectation, such that $u(y,s)$ specifies the expected value of X_t conditioned on its value at a time s. One can show the dynamics of $u(y,s)$ are given by

$$\partial_s u(y,s) = -\mathcal{L}u(y,s), \tag{11.3}$$

where $s < t$ and the operator $\mathcal{L}$ is given

$$\mathcal{L}f = \mathbf{b}(\mathbf{X_t},t)\cdot\nabla f(\mathbf{X_t}) + \sum_{ij}\boldsymbol{\sigma}_i(\mathbf{X_t},t)\boldsymbol{\sigma}_j(\mathbf{X_t},t)\nabla_i\nabla_j f(\mathbf{X_t}). \tag{11.4}$$

We omit the proof as it is beyond the scope of this work, though it is readily found in standard texts [92]. The operator, $\mathcal{L}$, is the *Backward Kolmogorov operator* as it indicates the change in expected value of the function as one propagates the dynamics backward in time. For a stationary process Eq. (11.3) may be simplified even further [92]. Defining,

$$v(x,t) \equiv \mathbb{E}[f(X_t)|X_0 = x], \tag{11.5}$$

Eq. (11.3) yields

$$\partial_t u(x,t) = \mathcal{L}u(x,t), \tag{11.6}$$

which is to say, for stationary diffusion processes, the Kolmogorov backward operator indicates the time evolution of expectation values of functions conditioned on some initial value.

Let us now consider the quantity

$$\int d\mathbf{y}u(\mathbf{y},s)\rho(\mathbf{y},s), \tag{11.7}$$

where $u(\mathbf{y},s) = \mathbb{E}[f(X_t)|X_s = y]$ as before for $0 \le s \le t$ and $\rho(\mathbf{x},t)$ is the distribution function of $\mathbf{X}_t$. We may expand this expression:

$$\begin{aligned}\int d\mathbf{y}u(\mathbf{y},s)\rho(\mathbf{y},s) &= \int d\mathbf{y}\left[\int d\mathbf{x}f(x)p(\mathbf{x},t|\mathbf{y},s)\right]\left[\int d\mathbf{z}p(\mathbf{y},s|\mathbf{z},0)\rho(\mathbf{z},0)\right]\\ &= \int d\mathbf{x}d\mathbf{z}f(x)p(\mathbf{x},t|\mathbf{z},0)\rho(\mathbf{z},0),\end{aligned} \tag{11.8}$$

which is, critically, independent of s. We may therefore differentiate:

$$\begin{aligned}0 = \frac{\partial}{\partial s}\int d\mathbf{y}u(\mathbf{y},s)\rho(\mathbf{y},s) &= \int d\mathbf{y}(\rho(\mathbf{y},s)\partial_s u(\mathbf{y},s) + u(\mathbf{y},s)\partial_s\rho(\mathbf{y},s))\\ &= \int d\mathbf{y}(\rho(\mathbf{y},s)(-\mathcal{L})u(\mathbf{y},s) + u(\mathbf{y},s)\partial_s\rho(\mathbf{y},s))\\ &= \int d\mathbf{y}u(\mathbf{y},s)(-\mathcal{L}^\dagger\rho(\mathbf{y},s) + \partial_s\rho(\mathbf{y},s)),\end{aligned} \tag{11.9}$$

where $\mathcal{L}^\dagger$ is the L^2 adjoint operator to $\mathcal{L}$ given

$$\mathcal{L}^\dagger f(\mathbf{X},t) = -\nabla\cdot(\mathbf{b}(\mathbf{X_t},t)f(\mathbf{X_t})) + \sum_{ij}\nabla_i\nabla_j\boldsymbol{\sigma}_i(\mathbf{X_t},t)\boldsymbol{\sigma}_j(\mathbf{X_t},t)f(\mathbf{X_t}). \tag{11.10}$$

This construction holds for an arbitrary function f, such that we may conclude

$$\partial_s\rho(\mathbf{y},t) = \mathcal{L}^\dagger\rho(\mathbf{y},t). \tag{11.11}$$

The operator $\mathcal{L}^\dagger$ is the *Kolmogorov forward operator*, commonly referred to as the Fokker-Planck operator in the physics literature. It is the same operator $\mathcal{L}^\dagger$ as first introduced in Ch. 4 which determines forward time evolution of a probability distribution under a set of dynamics. With these mathematical preliminaries, we proceed to studying shortcut geometries and their connections to thermodynamic geometries.

11.2 Shortcuts to Isothermality

As first introduced in Chapter 5, we recall Shortcuts to Isothermality (STI), a counterdiabatic method of shortcutting relaxation dynamics in open classical systems. This is carried out through an auxiliary Hamiltonian, similar to how it was carried out in Chapter 6:

$$H(t) = H_{\text{base}}(t) + H_{\text{aux}}(t), \tag{11.12}$$

where $H_{\text{aux}}(t)$ is chosen so that $\rho(t) = \rho_{\text{eq,base}}(t) \propto \exp[-\beta H_{\text{base}}(t)]$. These methods were first introduced in [77]. We here derive the necessary conditions for the shortcut auxiliary Hamiltonian for both overdamped and underdamped dynamics.

Overdamped dynamics

We consider the classical overdamped dynamics of a system subject to some potential $V(\mathbf{x},t)$. The probability distribution evolves as [77]

$$\partial_t\rho = \mathcal{L}^\dagger\rho = -\nabla\cdot(\rho\mathbf{v}) \tag{11.13}$$

where we recall the local mean velocity (see Eq. (4.4)),

$$\mathbf{v} = -\gamma\nabla(V + k_BT\log\rho). \tag{11.14}$$

We now specify the form of V as

$$V = V_{\text{base}}(\mathbf{x};\boldsymbol{\lambda}(t)) + V_{\text{aux}}(\mathbf{x},t), \tag{11.15}$$

where $\{\boldsymbol{\lambda}\}$ is a set of parametric control variables and we desire the system to assume the equilibrium distribution given by $V_{\text{base}}(\mathbf{x};\boldsymbol{\lambda}(t))$ at all times:

$$\rho(\mathbf{x},t) = \rho_{\text{eq}}(\mathbf{x};\boldsymbol{\lambda}) = e^{-\beta(V_{\text{base}}(\mathbf{x};\boldsymbol{\lambda})-F_{\text{base}}(\boldsymbol{\lambda}))}, \tag{11.16}$$

where, as always, $F_{\text{base}}(\boldsymbol{\lambda}) = -k_B T \log Z_{\text{base}} = -k_B T \log \int d\mathbf{x} e^{-\beta V_{\text{base}}}$ is the equilibrium free energy associated with $V_{\text{base}}(\mathbf{x}; \boldsymbol{\lambda})$ and $\beta = 1/(k_B T)$. Plugging this ansatz into Eq. (11.13), we have

$$-\nabla_{\boldsymbol{\lambda}}(V_{\text{base}} - F_{\text{base}}) \cdot \dot{\boldsymbol{\lambda}} = D\rho_{\text{eq}}^{-1} \nabla \cdot (\rho_{\text{eq}} \nabla V_{\text{aux}}). \tag{11.17}$$

Focusing first on the left hand side of Eq. (11.17), we recognize $\partial V/\partial \lambda_i = -X_i$ as the thermodynamic force conjugate to λ_i, whereas

$$\frac{\partial F}{\partial \lambda_i} = \frac{\partial}{\partial \lambda_i}(-k_B T \log Z) = \frac{\partial}{\partial \lambda_i}(-k_B T \log \int dx e^{-\beta V}) = -\frac{\int \frac{\partial V}{\partial \lambda_i} e^{-\beta V}}{Z} = \langle X_i \rangle_{\text{eq,base}}, \tag{11.18}$$

where $\langle \cdot \rangle_{\text{eq,base}}$ denotes an equilibrium average for the base dynamics. The left hand side of Eq. (11.17) is therefore simply

$$-\nabla_{\boldsymbol{\lambda}}(V_{\text{base}} - F_{\text{base}}) \cdot \dot{\boldsymbol{\lambda}} = (\mathbf{X}_{\text{base}} - \langle \mathbf{X}_{\text{base}} \rangle_{\text{eq,base}}) \cdot \dot{\boldsymbol{\lambda}} = \delta \mathbf{X}_{\text{base}} \cdot \dot{\boldsymbol{\lambda}}.$$

Following Eq. (11.4), a relatively straightforward manipulation demonstrates that the right hand side, in contrast, can be written succinctly in terms of the Backward Kolmogorov operator:

$$\rho_{\text{eq}}^{-1} \nabla \cdot (\rho_{\text{eq}} \nabla V_{\text{aux}}) = \mathcal{L} V_{\text{aux}}, \tag{11.19}$$

such that, altogether, Eq. (11.17) may finally be written as

$$\mathcal{L} V_{\text{aux}} = \delta \mathbf{X}_{\text{base}} \cdot \dot{\boldsymbol{\lambda}}. \tag{11.20}$$

Underdamped dynamics

For systems in which we cannot ignore the inertial degrees of freedom, we instead adopt underrdamped dynamics. This set of dynamics is given [77]

$$\partial_t \rho = \mathcal{L}_u^\dagger \rho = -\nabla_u \cdot (\rho \mathbf{v}_u), \tag{11.21}$$

where we identify

$$\nabla_u = \begin{pmatrix} \nabla_{\mathbf{x}} \\ \nabla_{\mathbf{p}} \end{pmatrix} \tag{11.22}$$

and

$$\mathbf{v}_u = -\begin{pmatrix} 0 & -1 \\ 1 & \gamma \end{pmatrix} \cdot \begin{pmatrix} \nabla_{\mathbf{x}} \\ \nabla_{\mathbf{p}} \end{pmatrix} (H + k_B T \log \rho). \tag{11.23}$$

Note, further, if we identify

$$\boldsymbol{\Gamma} = \begin{pmatrix} 0 & -1 \\ 1 & \gamma \end{pmatrix} \tag{11.24}$$

and

$$\mathbf{v}_{\text{bare}} = -\nabla_u (H + k_B T \log \rho) \tag{11.25}$$

we may write

$$\mathbf{v}_u = \mathbf{\Gamma} \cdot \mathbf{v}_{\text{bare}}, \tag{11.26}$$

which may be interpreted as the underdamped analogy of Eqs. (4.4) and (11.14)[1]. Note that the matrix $\mathbf{\Gamma}$ serves to encode both the Liouvillian dynamics and the Langevin damping.

Under this identification, we may carry out a similar procedure as was done for overdamped dynamics. We write the Hamiltonian as

$$H = H_{\text{base}}(\mathbf{x}, \mathbf{p}; \boldsymbol{\lambda}(t)) + H_{\text{aux}}(\mathbf{x}, \mathbf{p}, t) \tag{11.27}$$

We now seek to enact a shortcut, such that, at all times

$$\rho(\mathbf{x}, \mathbf{p}, t) = \rho_{\text{eq}}(\mathbf{x}, \mathbf{p}; \boldsymbol{\lambda}(t)) = e^{-\beta(H_{\text{base}}(\mathbf{x},\mathbf{p};\boldsymbol{\lambda}) - F_{\text{base}}(\boldsymbol{\lambda}))}. \tag{11.28}$$

Evaluating Eq. (11.21) with this ansatz, we need to satisfy

$$-\nabla_{\boldsymbol{\lambda}}(H_{\text{base}} - F_{\text{base}}) \cdot \dot{\boldsymbol{\lambda}} = \rho_{\text{eq}}^{-1} \nabla_u \cdot (\rho_{\text{eq}} \mathbf{\Gamma} \cdot \nabla_u H_{\text{aux}}). \tag{11.29}$$

The left hand side of this equation follows an identical argument as in the overdamped case and is therefore δX. However, much as the analogy seems promising, the right hand side does *not* represent the action of the backward Kolmogorov operator. Seeing as the backward Kolmogorov operator is an adjoint of $\mathcal{L}^\dagger$, it is described for underdamped dynamics as

$$\mathcal{L}_u H_{\text{aux}} = \rho_{\text{eq}}^{-1} \nabla_u \cdot (\rho_{\text{eq}} \mathbf{\Gamma}^\dagger \cdot \nabla_u H_{\text{aux}}), \tag{11.30}$$

where $M^\dagger$ is the conjugate transpose of the matrix M. The left hand side of Eq. (11.29) is quite similar to Eq. (11.30) but critically lacks the necessary conjugate transpose of $\mathbf{\Gamma}$. Rather, the operator on the RHS of Eq. (11.29) denotes the action of $\mathcal{L}_u$ under a transformation $p \to \bar{\mathbf{p}} = -\mathbf{p}$:

$$\bar{\mathcal{L}}_u H_{\text{aux}} = \rho_{\text{eq}}^{-1} \nabla_u \cdot (\rho_{\text{eq}} \mathbf{\Gamma} \cdot \nabla_u H_{\text{aux}}), \tag{11.31}$$

where we adopt the notation $\bar{f}$ to denote the operator f under the transformation $\mathbf{p} \to -\mathbf{p}$. With these identifications, we may write Eq. (11.29) as

$$\bar{\mathcal{L}} H_{\text{aux}} = \delta \mathbf{X} \cdot \dot{\boldsymbol{\lambda}}. \tag{11.32}$$

Looking back at the overdamped dynamics, we recognize that there is no dependence on momenta and that the Hamiltonian is simply given by the potential. Importantly, for overdamped dynamics $\mathcal{L} = \bar{\mathcal{L}}$ and $V_{\text{aux}} = H_{\text{aux}}$. Therefore, Eq. (11.32) applies to both overdamped and underdamped dynamics. Additionally, if we further choose $H_{\text{aux}} = \mathbf{f} \cdot \dot{\boldsymbol{\lambda}}$ and given that Eq. (11.32) holds for arbitrary driving, we arrive at the following condition for $\mathbf{f}$:

$$\bar{\mathcal{L}} H_{\text{aux}} = \delta \mathbf{X} \cdot \dot{\boldsymbol{\lambda}} \implies \bar{\mathcal{L}} \mathbf{f} = \delta \mathbf{X}. \tag{11.33}$$

[1]For technical reasons beyond the scope of this work, $\mathbf{v}_u$ is not the exact underdamped local mean velocity, but it differs from the actual local mean velocity by to a correction that does not alter the dynamics.

11.3 Optimal shortcut geometry

A key insight from [77] was further expanded in [80]: for both overdamped and underdamped dynamics, the dissipation during a shortcutted protocol may be written as a simple quadratic in the auxiliary Hamiltonians

$$W_{\text{ex,over}} = \frac{1}{\gamma}\int_0^\tau \langle \nabla H_{\text{aux}}^2 \rangle_{\text{eq,base}} \tag{11.34a}$$

$$W_{\text{ex,under}} = \gamma \int_0^\tau \langle \nabla_{\mathbf{p}} H_{\text{aux}}^2 \rangle_{\text{eq,base}} \, , \tag{11.34b}$$

where γ is the damping coefficient and $\langle \cdot \rangle_{\text{eq,base}}$ indicates an instantaneous equilibrium average, i.e. carrying out the average at each time for $\rho(t) = \rho_{\text{eq,base}}(t)$. If, as is often the case, we are interested particularly in parametric control such that $H_{\text{base}}(t) = H_{\text{base}}(\boldsymbol{\lambda}(t))$, then the governing dynamics ensure $H_{\text{aux}}(t)$ may be written as $H_{\text{aux}}(t) = \mathbf{f}(t) \cdot \dot{\boldsymbol{\lambda}}$ as noted previously (see above Eq. (11.33)). Under this construction,

$$W_{\text{ex,over}} = \frac{1}{\gamma}\int_0^\tau \sum_{\mu\nu} \dot{\lambda}_\mu \langle \nabla f_\mu \cdot \nabla f_\nu \rangle_{\text{eq,base}} \dot{\lambda}_\nu \tag{11.35a}$$

$$W_{\text{ex,under}} = \gamma \int_0^\tau \sum_{\mu\nu} \dot{\lambda}_\mu \langle \nabla_{\mathbf{p}} f_\mu \cdot \nabla_{\mathbf{p}} f_\nu \rangle_{\text{eq,base}} \dot{\lambda}_\nu . \tag{11.35b}$$

Importantly, much like in thermdoynamic geometry [106], the matrices $\langle \nabla f_\mu \cdot \nabla f_\nu \rangle_{\text{eq,base}}$ in the overdamped case and $\langle \nabla_{\mathbf{p}} f_\mu \cdot \nabla_{\mathbf{p}} f_\nu \rangle_{\text{ieq}}$ in the underdamped case both satisfy the requisite axioms to be a metric tensor in the space of parametric control parameters, again lending a geometric interpretation to the space of control [80]. We define them as the *shortcut tensor*, $g_{\mu\nu}^{\text{shortcut}}$. One can then carry out geometric optimization following precisely the same line of reasoning as for thermodynamic geometry. We would like to clarify, however, that *a priori* these are distinct geometries solving distinct problems. Thermodynamic geometry stems from dynamic linear response and accurately describes parametric control for slowly driven systems. Shortcut geometry, in contrast, places no constraint on the protocol duration, so long as an auxiliary Hamiltonian is added ensuring the system stays in an instantaneous (base) equilibrium state at all times. Nevertheless, these two problems are intimately linked.

11.4 Unifying thermodynamic geometries

To proceed, let us consider the thermodynamic metric introduced in Part III:

$$g_{\mu\nu} = \int dt \, \langle \delta X_\mu(0) \delta X_\nu(t) \rangle \, . \tag{11.36}$$

We may write this equation in a more universal manner by utilizing the Backward Kolmogorov operator. In particular, we may write the (formal) expression

$$\delta X_\mu(t) = e^{\mathcal{L}t}\delta X_\mu \tag{11.37}$$

Combining Eqs. 11.36 and 11.37, we may write

$$g_{\mu\nu} = \int dt\, \langle \delta X_\mu e^{\mathcal{L}t}\delta X_\nu\rangle \tag{11.38}$$

Now, let us restrict our attention to the case where the Hamiltonian and the thermodynamic forces are both even in momenta. Although seemingly restrictive, this is the typical case, especially for Hamiltonians of the form $H = \mathbf{p}^2/2m + V(\mathbf{x}, \boldsymbol{\lambda})$. We should further note, this places no restriction whatsoever on overdamped systems that, by definition, have no dependence on $\mathbf{p}$. Under this assumption, we define the overbar operation as

$$\bar{f}(\mathbf{p}) = f(-\mathbf{p}). \tag{11.39}$$

for an arbitrary function f. By symmetry, we must have

$$g_{\mu\nu} = \int dt \int d\mathbf{x} d\overline{\mathbf{p}\rho_{\rm eq}}\overline{\delta X_\mu} e^{\bar{\mathcal{L}}t}\overline{\delta X_\nu} = \int dt \int d\mathbf{x} d\overline{\mathbf{p}}\rho_{\rm eq}\delta X_\mu e^{\bar{\mathcal{L}}t}\delta X_\nu = \int dt\, \langle \delta X_\mu e^{\bar{\mathcal{L}}t}\delta X_\nu\rangle\,. \tag{11.40}$$

Finally, let us carry out a formal integration in t:

$$g_{\mu\nu} = \int dt\, \langle \delta X_\mu e^{\bar{\mathcal{L}}t}\delta X_\nu\rangle = -\langle \delta X_\mu \bar{\mathcal{L}}^{-1}\delta X_\nu\rangle\,, \tag{11.41}$$

where the inverse is defined in terms of the appropriate Green's function of the momentum-reversed Backward Kolmogorov operator [272]. Critically, following Eq. (11.33), this expectation may be rewritten in terms of the shortcut auxiliary Hamiltonian:

$$g_{\mu\nu} = -\langle \delta X_\mu \bar{\mathcal{L}}^{-1}\delta X_\nu\rangle = -\langle f_\mu \bar{\mathcal{L}} f_\nu\rangle\,, \tag{11.42}$$

where we have implicitly invoked the symmetry of $g_{\mu\nu}$. The forms of the time-reversed Backward Kolmogorov operator are given in Eqs. (11.19) and (11.31):

$$\begin{aligned} g^{\rm over}_{\mu\nu} &= -\langle f_\mu \bar{\mathcal{L}} f_\nu\rangle = -\langle f_\mu \rho_{\rm eq}^{-1}\nabla\cdot(\rho_{\rm eq}\nabla f_\nu)\rangle \\ &= \langle \nabla f_\mu\cdot\nabla f_\nu\rangle = g^{\rm over,\ shortcut}_{\mu\nu} \end{aligned} \tag{11.43a}$$

$$\begin{aligned} g^{\rm under}_{\mu\nu} &= -\langle f_\mu \bar{\mathcal{L}} f_\nu\rangle = -\langle f_\mu \rho_{\rm eq}^{-1}\nabla_u\cdot(\rho_{\rm eq}\Gamma\cdot\nabla_u f_\nu)\rangle \\ &= \langle \nabla_u f_\mu\cdot\Gamma\nabla_u f_\nu\rangle = \langle \nabla_{\mathbf{p}} f_\mu\cdot\nabla_{\mathbf{p}} f_\nu\rangle = g^{\rm under,\ shortcut}_{\mu\nu}, \end{aligned} \tag{11.43b}$$

which is to say the thermodynamic and shortcut geometries are *identical*. This unifies the two main topics of this thesis: optimization of engineered dynamics for shortcutted open classical systems is an *identical* problem to the optimal control problem of thermodynamic geometry.

11.5 Thermodynamic geometry and the equilibrium Wasserstein manifold

Over the last few years, a major advance in optimal control of nonequilibriium thermodynamics has revealed a connection to the mathematical field of Optimal Transport (OT) [293, 97, 63, 98, 94]. OT deals with the question of how to transform between two probability distributions while minimizing some objective function. For example, for a distribution over one variable, we may consider the cost to transport between $\rho_0(x)$ and $\rho_f(y)$. A standard cost function could be the L^p norm to move a unit of probability mass:

$$\left(\int |x-y|^p dJ(x,y) \right)^{1/p}, \tag{11.44}$$

where $J(x,y)$ is a joint distribution with marginals given $\int J(x,y)dy = \rho_0(x)$, and $\int J(x,y)dx = \rho_f(y)$. This notion of cost therefore measures the *horizontal* distance transported by each unit of probability mass during the transformation. OT, growing initially out of questions in optimal engineering design, seeks to minimize this quantity and has yielded a number of profound results over the recent few decades [293]. For our case, we highlight that the infinum of the cost in Eq. (11.44) over all joint distributions defines a metric,

$$\mathcal{W}_p(\rho_0,\rho_f) = \inf_{J\in\mathcal{J}(p_0,p_f)} \left(\int |\mathbf{x}-\mathbf{y}|^p dJ(\mathbf{x},\mathbf{y}) \right)^{1/p}, \tag{11.45}$$

where $\mathcal{J}(p_0,p_f)$ denotes the set of all possible joint distributions. This is the *p-Wasserstein distance*, inducing a metric structure on the space of joint probability distributions.

Following a reformulation due to Benamou and Brenier [294], the Wasserstein distance can be brought into a form that is directly connected with stochastic thermodynamics. In particular, for continuous overdamped systems, the minimum entropy production is given by the 2-Wasserstein distance between initial and final distributions [295, 296]:

$$\Sigma_\tau \geq \frac{\mathcal{W}_2(\rho_0,\rho_f)^2}{\tau D}, \tag{11.46}$$

where Σ_τ denotes total entropy production over duration τ, and D is the diffusion constant. Similar notions have since been extended to discrete classical and quantum systems [98] and there have been some suggestive results for underdamped dynamics [295]. It bears mentioning that, although Eq. (11.46) is a strict bound, it is not always accessible given possible limitations of experimental control. For full control of the potential in 1D, one can always construct the sufficient protocol to meet the bound, though generically, and especially for parametric control, the control may not be sufficiently *expressive* to saturate Eq. (11.46).

In a recent work [99], focusing exclusively on continuous overdamped systems, Zhong and DeWeese showed a far broader unification beyond simply the thermodynamic and shortcut geometries. In particular, they demonstrated that both thermodynamic geometry and shortcut geometry are manifestations of Wasserstein geometry for paths in probability space restricted to follow equilibrium manifolds: the equilibrium Wasserstein manifold. This captures not only the simple unification of thermodynamic and shortcut geometries as shown previously, but also demonstrates how they fit into the broader picture of absolute optimal control. Here, we have demonstrated not only that thermodynamic and shortcut gemeotries are identical for overdamped systems but also for underdamped systems so long as these systems satisfy the symmetry $p \to -p$. This is a highly suggestive result, leading us to conjecture that there may likewise be an equilibrium Wasserstein-like manifold for underdamped dynamics, and more broadly for the increasing class of systems observed to be well-described by Optimal Transport.

11.6 Outlook

In this chapter, we have demonstrated a connection between shortcut protocols, which formed the major focus of Part II, and thermodynamic geometry, which was the major focus of Part III. In particular, we derived a unification of geometric descriptions for optimal control of classical thermodynamic systems when driven out of equilibrium, either via a finite-time engineered shortcut or through slow manipulation.

Beyond the inherent value of this result, the unification also has pragmatic implications. Calculations of the thermodynamic metric generally involves the evaluation of correlation functions by analytical techniques or simulation. Evaluation of the shortcut metric involves the solution of a partial differential equation Eq. (11.33). Given the equivalence of these metrics, either method can now be used to derive either metric, making the derivation significantly more flexible and feasible for a wider class of physical systems. In particular, shortcut geometries have been analytically derived for Hamiltonians of the form $H = p^2 + 1/nx^n$ for even integers n [77], whereas analytical results for underdamped thermodynamic geometries are typically restricted to quadratic potentials. This unification immediately allows us to identify the thermodynamic metric for these more complicated potentials as the same as the previously derived ones for shortcut geometry [77].

This unification was previously known for overdamped systems, though we extended it here for the first time to underdamped systems. That said, we restricted our attention to systems that are even in momenta. This immediately begs the question of whether there is a broader class for which this equivalence may hold, particularly for systems satisfying time-reversal symmetry. Although not technically the same constraint, reversal of momenta is a major component of the time-reversal operation. Extending this result would allow for wider application of these methods and deeper understanding of the fundamental connection between these two geometric approaches. Further, the connection to Optimal Transport theory and Wasserstein geometry that this unification entails in the overdamped limit is

highly suggestive of similar results for the underdamped regime.

It bears mentioning that we only focused here on classical open systems, though, as detailed in Ch. 5, shortcut engineering techniques have been applied widely, such as for quantum dynamics and even active matter, as we demonstrated in Ch. 7. To date, there already exist thermodynamic geometric techniques for quantum and, recently, active systems, but to our knowledge there are no major geometric techniques for quantum or active shortcuts. This unification suggests both the potential for the existence of such a geometric construction and its identification with the thermodynamic geometric methods that have already been developed.

Finally, as described in Sec. 4.3, there are a wide range of approximation schemes used for various parameter regimes in optimal control. Ultimately, as given in Eq. (11.46), the Wasserstein metric sets a fundamental bound on overdamped thermodynamic systems. The previous unification [99] of thermodynamic geometry with Wasserstein geometry demonstrated that thermodynamic geometry is *precisely* Wasserstein geometry when restricted to paths on an equilibrium manifold for the parametric control $\rho(t) = \rho_{\text{eq}}(\boldsymbol{\lambda})$. Following this case, we conjecture that there may be further unifications to be established reinterpreting various approximation regimes as restricted forms of the absolute optimal control problem, Wasserstein geometry.

Bibliography

[1] Erwin Schrödinger. *What is life? The physical aspect of the living cell*. Cambridge University Press, 1944.

[2] George E. Smith. "The vis viva dispute: A controversy at the dawn of dynamics". In: *Physics Today* 59.10 (July 2006), pp. 31–36. DOI: 10.1063/1.2387086. URL: https://doi.org/10.1063/1.2387086.

[3] Thomas Young. *A course of lectures on natural philosophy and the mechanical arts: in two volumes*. Vol. 2. Johnson, 1807.

[4] Sadi Carnot. "Reflections on the motive power of fire, and on machines fitted to develop that power". In: *Paris: Bachelier* 108.1824 (1824), p. 1824.

[5] Florian Cajori. "On the history of caloric". In: *Isis* 4.3 (1922), pp. 483–492.

[6] Benoit-Paul Emile Clapeyron. "Memoir sur la puissance motrice de la chaleur". In: *Journal de l'École royale polytechnique* (1834), pp. 153–190.

[7] Hermann von Helmholtz. *Über die Erhaltung der Kraft*. Humboldt-Universität zu Berlin, 1847.

[8] Rudolf Clausius. "Über die bewegende Kraft der Wärme und die Gesetze, welche sich daraus für die Wärmelehre selbst ableiten lassen". In: *Annalen der Physik* 155.3 (1850), pp. 368–397.

[9] Rudolf Clausius. "Über eine veränderte Form des zweiten Hauptsatzes der mechanischen Wärmetheorie". In: *Annalen der Physik* 169.12 (1854), pp. 481–506.

[10] Daniel V Schroeder. *An introduction to thermal physics*. Oxford University Press, 2020.

[11] Rudolf Clausius. *The Mechanical Theory of Heat*. Macmillan, 1879.

[12] Rudolf Julius Emanuel Clausius. *Über die Art der Bewegung, welche wir Wärme nennen*. Verlag nicht ermittelbar, 1857.

[13] James Clerk Maxwell. "Illustrations of the Dynamical Theory of Gases". In: *The Kinetic Theory of Gases*. Vol. Volume 1. History of Modern Physical Sciences. Imperial College Press, 2024/07/10 2003, pp. 148–171. ISBN: 978-1-86094-347-8. DOI: doi:10.1142/9781848161337{_}0011. URL: https://doi.org/10.1142/9781848161337_0011.

[14] Carlo Cercignani and Roger Penrose. *Ludwig Boltzmann: The Man Who Trusted Atoms*. Oxford University Press, July 2006. ISBN: 9780198570646. DOI: 10.1093/acprof:oso/9780198570646.001.0001. URL: https://doi.org/10.1093/acprof:oso/9780198570646.001.0001.

[15] "Weitere Studien über das Wärmegleichgewicht unter Gas-molekülen". In: *Wissenschaftliche Abhandlungen*. Ed. by Ludwig Boltzmann and Friedrich Hasenöhrl. Vol. 1. Cambridge Library Collection - Physical Sciences. Cambridge: Cambridge University Press, 2012, pp. 316–402. ISBN: 9781108052795. DOI: DOI:10.1017/CBO9781139381420.023. URL: https://www.cambridge.org/core/product/A5DBDBCADB8E78D27D1E8DFCFF31443D.

[16] S. H. Burbury. "XXXV. On some problems in the kinetic theory of gases". In: *The London, Edinburgh, and Dublin Philosophical Magazine and Journal of Science* 30.185 (Oct. 1890), pp. 298–317. DOI: 10.1080/14786449008620029. URL: https://doi.org/10.1080/14786449008620029.

[17] Clayton A. Gearhart. "Boltzmann's Atom: The Great Debate that Launched a Revolution in Physics". In: *Physics Today* 54.9 (July 2001), pp. 53–53. DOI: 10.1063/1.1420513. URL: https://doi.org/10.1063/1.1420513.

[18] Ta-You Wu. "Boltzmann'sH theorem and the Loschmidt and the Zermelo paradoxes". In: *International Journal of Theoretical Physics* 14.5 (1975), pp. 289–294. DOI: 10.1007/BF01807856. URL: https://doi.org/10.1007/BF01807856.

[19] Jos Uffink. "Boltzmann's Work in Statistical Physics". In: ed. by Edward N. Zalta. Summer 2022. 2022.

[20] Max Planck. "Über das Gesetz der Energieverteilung im Normalspectrum". In: *Annalen der Physik* 309.3 (2024/07/10 1901), pp. 553–563. DOI: https://doi.org/10.1002/andp.19013090310. URL: https://doi.org/10.1002/andp.19013090310.

[21] "The Collected Works of J. Willard Gibbs". In: *Nature* 124.3117 (1929), pp. 119–120. DOI: 10.1038/124119a0. URL: https://doi.org/10.1038/124119a0.

[22] Josiah Willard Gibbs. *Elementary Principles in Statistical Mechanics: Developed with Especial Reference to the Rational Foundation of Thermodynamics*. Cambridge Library Collection - Mathematics. Cambridge: Cambridge University Press, 2010. ISBN: 9781108017022. DOI: DOI:10.1017/CBO9780511686948. URL: https://www.cambridge.org/core/product/E7AB3B94A215CF4E3A193C092F29856A.

[23] Paul Ehrenfest. "Welche Züge der Lichtquantenhypothese spielen in der Theorie der Wärmestrahlung eine wesentliche Rolle?" In: *Annalen der Physik* 341.11 (1911), pp. 91–118.

[24] Lars Onsager. "Reciprocal Relations in Irreversible Processes. I." In: *Phys. Rev.* 37 (4 Feb. 1931), pp. 405–426. DOI: 10.1103/PhysRev.37.405. URL: https://link.aps.org/doi/10.1103/PhysRev.37.405.

[25] "Über den Magnetismus der galvanischen Kette". In: *Abhadlungen der Physikalischen Klasse der Königlisch-Preußsischen* (1822).

[26] Peltier. "Nouvelles expériences sur la caloricité des courants électrique". In: *Annales de Chimie et de Physique* 56 (1834).

[27] Herbert B. Callen. "The Application of Onsager's Reciprocal Relations to Thermoelectric, Thermomagnetic, and Galvanomagnetic Effects". In: *Phys. Rev.* 73 (11 June 1948), pp. 1349–1358. DOI: 10.1103/PhysRev.73.1349. URL: https://link.aps.org/doi/10.1103/PhysRev.73.1349.

[28] URL: https://www.nobelprize.org/prizes/chemistry/1968/.

[29] "Moderation et Transformations Irreversibles des Systemes Ouverts". In: *Bulletin de la Classe des Sciences* 31 (1945).

[30] Martin J. Klein and Paul H. E. Meijer. "Principle of Minimum Entropy Production". In: *Phys. Rev.* 96 (2 Oct. 1954), pp. 250–255. DOI: 10.1103/PhysRev.96.250. URL: https://link.aps.org/doi/10.1103/PhysRev.96.250.

[31] Lars Onsager. *The Motion of Ions: Principles and Concepts*. Dec. 1968. URL: https://www.nobelprize.org/prizes/chemistry/1968/onsager/lecture/.

[32] L. Onsager and S. Machlup. "Fluctuations and Irreversible Processes". In: *Phys. Rev.* 91 (6 Sept. 1953), pp. 1505–1512. DOI: 10.1103/PhysRev.91.1505. URL: https://link.aps.org/doi/10.1103/PhysRev.91.1505.

[33] S. Machlup and L. Onsager. "Fluctuations and Irreversible Process. II. Systems with Kinetic Energy". In: *Phys. Rev.* 91 (6 Sept. 1953), pp. 1512–1515. DOI: 10.1103/PhysRev.91.1512. URL: https://link.aps.org/doi/10.1103/PhysRev.91.1512.

[34] R Kubo. "The fluctuation-dissipation theorem". In: *Reports on Progress in Physics* 29.1 (Jan. 1966), p. 255. DOI: 10.1088/0034-4885/29/1/306. URL: https://dx.doi.org/10.1088/0034-4885/29/1/306.

[35] Melville S. Green. "Markoff Random Processes and the Statistical Mechanics of Time-Dependent Phenomena". In: *The Journal of Chemical Physics* 20.8 (Aug. 1952), pp. 1281–1295. ISSN: 0021-9606. DOI: 10.1063/1.1700722. eprint: https://pubs.aip.org/aip/jcp/article-pdf/20/8/1281/18800929/1281_1_online.pdf. URL: https://doi.org/10.1063/1.1700722.

[36] Melville S. Green. "Markoff Random Processes and the Statistical Mechanics of Time-Dependent Phenomena. II. Irreversible Processes in Fluids". In: *The Journal of Chemical Physics* 22.3 (Mar. 1954), pp. 398–413. ISSN: 0021-9606. DOI: 10.1063/1.1740082. eprint: https://pubs.aip.org/aip/jcp/article-pdf/22/3/398/18804401/398_1_online.pdf. URL: https://doi.org/10.1063/1.1740082.

[37] Ryogo Kubo. "Statistical-Mechanical Theory of Irreversible Processes. I. General Theory and Simple Applications to Magnetic and Conduction Problems". In: *Journal of the Physical Society of Japan* 12.6 (1957), pp. 570–586. DOI: 10.1143/JPSJ.12.570. eprint: https://doi.org/10.1143/JPSJ.12.570. URL: https://doi.org/10.1143/JPSJ.12.570.

[38] R Zwanzig. "Time-Correlation Functions and Transport Coefficients in Statistical Mechanics". In: *Annual Review of Physical Chemistry* 16.Volume 16, (1965), pp. 67–102. ISSN: 1545-1593. DOI: https://doi.org/10.1146/annurev.pc.16.100165.000435. URL: https://www.annualreviews.org/content/journals/10.1146/annurev.pc.16.100165.000435.

[39] David Chandler. *Introduction to modern statistical mechanics*. New York, NY: Oxford University Press, Sept. 1987.

[40] *Time, Structure and Fluctuations*. Dec. 1977. URL: https://www.nobelprize.org/prizes/chemistry/1977/prigogine/lecture/.

[41] Denis J. Evans, E. G. D. Cohen, and G. P. Morriss. "Probability of second law violations in shearing steady states". In: *Phys. Rev. Lett.* 71 (15 Oct. 1993), pp. 2401–2404. DOI: 10.1103/PhysRevLett.71.2401. URL: https://link.aps.org/doi/10.1103/PhysRevLett.71.2401.

[42] G. Gallavotti and E. G. D. Cohen. "Dynamical Ensembles in Nonequilibrium Statistical Mechanics". In: *Phys. Rev. Lett.* 74 (14 Apr. 1995), pp. 2694–2697. DOI: 10.1103/PhysRevLett.74.2694. URL: https://link.aps.org/doi/10.1103/PhysRevLett.74.2694.

[43] Jorge Kurchan. "Fluctuation theorem for stochastic dynamics". In: *Journal of Physics A: Mathematical and General* 31.16 (Apr. 1998), p. 3719. DOI: 10.1088/0305-4470/31/16/003. URL: https://dx.doi.org/10.1088/0305-4470/31/16/003.

[44] Joel L. Lebowitz and Herbert Spohn. "A Gallavotti–Cohen-Type Symmetry in the Large Deviation Functional for Stochastic Dynamics". In: *Journal of Statistical Physics* 95.1 (1999), pp. 333–365. DOI: 10.1023/A:1004589714161. URL: https://doi.org/10.1023/A:1004589714161.

[45] Udo Seifert. "Stochastic thermodynamics, fluctuation theorems and molecular machines". In: *Reports on Progress in Physics* 75.12 (Nov. 2012), p. 126001. DOI: 10.1088/0034-4885/75/12/126001. URL: https://doi.org/10.1088/0034-4885/75/12/126001.

[46] C. Jarzynski. "Nonequilibrium Equality for Free Energy Differences". In: *Phys. Rev. Lett.* 78 (14 Apr. 1997), pp. 2690–2693. DOI: 10.1103/PhysRevLett.78.2690. URL: https://link.aps.org/doi/10.1103/PhysRevLett.78.2690.

[47] C. Jarzynski. "Equilibrium free-energy differences from nonequilibrium measurements: A master-equation approach". In: *Phys. Rev. E* 56 (5 Nov. 1997), pp. 5018–5035. DOI: 10.1103/PhysRevE.56.5018. URL: https://link.aps.org/doi/10.1103/PhysRevE.56.5018.

[48] D. H. E. Gross. *Flaw of Jarzynski's equality when applied to systems with several degrees of freedom*. 2005. arXiv: cond-mat/0508721 [cond-mat.stat-mech]. URL: https://arxiv.org/abs/cond-mat/0508721.

[49] Christopher Jarzynski. *Reply to comments by D.H.E. Gross*. 2005. arXiv: cond-mat/0509344 [cond-mat.stat-mech]. URL: https://arxiv.org/abs/cond-mat/0509344.

[50] Gavin E. Crooks. "Entropy production fluctuation theorem and the nonequilibrium work relation for free energy differences". In: *Phys. Rev. E* 60 (3 Sept. 1999), pp. 2721–2726. DOI: 10.1103/PhysRevE.60.2721. URL: https://link.aps.org/doi/10.1103/PhysRevE.60.2721.

[51] D. Collin et al. "Verification of the Crooks fluctuation theorem and recovery of RNA folding free energies". In: *Nature* 437.7056 (2005), pp. 231–234. DOI: 10.1038/nature04061. URL: https://doi.org/10.1038/nature04061.

[52] Massimiliano Esposito et al. "Efficiency at Maximum Power of Low-Dissipation Carnot Engines". In: *Phys. Rev. Lett.* 105 (15 Oct. 2010), p. 150603. DOI: 10.1103/PhysRevLett.105.150603. URL: https://link.aps.org/doi/10.1103/PhysRevLett.105.150603.

[53] Ken Sekimoto. "Langevin Equation and Thermodynamics". In: *Progress of Theoretical Physics Supplement* 130 (1998), pp. 17–27. DOI: 10.1143/PTPS.130.17. URL: https://doi.org/10.1143/PTPS.130.17.

[54] Udo Seifert. "Entropy Production along a Stochastic Trajectory and an Integral Fluctuation Theorem". In: *Phys. Rev. Lett.* 95 (4 July 2005), p. 040602. DOI: 10.1103/PhysRevLett.95.040602. URL: https://link.aps.org/doi/10.1103/PhysRevLett.95.040602.

[55] L.P. Kadanoff. *Statics, Dynamics and Renormalization*. World Scientific Publishing Company, 2000.

[56] James Maxwell. *Theory of heat*. Dover Books on Physics. Mineola, NY: Dover Publications, June 2001.

[57] L Szilard. "Über die Entropieverminderung in einem thermodynamischen System bei Eingriffen intelligenter Wesen". de. In: *Eur. Phys. J. A* 53.11-12 (Nov. 1929), pp. 840–856.

[58] Andrew Rex. "Maxwell's Demon—A Historical Review". In: *Entropy* 19.6 (2017). DOI: 10.3390/e19060240.

[59] Takahiro Sagawa and Masahito Ueda. "Nonequilibrium thermodynamics of feedback control". In: *Phys. Rev. E* 85 (2 Feb. 2012), p. 021104. DOI: 10.1103/PhysRevE.85.021104. URL: https://link.aps.org/doi/10.1103/PhysRevE.85.021104.

[60] Tushar K Saha et al. "Maximizing power and velocity of an information engine". en. In: *Proc. Natl. Acad. Sci.* 118.20 (May 2021), e2023356118.

[61] Juan M. R. Parrondo, Jordan M. Horowitz, and Takahiro Sagawa. "Thermodynamics of information". In: *Nature Physics* 11.2 (2015), pp. 131–139. DOI: 10.1038/nphys3230. URL: https://doi.org/10.1038/nphys3230.

[62] Charles H Bennett. "Notes on Landauer's principle, reversible computation, and Maxwell's Demon". en. In: *Stud. Hist. Philos. Sci. B Stud. Hist. Philos. Modern Phys.* 34.3 (Sept. 2003), pp. 501–510.

[63] Karel Proesmans, Jannik Ehrich, and John Bechhoefer. "Finite-Time Landauer Principle". In: *Phys. Rev. Lett.* 125 (10 Sept. 2020), p. 100602. DOI: 10.1103/PhysRevLett.125.100602. URL: https://link.aps.org/doi/10.1103/PhysRevLett.125.100602.

[64] Karel Proesmans, Jannik Ehrich, and John Bechhoefer. "Optimal finite-time bit erasure under full control". In: *Phys. Rev. E* 102 (3 Sept. 2020), p. 032105. DOI: 10.1103/PhysRevE.102.032105. URL: https://link.aps.org/doi/10.1103/PhysRevE.102.032105.

[65] Stuart A. Rice. "Ilya Prigogine". In: *Physics Today* 57.4 (July 2004), pp. 102–103. DOI: 10.1063/1.1752434. URL: https://doi.org/10.1063/1.1752434.

[66] Tim Schmiedl and Udo Seifert. "Stochastic thermodynamics of chemical reaction networks". In: *The Journal of Chemical Physics* 126.4 (July 2007), p. 044101. DOI: 10.1063/1.2428297. URL: https://doi.org/10.1063/1.2428297.

[67] Riccardo Rao and Massimiliano Esposito. "Nonequilibrium Thermodynamics of Chemical Reaction Networks: Wisdom from Stochastic Thermodynamics". In: *Phys. Rev. X* 6 (4 Dec. 2016), p. 041064. DOI: 10.1103/PhysRevX.6.041064. URL: https://link.aps.org/doi/10.1103/PhysRevX.6.041064.

[68] Yoshitsugu Oono and Marco Paniconi. "Steady State Thermodynamics". In: *Progress of Theoretical Physics Supplement* 130 (July 1998), pp. 29–44. DOI: 10.1143/PTPS.130.29. URL: https://doi.org/10.1143/PTPS.130.29.

[69] Takahiro Hatano and Shin-ichi Sasa. "Steady-State Thermodynamics of Langevin Systems". In: *Phys. Rev. Lett.* 86 (16 Apr. 2001), pp. 3463–3466. DOI: 10.1103/PhysRevLett.86.3463. URL: https://link.aps.org/doi/10.1103/PhysRevLett.86.3463.

[70] J. Prost, J.-F. Joanny, and J. M. R. Parrondo. "Generalized Fluctuation-Dissipation Theorem for Steady-State Systems". In: *Phys. Rev. Lett.* 103 (9 Aug. 2009), p. 090601. DOI: 10.1103/PhysRevLett.103.090601. URL: https://link.aps.org/doi/10.1103/PhysRevLett.103.090601.

[71] Andre C. Barato and Udo Seifert. "Thermodynamic Uncertainty Relation for Biomolecular Processes". In: *Phys. Rev. Lett.* 114 (15 Apr. 2015), p. 158101. DOI: 10.1103/PhysRevLett.114.158101. URL: https://link.aps.org/doi/10.1103/PhysRevLett.114.158101.

[72] Todd R. Gingrich et al. "Dissipation Bounds All Steady-State Current Fluctuations". In: *Phys. Rev. Lett.* 116 (12 Mar. 2016), p. 120601. DOI: 10.1103/PhysRevLett.116.120601. URL: https://link.aps.org/doi/10.1103/PhysRevLett.116.120601.

[73] Jordan M. Horowitz and Todd R. Gingrich. "Thermodynamic uncertainty relations constrain non-equilibrium fluctuations". In: *Nature Physics* 16.1 (2020), pp. 15–20. DOI: 10.1038/s41567-019-0702-6. URL: https://doi.org/10.1038/s41567-019-0702-6.

[74] Bjarne Andresen, Peter Salamon, and R. Stephen Berry. "Thermodynamics in finite time". In: *Physics Today* 37.9 (July 1984), pp. 62–70. DOI: 10.1063/1.2916405. URL: https://doi.org/10.1063/1.2916405.

[75] Bjarne Andresen and Peter Salamon. "Future Perspectives of Finite-Time Thermodynamics". In: *Entropy* 24.5 (2022). DOI: 10.3390/e24050690.

[76] Kay Brandner and Keiji Saito. "Thermodynamic Geometry of Microscopic Heat Engines". In: *Phys. Rev. Lett.* 124 (4 Jan. 2020), p. 040602. DOI: 10.1103/PhysRevLett.124.040602. URL: https://link.aps.org/doi/10.1103/PhysRevLett.124.040602.

[77] Geng Li, H. T. Quan, and Z. C. Tu. "Shortcuts to isothermality and nonequilibrium work relations". In: *Phys. Rev. E* 96 (1 July 2017), p. 012144. DOI: 10.1103/PhysRevE.96.012144. URL: https://link.aps.org/doi/10.1103/PhysRevE.96.012144.

[78] D. Guéry-Odelin et al. "Shortcuts to adiabaticity: Concepts, methods, and applications". In: *Rev. Mod. Phys.* 91 (4 Oct. 2019), p. 045001. DOI: 10.1103/RevModPhys.91.045001. URL: https://link.aps.org/doi/10.1103/RevModPhys.91.045001.

[79] Alexander B. Boyd et al. "Shortcuts to Thermodynamic Computing: The Cost of Fast and Faithful Information Processing". In: *Journal of Statistical Physics* 187.2 (2022), p. 17. DOI: 10.1007/s10955-022-02871-0. URL: https://doi.org/10.1007/s10955-022-02871-0.

[80] Geng Li et al. "Geodesic Path for the Minimal Energy Cost in Shortcuts to Isothermality". In: *Phys. Rev. Lett.* 128 (23 June 2022), p. 230603. DOI: 10.1103/PhysRevLett.128.230603. URL: https://link.aps.org/doi/10.1103/PhysRevLett.128.230603.

[81] Yonggun Jun and Pik-Yin Lai. "Minimal dissipation protocols of an instantaneous equilibrium Brownian particle under time-dependent temperature and potential variations". In: *Phys. Rev. Res.* 4 (2 May 2022), p. 023157. DOI: 10.1103/PhysRevResearch.4.023157. URL: https://link.aps.org/doi/10.1103/PhysRevResearch.4.023157.

[82] Sai Vinjanampathy and Janet Anders. "Quantum thermodynamics". In: *Contemporary Physics* 57.4 (Oct. 2016), pp. 545–579. DOI: 10.1080/00107514.2016.1201896. URL: https://doi.org/10.1080/00107514.2016.1201896.

[83] Nathan M. Myers, Obinna Abah, and Sebastian Deffner. "Quantum thermodynamic devices: From theoretical proposals to experimental reality". In: *AVS Quantum Science* 4.2 (July 2022), p. 027101. DOI: 10.1116/5.0083192. URL: https://doi.org/10.1116/5.0083192.

[84] Ken Funo, Masahito Ueda, and Takahiro Sagawa. "Quantum Fluctuation Theorems". In: *Thermodynamics in the Quantum Regime: Fundamental Aspects and New Directions*. Ed. by Felix Binder et al. Cham: Springer International Publishing, 2018, pp. 249–273. ISBN: 978-3-319-99046-0. DOI: 10.1007/978-3-319-99046-0{_}10. URL: https://doi.org/10.1007/978-3-319-99046-0_10.

[85] Nobuhiko Taniguchi. "Quantum thermodynamics of nanoscale steady states far from equilibrium". In: *Phys. Rev. B* 97 (15 Apr. 2018), p. 155404. DOI: 10.1103/PhysRevB.97.155404. URL: https://link.aps.org/doi/10.1103/PhysRevB.97.155404.

[86] Yoshihiko Hasegawa. "Quantum Thermodynamic Uncertainty Relation for Continuous Measurement". In: *Phys. Rev. Lett.* 125 (5 July 2020), p. 050601. DOI: 10.1103/PhysRevLett.125.050601. URL: https://link.aps.org/doi/10.1103/PhysRevLett.125.050601.

[87] Patrick R. Zulkowski and Michael R. DeWeese. "Optimal protocols for slowly driven quantum systems". In: *Phys. Rev. E* 92 (3 Sept. 2015), p. 032113. DOI: 10.1103/PhysRevE.92.032113. URL: https://link.aps.org/doi/10.1103/PhysRevE.92.032113.

[88] Matteo Scandi and Martí Perarnau-Llobet. "Thermodynamic length in open quantum systems". In: *Quantum* 3 (Oct. 2019), p. 197. ISSN: 2521-327X. DOI: 10.22331/q-2019-10-24-197. URL: https://doi.org/10.22331/q-2019-10-24-197.

[89] Sebastian Deffner and Marcus V. S. Bonança. "Thermodynamic control —An old paradigm with new applications". In: *Europhysics Letters* 131.2 (2020), p. 20001. DOI: 10.1209/0295-5075/131/20001. URL: https://dx.doi.org/10.1209/0295-5075/131/20001.

[90] John Watrous. *The Theory of Quantum Information*. Cambridge University Press, Apr. 2018. ISBN: 9781107180567. DOI: 10.1017/9781316848142. URL: http://dx.doi.org/10.1017/9781316848142.

[91] Sebastian Deffner and Steve Campbell. *Quantum Thermodynamics*. 2053-2571. Morgan & Claypool Publishers, 2019. ISBN: 978-1-64327-658-8. DOI: 10.1088/2053-2571/ab21c6. URL: https://dx.doi.org/10.1088/2053-2571/ab21c6.

[92] Grigorios A. Pavliotis. *Stochastic Processes and Applications: Diffusion Processes, the Fokker-Planck and Langevin Equations*. Springer New York, 2014. ISBN: 9781493913237. DOI: 10.1007/978-1-4939-1323-7. URL: http://dx.doi.org/10.1007/978-1-4939-1323-7.

[93] Raphaël Chetrite, Paolo Muratore-Ginanneschi, and Kay Schwieger. "E. Schrödinger's 1931 paper "On the Reversal of the Laws of Nature"["Über die Umkehrung der Naturgesetze", Sitzungsberichte der preussischen Akademie der Wissenschaften, physikalisch-mathematische Klasse, 8 N9 144–153]". In: *The European Physical Journal H* 46.1 (2021), p. 28. DOI: 10.1140/epjh/s13129-021-00032-7. URL: https://doi.org/10.1140/epjh/s13129-021-00032-7.

[94] Steven Blaber and David A Sivak. "Optimal control in stochastic thermodynamics". In: *Journal of Physics Communications* 7.3 (2023), p. 033001. DOI: 10.1088/2399-6528/acbf04. URL: https://dx.doi.org/10.1088/2399-6528/acbf04.

[95] Paolo Abiuso et al. "Thermodynamics and optimal protocols of multidimensional quadratic Brownian systems". In: *Journal of Physics Communications* 6.6 (2022), p. 063001. DOI: 10.1088/2399-6528/ac72f8. URL: https://dx.doi.org/10.1088/2399-6528/ac72f8.

[96] Megan C. Engel, Jamie A. Smith, and Michael P. Brenner. "Optimal Control of Nonequilibrium Systems through Automatic Differentiation". In: *Phys. Rev. X* 13 (4 Nov. 2023), p. 041032. DOI: 10.1103/PhysRevX.13.041032. URL: https://link.aps.org/doi/10.1103/PhysRevX.13.041032.

[97] Erik Aurell, Carlos Mejía-Monasterio, and Paolo Muratore-Ginanneschi. "Optimal Protocols and Optimal Transport in Stochastic Thermodynamics". In: *Phys. Rev. Lett.* 106 (25 June 2011), p. 250601. DOI: 10.1103/PhysRevLett.106.250601. URL: https://link.aps.org/doi/10.1103/PhysRevLett.106.250601.

[98] Tan Van Vu and Keiji Saito. "Thermodynamic Unification of Optimal Transport: Thermodynamic Uncertainty Relation, Minimum Dissipation, and Thermodynamic Speed Limits". In: *Phys. Rev. X* 13 (1 Feb. 2023), p. 011013. DOI: 10.1103/PhysRevX.13.011013. URL: https://link.aps.org/doi/10.1103/PhysRevX.13.011013.

[99] Adrianne Zhong and Michael R. DeWeese. *Beyond Linear Response: Equivalence between Thermodynamic Geometry and Optimal Transport*. 2024. arXiv: 2404.01286 [cond-mat.stat-mech]. URL: https://arxiv.org/abs/2404.01286.

[100] Adrianne Zhong and Michael R. DeWeese. "Limited-control optimal protocols arbitrarily far from equilibrium". In: *Phys. Rev. E* 106 (4 Oct. 2022), p. 044135. DOI: 10.1103/PhysRevE.106.044135. URL: https://link.aps.org/doi/10.1103/PhysRevE.106.044135.

[101] Luke K. Davis, Karel Proesmans, and Étienne Fodor. "Active Matter under Control: Insights from Response Theory". In: *Phys. Rev. X* 14 (1 Feb. 2024), p. 011012. DOI: 10.1103/PhysRevX.14.011012. URL: https://link.aps.org/doi/10.1103/PhysRevX.14.011012.

[102] S. Ciliberto. "Experiments in Stochastic Thermodynamics: Short History and Perspectives". In: *Phys. Rev. X* 7 (2 June 2017), p. 021051. DOI: 10.1103/PhysRevX.7.021051. URL: https://link.aps.org/doi/10.1103/PhysRevX.7.021051.

[103] Lucas P. Kamizaki, Marcus V. S. Bonan ça, and Sérgio R. Muniz. "Performance of optimal linear-response processes in driven Brownian motion far from equilibrium". In: *Phys. Rev. E* 106 (6 Dec. 2022), p. 064123. DOI: 10.1103/PhysRevE.106.064123. URL: https://link.aps.org/doi/10.1103/PhysRevE.106.064123.

[104] Steven Blaber, Miranda D. Louwerse, and David A. Sivak. "Steps minimize dissipation in rapidly driven stochastic systems". In: *Phys. Rev. E* 104 (2 Aug. 2021), p. L022101. DOI: 10.1103/PhysRevE.104.L022101. URL: https://link.aps.org/doi/10.1103/PhysRevE.104.L022101.

[105] Pierre Nazé, Sebastian Deffner, and Marcus V S Bonança. "Optimal finite-time processes in weakly driven overdamped Brownian motion". In: *Journal of Physics Communications* 6.8 (2022), p. 083001. DOI: 10.1088/2399-6528/ac871d. URL: https://dx.doi.org/10.1088/2399-6528/ac871d.

[106] David A. Sivak and Gavin E. Crooks. "Thermodynamic Metrics and Optimal Paths". In: *Phys. Rev. Lett.* 108 (19 May 2012), p. 190602. DOI: 10.1103/PhysRevLett.108.190602. URL: https://link.aps.org/doi/10.1103/PhysRevLett.108.190602.

[107] Patrick R. Zulkowski et al. "Geometry of thermodynamic control". In: *Phys. Rev. E* 86 (4 Oct. 2012), p. 041148. DOI: 10.1103/PhysRevE.86.041148. URL: https://link.aps.org/doi/10.1103/PhysRevE.86.041148.

[108] Patrick R. Zulkowski and Michael R. DeWeese. "Optimal control of overdamped systems". In: *Physical Review E* 92.3 (Sept. 2015), p. 032117. ISSN: 1539-3755, 1550-2376. DOI: 10.1103/PhysRevE.92.032117. URL: https://link.aps.org/doi/10.1103/PhysRevE.92.032117.

[109] David A. Sivak and Gavin E. Crooks. "Thermodynamic geometry of minimum-dissipation driven barrier crossing". In: *Phys. Rev. E* 94 (5 Nov. 2016), p. 052106. DOI: 10.1103/PhysRevE.94.052106. URL: https://link.aps.org/doi/10.1103/PhysRevE.94.052106.

[110] Adam G. Frim and Michael R. DeWeese. "Optimal finite-time Brownian Carnot engine". In: *Phys. Rev. E* 105.5 (May 2022), p. L052103.

[111] Adam G. Frim and Michael R. DeWeese. "Geometric Bound on the Efficiency of Irreversible Thermodynamic Cycles". In: *Phys. Rev. Lett.* 128 (23 June 2022), p. 230601. DOI: 10.1103/PhysRevLett.128.230601. URL: https://link.aps.org/doi/10.1103/PhysRevLett.128.230601.

[112] Erik Torrontegui et al. "Chapter 2 - Shortcuts to Adiabaticity". In: *Advances in Atomic, Molecular, and Optical Physics*. Ed. by Ennio Arimondo, Paul R. Berman, and Chun C. Lin. Vol. 62. Academic Press, 2013, pp. 117–169. DOI: https://doi.org/10.1016/B978-0-12-408090-4.00002-5. URL: http://www.sciencedirect.com/science/article/pii/B9780124080904000025.

[113] David Guéry-Odelin et al. "Driving rapidly while remaining in control: classical shortcuts from Hamiltonian to stochastic dynamics". In: *Reports on Progress in Physics* 86.3 (Jan. 2023), p. 035902. DOI: 10.1088/1361-6633/acacad. URL: https://dx.doi.org/10.1088/1361-6633/acacad.

[114] Xi Chen et al. "Fast Optimal Frictionless Atom Cooling in Harmonic Traps: Shortcut to Adiabaticity". In: *Phys. Rev. Lett.* 104 (6 Feb. 2010), p. 063002. DOI: 10.1103/PhysRevLett.104.063002. URL: https://link.aps.org/doi/10.1103/PhysRevLett.104.063002.

[115] Mustafa Demirplak and Stuart A. Rice. "Adiabatic Population Transfer with Control Fields". In: *The Journal of Physical Chemistry A* 107.46 (Nov. 2003), pp. 9937–9945. DOI: 10.1021/jp030708a. URL: https://doi.org/10.1021/jp030708a.

[116] Mustafa Demirplak and Stuart A. Rice. "Assisted Adiabatic Passage Revisited". In: *The Journal of Physical Chemistry B* 109.14 (Apr. 2005), pp. 6838–6844. DOI: 10.1021/jp040647w. URL: https://doi.org/10.1021/jp040647w.

[117] A. Couvert et al. "Optimal transport of ultracold atoms in the non-adiabatic regime". In: *Europhysics Letters* 83.1 (2008), p. 13001. DOI: 10.1209/0295-5075/83/13001. URL: https://dx.doi.org/10.1209/0295-5075/83/13001.

[118] M V Berry. "Transitionless quantum driving". In: *Journal of Physics A: Mathematical and Theoretical* 42.36 (Aug. 2009), p. 365303. DOI: 10.1088/1751-8113/42/36/365303. URL: https://doi.org/10.1088%2F1751-8113%2F42%2F36%2F365303.

[119] F. Motzoi et al. "Simple Pulses for Elimination of Leakage in Weakly Nonlinear Qubits". In: *Phys. Rev. Lett.* 103 (11 Sept. 2009), p. 110501. DOI: 10.1103/PhysRevLett.103.110501. URL: https://link.aps.org/doi/10.1103/PhysRevLett.103.110501.

[120] Tim Schmiedl et al. "Optimal protocols for Hamiltonian and Schrödinger dynamics". In: *Journal of Statistical Mechanics: Theory and Experiment* 2009.07 (2009), P07013. DOI: 10.1088/1742-5468/2009/07/P07013. URL: https://dx.doi.org/10.1088/1742-5468/2009/07/P07013.

[121] Shumpei Masuda and Katsuhiro Nakamura. "Acceleration of adiabatic quantum dynamics in electromagnetic fields". In: *Phys. Rev. A* 84 (4 Oct. 2011), p. 043434. DOI: 10.1103/PhysRevA.84.043434. URL: https://link.aps.org/doi/10.1103/PhysRevA.84.043434.

[122] M. Born and V. Fock. "Beweis des Adiabatensatzes". In: *Zeitschrift für Physik* 51.3 (1928), pp. 165–180. DOI: 10.1007/BF01343193. URL: https://doi.org/10.1007/BF01343193.

[123] Adolfo del Campo. "Shortcuts to Adiabaticity by Counterdiabatic Driving". In: *Phys. Rev. Lett.* 111 (10 Sept. 2013), p. 100502. DOI: 10.1103/PhysRevLett.111.100502. URL: https://link.aps.org/doi/10.1103/PhysRevLett.111.100502.

[124] Shuoming An et al. "Shortcuts to adiabaticity by counterdiabatic driving for trapped-ion displacement in phase space". In: *Nature Communications* 7.1 (2016), p. 12999. DOI: 10.1038/ncomms12999. URL: https://doi.org/10.1038/ncomms12999.

[125] Steve Campbell and Sebastian Deffner. "Trade-Off Between Speed and Cost in Shortcuts to Adiabaticity". In: *Phys. Rev. Lett.* 118 (10 Mar. 2017), p. 100601. DOI: 10.1103/PhysRevLett.118.100601. URL: https://link.aps.org/doi/10.1103/PhysRevLett.118.100601.

[126] Obinna Abah and Eric Lutz. "Performance of shortcut-to-adiabaticity quantum engines". In: *Phys. Rev. E* 98 (3 Sept. 2018), p. 032121. DOI: 10.1103/PhysRevE.98.032121. URL: https://link.aps.org/doi/10.1103/PhysRevE.98.032121.

[127] Roie Dann, Ander Tobalina, and Ronnie Kosloff. "Shortcut to Equilibration of an Open Quantum System". In: *Phys. Rev. Lett.* 122 (25 June 2019), p. 250402. DOI: 10.1103/PhysRevLett.122.250402. URL: https://link.aps.org/doi/10.1103/PhysRevLett.122.250402.

[128] Christopher Jarzynski. "Generating shortcuts to adiabaticity in quantum and classical dynamics". In: *Phys. Rev. A* 88 (4 Oct. 2013), 040101(R). DOI: 10.1103/PhysRevA.88.040101. URL: https://link.aps.org/doi/10.1103/PhysRevA.88.040101.

[129] Sebastian Deffner, Christopher Jarzynski, and Adolfo del Campo. "Classical and Quantum Shortcuts to Adiabaticity for Scale-Invariant Driving". In: *Phys. Rev. X* 4 (2 Apr. 2014), p. 021013. DOI: 10.1103/PhysRevX.4.021013. URL: https://link.aps.org/doi/10.1103/PhysRevX.4.021013.

[130] Ignacio A. Martínez et al. "Engineered swift equilibration of a Brownian particle". In: *Nature Physics* 12.9 (2016), pp. 843–846. DOI: 10.1038/nphys3758. URL: https://doi.org/10.1038/nphys3758.

[131] Marie Chupeau et al. "Engineered swift equilibration for Brownian objects: from underdamped to overdamped dynamics". In: *New Journal of Physics* 20.7 (July 2018), p. 075003. DOI: 10.1088/1367-2630/aac875. URL: https://doi.org/10.1088/1367-2630/aac875.

[132] Dago Salambô et al. "Engineered Swift Equilibration of brownian particles: consequences of hydrodynamic coupling". In: *SciPost Phys.* 9 (5 2020), p. 64. DOI: 10.21468/SciPostPhys.9.5.064. URL: https://scipost.org/10.21468/SciPostPhys.9.5.064.

[133] A. Baldassarri, A. Puglisi, and L. Sesta. "Engineered swift equilibration of a Brownian gyrator". In: *Phys. Rev. E* 102 (3 Sept. 2020), p. 030105. DOI: 10.1103/PhysRevE.102.030105. URL: https://link.aps.org/doi/10.1103/PhysRevE.102.030105.

[134] Adam G. Frim et al. "Engineered swift equilibration for arbitrary geometries". In: *Phys. Rev. E* 103 (3 Mar. 2021), p. L030102. DOI: 10.1103/PhysRevE.103.L030102. URL: https://link.aps.org/doi/10.1103/PhysRevE.103.L030102.

[135] Adam G. Frim and Michael R. DeWeese. *Shortcut engineering of active matter: run-and-tumble particles*. 2023. arXiv: 2304.06023 [cond-mat.stat-mech]. URL: https://arxiv.org/abs/2304.06023.

[136] Ayoti Patra and Christopher Jarzynski. "Shortcuts to adiabaticity using flow fields". In: *New Journal of Physics* 19.12 (Dec. 2017), p. 125009. DOI: 10.1088/1367-2630/aa924c. URL: https://doi.org/10.1088/1367-2630/aa924c.

[137] Jin-Fu Chen. "Optimizing Brownian heat engine with shortcut strategy". In: *Phys. Rev. E* 106 (5 Nov. 2022), p. 054108. DOI: 10.1103/PhysRevE.106.054108. URL: https://link.aps.org/doi/10.1103/PhysRevE.106.054108.

[138] Xiu-Hua Zhao, Zheng-Nan Gong, and Z. C. Tu. "Low-dissipation engines: Microscopic construction via shortcuts to adiabaticity and isothermality, the optimal relation between power and efficiency". In: *Phys. Rev. E* 106 (6 Dec. 2022), p. 064117. DOI: 10.1103/PhysRevE.106.064117. URL: https://link.aps.org/doi/10.1103/PhysRevE.106.064117.

[139] Sahar Alipour et al. "Shortcuts to Adiabaticity in Driven Open Quantum Systems: Balanced Gain and Loss and Non-Markovian Evolution". In: *Quantum* 4 (Sept. 2020), p. 336. ISSN: 2521-327X. DOI: 10.22331/q-2020-09-28-336. URL: https://doi.org/10.22331/q-2020-09-28-336.

[140] A Pedram et al. "A quantum Otto engine with shortcuts to thermalization and adiabaticity". In: *New Journal of Physics* 25.11 (2023), p. 113014. DOI: 10.1088/1367-2630/ad0857. URL: https://dx.doi.org/10.1088/1367-2630/ad0857.

[141] Kazutaka Takahashi and Adolfo del Campo. "Shortcuts to Adiabaticity in Krylov Space". In: *Phys. Rev. X* 14 (1 Feb. 2024), p. 011032. DOI: 10.1103/PhysRevX.14.011032. URL: https://link.aps.org/doi/10.1103/PhysRevX.14.011032.

[142] Sebastian Deffner and Steve Campbell. "Quantum speed limits: from Heisenberg's uncertainty principle to optimal quantum control". In: *Journal of Physics A: Mathematical and Theoretical* 50.45 (2017), p. 453001. DOI: 10.1088/1751-8121/aa86c6. URL: https://dx.doi.org/10.1088/1751-8121/aa86c6.

[143] Ricardo Puebla, Sebastian Deffner, and Steve Campbell. "Kibble-Zurek scaling in quantum speed limits for shortcuts to adiabaticity". In: *Phys. Rev. Res.* 2 (3 July 2020), p. 032020. DOI: 10.1103/PhysRevResearch.2.032020. URL: https://link.aps.org/doi/10.1103/PhysRevResearch.2.032020.

[144] Shamreen Iram et al. "Controlling the speed and trajectory of evolution with counter-diabatic driving". In: *Nature Physics* 17.1 (2021), pp. 135–142. DOI: 10.1038/s41567-020-0989-3. URL: https://doi.org/10.1038/s41567-020-0989-3.

[145] Efe Ilker et al. "Shortcuts in Stochastic Systems and Control of Biophysical Processes". In: *Phys. Rev. X* 12 (2 May 2022), p. 021048. DOI: 10.1103/PhysRevX.12.021048. URL: https://link.aps.org/doi/10.1103/PhysRevX.12.021048.

[146] S.L. Wu et al. "Shortcuts to Adiabaticity for Open Quantum Systems and a Mixed-State Inverse Engineering Scheme". In: *Phys. Rev. Appl.* 16 (4 Oct. 2021), p. 044028. DOI: 10.1103/PhysRevApplied.16.044028. URL: https://link.aps.org/doi/10.1103/PhysRevApplied.16.044028.

[147] Marco Baldovin, David Guéry-Odelin, and Emmanuel Trizac. "Control of Active Brownian Particles: An exact solution". In: *Phys. Rev. Lett.* 131.11 (Sept. 2023), p. 118302.

[148] John Preskill. "Quantum Computing in the NISQ era and beyond". In: *Quantum* 2 (Aug. 2018), p. 79. ISSN: 2521-327X. DOI: 10.22331/q-2018-08-06-79. URL: https://doi.org/10.22331/q-2018-08-06-79.

[149] Ethan N. Evans et al. "Learning quantum-state feedback control with backpropagation-free stochastic optimization". In: *Phys. Rev. A* 106 (5 Nov. 2022), p. 052405. DOI: 10.1103/PhysRevA.106.052405. URL: https://link.aps.org/doi/10.1103/PhysRevA.106.052405.

[150] Kang Cai et al. *Quantum Shortcut to Adiabaticity for State Preparation in a Finite-Sized Jaynes-Cummings Lattice*. 2024. arXiv: 2402.12485 [quant-ph]. URL: https://arxiv.org/abs/2402.12485.

[151] Qi Zhang, Xi Chen, and David Guéry-Odelin. "Connection between Inverse Engineering and Optimal Control in Shortcuts to Adiabaticity". In: *Entropy* 23.1 (2021). DOI: 10.3390/e23010084.

[152] A. Emmanouilidou et al. "Steering an Eigenstate to a Destination". In: *Phys. Rev. Lett.* 85 (8 Aug. 2000), pp. 1626–1629. DOI: 10.1103/PhysRevLett.85.1626. URL: https://link.aps.org/doi/10.1103/PhysRevLett.85.1626.

[153] Ken Funo et al. "Universal Work Fluctuations During Shortcuts to Adiabaticity by Counterdiabatic Driving". In: *Phys. Rev. Lett.* 118 (10 Mar. 2017), p. 100602. DOI: 10.1103/PhysRevLett.118.100602. URL: https://link.aps.org/doi/10.1103/PhysRevLett.118.100602.

[154] Obinna Abah, Mauro Paternostro, and Eric Lutz. "Shortcut-to-adiabaticity quantum Otto refrigerator". In: *Phys. Rev. Research* 2 (2 May 2020), p. 023120. DOI: 10.1103/PhysRevResearch.2.023120. URL: https://link.aps.org/doi/10.1103/PhysRevResearch.2.023120.

[155] Marie Chupeau et al. "Thermal bath engineering for swift equilibration". In: *Phys. Rev. E* 98 (1 July 2018), 010104(R). DOI: 10.1103/PhysRevE.98.010104. URL: https://link.aps.org/doi/10.1103/PhysRevE.98.010104.

[156] Tim Schmiedl and Udo Seifert. "Optimal Finite-Time Processes In Stochastic Thermodynamics". In: *Phys. Rev. Lett.* 98 (10 Mar. 2007), p. 108301. DOI: 10.1103/PhysRevLett.98.108301. URL: https://link.aps.org/doi/10.1103/PhysRevLett.98.108301.

[157] T. Schmiedl and U. Seifert. "Efficiency at maximum power: An analytically solvable model for stochastic heat engines". In: *EPL (Europhysics Letters)* 81.2 (Dec. 2007), p. 20003. DOI: 10.1209/0295-5075/81/20003. URL: https://doi.org/10.1209%2F0295-5075%2F81%2F20003.

[158] Patrick R. Zulkowski and Michael R. DeWeese. "Optimal finite-time erasure of a classical bit". In: *Phys. Rev. E* 89 (5 May 2014), p. 052140. DOI: 10.1103/PhysRevE.89.052140. URL: https://link.aps.org/doi/10.1103/PhysRevE.89.052140.

[159] Ignacio A. Martínez et al. "Colloidal heat engines: a review". In: *Soft Matter* 13 (1 2017), pp. 22–36. DOI: 10.1039/C6SM00923A. URL: http://dx.doi.org/10.1039/C6SM00923A.

[160] Valentin Blickle and Clemens Bechinger. "Realization of a micrometre-sized stochastic heat engine". In: *Nature Physics* 8.2 (Feb. 2012), pp. 143–146. DOI: 10.1038/nphys2163. URL: https://doi.org/10.1038/nphys2163.

[161] M. Nakahara. *Geometry, Topology and Physics*. 2nd. CRC Press, 2003.

[162] Claire Voisin. "Harmonic Forms and Cohomology". In: *Hodge Theory and Complex Algebraic Geometry I*. Vol. 1. Cambridge Studies in Advanced Mathematics. Cambridge University Press, 2002, pp. 117–136. DOI: 10.1017/CBO9780511615344.006.

[163] John David Jackson. *Classical Electrodynamics, Third Edition*. Wiley, Aug. 1998. ISBN: 9780471309321.

[164] Peter E. Kloeden and Eckhard Platen. *Numerical Solution of Stochastic Differential Equations*. Springer Berlin Heidelberg, 1992. DOI: 10.1007/978-3-662-12616-5. URL: https://doi.org/10.1007/978-3-662-12616-5.

[165] N. Kumar and K. Vijay Kumar. "Classical Langevin dynamics of a charged particle moving on a sphere and diamagnetism: A surprise". In: *EPL (Europhysics Letters)* 86.1 (Apr. 2009), p. 17001. DOI: 10.1209/0295-5075/86/17001. URL: https://doi.org/10.1209%2F0295-5075%2F86%2F17001.

[166] Leonardo Apaza and Mario Sandoval. "Brownian self-driven particles on the surface of a sphere". In: *Phys. Rev. E* 96 (2 Aug. 2017), p. 022606. DOI: 10.1103/PhysRevE.96.022606. URL: https://link.aps.org/doi/10.1103/PhysRevE.96.022606.

[167] Andrey L. Pankratov and Mario Salerno. "Adiabatic approximation and parametric stochastic resonance in a bistable system with periodically driven barrier". In: *Phys. Rev. E* 61 (2 Feb. 2000), pp. 1206–1210. DOI: 10.1103/PhysRevE.61.1206. URL: https://link.aps.org/doi/10.1103/PhysRevE.61.1206.

[168] Andrey L. Pankratov. "Suppression of noise in nonlinear systems subjected to strong periodic driving". In: *Phys. Rev. E* 65 (2 Jan. 2002), p. 022101. DOI: 10.1103/PhysRevE.65.022101. URL: https://link.aps.org/doi/10.1103/PhysRevE.65.022101.

[169] Patrick R. Zulkowski, David A. Sivak, and Michael R. DeWeese. "Optimal Control of Transitions between Nonequilibrium Steady States". In: *PLOS ONE* 8.12 (Dec. 2013), pp. 1–7. DOI: 10.1371/journal.pone.0082754. URL: https://doi.org/10.1371/journal.pone.0082754.

[170] Carlos A. Plata et al. "Optimal work in a harmonic trap with bounded stiffness". In: *Phys. Rev. E* 99 (1 Jan. 2019), p. 012140. DOI: 10.1103/PhysRevE.99.012140. URL: https://link.aps.org/doi/10.1103/PhysRevE.99.012140.

[171] Massimiliano Esposito et al. "Finite-time thermodynamics for a single-level quantum dot". In: *EPL (Europhysics Letters)* 89.2 (2010), p. 20003.

[172] Giovanni Diana, G. Baris Bagci, and Massimiliano Esposito. "Finite-time erasing of information stored in fermionic bits". In: *Phys. Rev. E* 87 (1 Jan. 2013), p. 012111. DOI: 10.1103/PhysRevE.87.012111. URL: https://link.aps.org/doi/10.1103/PhysRevE.87.012111.

[173] Rothschild. "Non-random Distribution of Bull Spermatozoa in a Drop of Sperm Suspension". In: *Nature* 198.4886 (1963), pp. 1221–1222. DOI: 10.1038/1981221a0. URL: https://doi.org/10.1038/1981221a0.

[174] Howard C. Berg and Robert A. Anderson. "Bacteria Swim by Rotating their Flagellar Filaments". In: *Nature* 245.5425 (Oct. 1973), pp. 380–382. DOI: 10.1038/245380a0. URL: https://doi.org/10.1038/245380a0.

[175] George H. Wadhams and Judith P. Armitage. "Making sense of it all: bacterial chemotaxis". In: *Nature Reviews Molecular Cell Biology* 5.12 (Dec. 2004), pp. 1024–1037. DOI: 10.1038/nrm1524. URL: https://doi.org/10.1038/nrm1524.

[176] Tamás Vicsek et al. "Novel Type of Phase Transition in a System of Self-Driven Particles". In: *Phys. Rev. Lett.* 75 (6 Aug. 1995), pp. 1226–1229. DOI: 10.1103/PhysRevLett.75.1226. URL: https://link.aps.org/doi/10.1103/PhysRevLett.75.1226.

[177] John Toner and Yuhai Tu. "Long-Range Order in a Two-Dimensional Dynamical XY Model: How Birds Fly Together". In: *Phys. Rev. Lett.* 75 (23 Dec. 1995), pp. 4326–4329. DOI: 10.1103/PhysRevLett.75.4326. URL: https://link.aps.org/doi/10.1103/PhysRevLett.75.4326.

[178] F. D. C. Farrell et al. "Pattern Formation in Self-Propelled Particles with Density-Dependent Motility". In: *Phys. Rev. Lett.* 108 (24 June 2012), p. 248101. DOI: 10.1103/PhysRevLett.108.248101. URL: https://link.aps.org/doi/10.1103/PhysRevLett.108.248101.

[179] Yaouen Fily and M. Cristina Marchetti. "Athermal Phase Separation of Self-Propelled Particles with No Alignment". In: *Phys. Rev. Lett.* 108 (23 June 2012), p. 235702. DOI: 10.1103/PhysRevLett.108.235702. URL: https://link.aps.org/doi/10.1103/PhysRevLett.108.235702.

[180] Michael E. Cates and Julien Tailleur. "Motility-Induced Phase Separation". In: *Annual Review of Condensed Matter Physics* 6.1 (2015), pp. 219–244. DOI: 10.1146/annurev-conmatphys-031214-014710. eprint: https://doi.org/10.1146/annurev-conmatphys-031214-014710. URL: https://doi.org/10.1146/annurev-conmatphys-031214-014710.

[181] Pasquale Digregorio et al. "Full Phase Diagram of Active Brownian Disks: From Melting to Motility-Induced Phase Separation". In: *Phys. Rev. Lett.* 121 (9 Aug. 2018), p. 098003. DOI: 10.1103/PhysRevLett.121.098003. URL: https://link.aps.org/doi/10.1103/PhysRevLett.121.098003.

[182] L. Caprini, U. Marini Bettolo Marconi, and A. Puglisi. "Spontaneous Velocity Alignment in Motility-Induced Phase Separation". In: *Phys. Rev. Lett.* 124 (7 Feb. 2020), p. 078001. DOI: 10.1103/PhysRevLett.124.078001. URL: https://link.aps.org/doi/10.1103/PhysRevLett.124.078001.

[183] Allison P. Berke et al. "Hydrodynamic Attraction of Swimming Microorganisms by Surfaces". In: *Phys. Rev. Lett.* 101 (3 July 2008), p. 038102. DOI: 10.1103/PhysRevLett.101.038102. URL: https://link.aps.org/doi/10.1103/PhysRevLett.101.038102.

[184] Yaouen Fily, Aparna Baskaran, and Michael F. Hagan. "Dynamics of self-propelled particles under strong confinement". In: *Soft Matter* 10 (30 2014), pp. 5609–5617. DOI: 10.1039/C4SM00975D. URL: http://dx.doi.org/10.1039/C4SM00975D.

[185] Xingbo Yang, M. Lisa Manning, and M. Cristina Marchetti. "Aggregation and segregation of confined active particles". In: *Soft Matter* 10.34 (2014), pp. 6477–6484. DOI: 10.1039/c4sm00927d. URL: https://doi.org/10.1039/c4sm00927d.

[186] A. P. Solon et al. "Pressure is not a state function for generic active fluids". In: *Nature Physics* 11.8 (June 2015), pp. 673–678. DOI: 10.1038/nphys3377. URL: https://doi.org/10.1038/nphys3377.

[187] Sho C. Takatori et al. "Acoustic trapping of active matter". In: *Nature Communications* 7.1 (2016), p. 10694. DOI: 10.1038/ncomms10694. URL: https://doi.org/10.1038/ncomms10694.

[188] Daniel Needleman and Zvonimir Dogic. "Active matter at the interface between materials science and cell biology". In: *Nature Reviews Materials* 2.9 (July 2017). DOI: 10.1038/natrevmats.2017.48. URL: https://doi.org/10.1038/natrevmats.2017.48.

[189] Tyler D. Ross et al. "Controlling organization and forces in active matter through optically defined boundaries". In: *Nature* 572.7768 (Aug. 2019), pp. 224–229. DOI: 10.1038/s41586-019-1447-1. URL: https://doi.org/10.1038/s41586-019-1447-1.

[190] Andrey Sokolov et al. "Swimming bacteria power microscopic gears". In: *Proceedings of the National Academy of Sciences* 107.3 (Dec. 2009), pp. 969–974. DOI: 10.1073/pnas.0913015107. URL: https://doi.org/10.1073/pnas.0913015107.

[191] Timothy Ekeh, Michael E. Cates, and Étienne Fodor. "Thermodynamic cycles with active matter". In: *Phys. Rev. E* 102 (1 July 2020), p. 010101. DOI: 10.1103/PhysRevE.102.010101. URL: https://link.aps.org/doi/10.1103/PhysRevE.102.010101.

[192] Patrick Pietzonka et al. "Autonomous Engines Driven by Active Matter: Energetics and Design Principles". In: *Phys. Rev. X* 9 (4 Nov. 2019), p. 041032. DOI: 10.1103/PhysRevX.9.041032. URL: https://link.aps.org/doi/10.1103/PhysRevX.9.041032.

[193] Thomas Speck. "Efficiency of isothermal active matter engines: Strong driving beats weak driving". In: *Phys. Rev. E* 105 (1 Jan. 2022), p. L012601. DOI: 10.1103/PhysRevE.105.L012601. URL: https://link.aps.org/doi/10.1103/PhysRevE.105.L012601.

[194] Étienne Fodor and Michael E. Cates. "Active engines: Thermodynamics moves forward". In: *Europhysics Letters* 134.1 (Apr. 2021), p. 10003. DOI: 10.1209/0295-5075/134/10003. URL: https://doi.org/10.1209/0295-5075/134/10003.

[195] J. Schwarz-Linek et al. "Phase separation and rotor self-assembly in active particle suspensions". In: *Proceedings of the National Academy of Sciences* 109.11 (Mar. 2012), pp. 4052–4057. DOI: 10.1073/pnas.1116334109. URL: https://doi.org/10.1073/pnas.1116334109.

[196] Tim Sanchez et al. "Spontaneous motion in hierarchically assembled active matter". In: *Nature* 491.7424 (Nov. 2012), pp. 431–434. DOI: 10.1038/nature11591. URL: https://doi.org/10.1038/nature11591.

[197] Joakim Stenhammar et al. "Light-induced self-assembly of active rectification devices". In: *Science Advances* 2.4 (Apr. 2016). DOI: 10.1126/sciadv.1501850. URL: https://doi.org/10.1126/sciadv.1501850.

[198] Stewart A. Mallory, Chantal Valeriani, and Angelo Cacciuto. "An Active Approach to Colloidal Self-Assembly". In: *Annual Review of Physical Chemistry* 69.1 (Apr. 2018), pp. 59–79. DOI: 10.1146/annurev-physchem-050317-021237. URL: https://doi.org/10.1146/annurev-physchem-050317-021237.

[199] Alberto Scacchi et al. "Self-assembly in soft matter with multiple length scales". In: *Phys. Rev. Res.* 3 (2 Apr. 2021), p. L022008. DOI: 10.1103/PhysRevResearch.3.L022008. URL: https://link.aps.org/doi/10.1103/PhysRevResearch.3.L022008.

[200] Guo Zhan Lum et al. "Shape-programmable magnetic soft matter". In: *Proceedings of the National Academy of Sciences* 113.41 (Sept. 2016). DOI: 10.1073/pnas.1608193113. URL: https://doi.org/10.1073/pnas.1608193113.

[201] Yulei Fu et al. "Microscopic Swarms: From Active Matter Physics to Biomedical and Environmental Applications". In: *Micromachines* 13.2 (Feb. 2022), p. 295. DOI: 10.3390/mi13020295. URL: https://doi.org/10.3390/mi13020295.

[202] Gaurav Gardi et al. "Microrobot collectives with reconfigurable morphologies, behaviors, and functions". In: *Nature Communications* 13.1 (Apr. 2022). DOI: 10.1038/s41467-022-29882-5. URL: https://doi.org/10.1038/s41467-022-29882-5.

[203] Erik Torrontegui et al. "Shortcuts to Adiabaticity". In: *Advances In Atomic, Molecular, and Optical Physics*. Elsevier, 2013, pp. 117–169. DOI: 10.1016/b978-0-12-408090-4.00002-5. URL: https://doi.org/10.1016%2Fb978-0-12-408090-4.00002-5.

[204] Adolfo del Campo and Kihwan Kim. "Focus on Shortcuts to Adiabaticity". In: *New Journal of Physics* 21.5 (May 2019), p. 050201. DOI: 10.1088/1367-2630/ab1437. URL: https://dx.doi.org/10.1088/1367-2630/ab1437.

[205] Christopher Jarzynski et al. "Fast forward to the classical adiabatic invariant". In: *Phys. Rev. E* 95 (3 Mar. 2017), p. 032122. DOI: 10.1103/PhysRevE.95.032122. URL: https://link.aps.org/doi/10.1103/PhysRevE.95.032122.

[206] J. Tailleur and M. E. Cates. "Statistical Mechanics of Interacting Run-and-Tumble Bacteria". In: *Phys. Rev. Lett.* 100 (21 May 2008), p. 218103. DOI: 10.1103/PhysRevLett.100.218103. URL: https://link.aps.org/doi/10.1103/PhysRevLett.100.218103.

[207] Olivier Dauchot and Vincent Démery. "Dynamics of a Self-Propelled Particle in a Harmonic Trap". In: *Phys. Rev. Lett.* 122 (6 Feb. 2019), p. 068002. DOI: 10.1103/PhysRevLett.122.068002. URL: https://link.aps.org/doi/10.1103/PhysRevLett.122.068002.

[208] Falko Schmidt et al. "Non-equilibrium properties of an active nanoparticle in a harmonic potential". In: *Nature Communications* 12.1 (2021), p. 1902. DOI: 10.1038/s41467-021-22187-z. URL: https://doi.org/10.1038/s41467-021-22187-z.

[209] Caleb G Wagner, Michael F Hagan, and Aparna Baskaran. "Steady-state distributions of ideal active Brownian particles under confinement and forcing". In: *Journal of Statistical Mechanics: Theory and Experiment* 2017.4 (Apr. 2017), p. 043203. DOI: 10.1088/1742-5468/aa60a8. URL: https://dx.doi.org/10.1088/1742-5468/aa60a8.

[210] Kanaya Malakar et al. "Steady state, relaxation and first-passage properties of a run-and-tumble particle in one-dimension". In: *Journal of Statistical Mechanics: Theory and Experiment* 2018.4 (Apr. 2018), p. 043215. DOI: 10.1088/1742-5468/aab84f. URL: https://dx.doi.org/10.1088/1742-5468/aab84f.

[211] Urna Basu et al. "Long-time position distribution of an active Brownian particle in two dimensions". In: *Phys. Rev. E* 100 (6 Dec. 2019), p. 062116. DOI: 10.1103/PhysRevE.100.062116. URL: https://link.aps.org/doi/10.1103/PhysRevE.100.062116.

[212] Kanaya Malakar et al. "Steady state of an active Brownian particle in a two-dimensional harmonic trap". In: *Phys. Rev. E* 101 (2 Feb. 2020), p. 022610. DOI: 10.1103/PhysRevE.101.022610. URL: https://link.aps.org/doi/10.1103/PhysRevE.101.022610.

[213] Debasish Chaudhuri and Abhishek Dhar. "Active Brownian particle in harmonic trap: exact computation of moments, and re-entrant transition". In: *Journal of Statistical Mechanics: Theory and Experiment* 2021.1 (Jan. 2021), p. 013207. DOI: 10.1088/1742-5468/abd031. URL: https://dx.doi.org/10.1088/1742-5468/abd031.

[214] Michele Caraglio and Thomas Franosch. "Analytic Solution of an Active Brownian Particle in a Harmonic Well". In: *Phys. Rev. Lett.* 129 (15 Oct. 2022), p. 158001. DOI: 10.1103/PhysRevLett.129.158001. URL: https://link.aps.org/doi/10.1103/PhysRevLett.129.158001.

[215] Abhishek Dhar et al. "Run-and-tumble particle in one-dimensional confining potentials: Steady-state, relaxation, and first-passage properties". In: *Phys. Rev. E* 99 (3 Mar. 2019), p. 032132. DOI: 10.1103/PhysRevE.99.032132. URL: https://link.aps.org/doi/10.1103/PhysRevE.99.032132.

[216] Rosalba Garcia-Millan and Gunnar Pruessner. "Run-and-tumble motion in a harmonic potential: field theory and entropy production". In: *Journal of Statistical Mechanics: Theory and Experiment* 2021.6 (June 2021), p. 063203. DOI: 10.1088/1742-5468/ac014d. URL: https://dx.doi.org/10.1088/1742-5468/ac014d.

[217] M. E. Cates and J. Tailleur. "When are active Brownian particles and run-and-tumble particles equivalent? Consequences for motility-induced phase separation". In: *Europhysics Letters* 101.2 (Feb. 2013), p. 20010. DOI: 10.1209/0295-5075/101/20010. URL: https://dx.doi.org/10.1209/0295-5075/101/20010.

[218] A. P. Solon, M. E. Cates, and J. Tailleur. "Active brownian particles and run-and-tumble particles: A comparative study". In: *The European Physical Journal Special Topics* 224.7 (2015), pp. 1231–1262. DOI: 10.1140/epjst/e2015-02457-0. URL: https://doi.org/10.1140/epjst/e2015-02457-0.

[219] Karel Proesmans, Bart Cleuren, and Christian Van den Broeck. "Power-Efficiency-Dissipation Relations in Linear Thermodynamics". In: *Phys. Rev. Lett.* 116 (22 June 2016), p. 220601. DOI: 10.1103/PhysRevLett.116.220601. URL: https://link.aps.org/doi/10.1103/PhysRevLett.116.220601.

[220] Patrick Pietzonka and Udo Seifert. "Universal Trade-Off between Power, Efficiency, and Constancy in Steady-State Heat Engines". In: *Phys. Rev. Lett.* 120 (19 May 2018), p. 190602. DOI: 10.1103/PhysRevLett.120.190602. URL: https://link.aps.org/doi/10.1103/PhysRevLett.120.190602.

[221] Naoto Shiraishi, Ken Funo, and Keiji Saito. "Speed Limit for Classical Stochastic Processes". In: *Phys. Rev. Lett.* 121 (7 Aug. 2018), p. 070601. DOI: 10.1103/PhysRevLett.121.070601. URL: https://link.aps.org/doi/10.1103/PhysRevLett.121.070601.

[222] Grant M. Rotskoff and Gavin E. Crooks. "Optimal control in nonequilibrium systems: Dynamic Riemannian geometry of the Ising model". In: *Phys. Rev. E* 92 (6 Dec. 2015), p. 060102. DOI: 10.1103/PhysRevE.92.060102. URL: https://link.aps.org/doi/10.1103/PhysRevE.92.060102.

[223] Paolo Abiuso and Martí Perarnau-Llobet. "Optimal Cycles for Low-Dissipation Heat Engines". In: *Phys. Rev. Lett.* 124 (11 Mar. 2020), p. 110606. DOI: 10.1103/PhysRevLett.124.110606. URL: https://link.aps.org/doi/10.1103/PhysRevLett.124.110606.

[224] Ana Cannas da Silva. *Lectures on Symplectic Geometry*. Springer Berlin Heidelberg, 2008. ISBN: 9783540453307. DOI: 10.1007/978-3-540-45330-7. URL: http://dx.doi.org/10.1007/978-3-540-45330-7.

[225] Hansjorg Geiges. *Cambridge studies in advanced mathematics: An introduction to contact topology series number 109*. Cambridge, England: Cambridge University Press, Mar. 2008.

[226] Anahita Eslami Rad. *Symplectic and Contact Geometry: A Concise Introduction*. Springer Nature Switzerland, 2024. ISBN: 9783031562259. DOI: 10.1007/978-3-031-56225-9. URL: http://dx.doi.org/10.1007/978-3-031-56225-9.

[227] F. Weinhold. "Metric geometry of equilibrium thermodynamics". In: *The Journal of Chemical Physics* 63.6 (1975), pp. 2479–2483. DOI: 10.1063/1.431689. eprint: https://doi.org/10.1063/1.431689. URL: https://doi.org/10.1063/1.431689.

[228] F. Weinhold. "Metric geometry of equilibrium thermodynamics. II. Scaling, homogeneity, and generalized Gibbs–Duhem relations". In: *The Journal of Chemical Physics* 63.6 (July 1975), pp. 2484–2487. DOI: 10.1063/1.431635. URL: https://doi.org/10.1063/1.431635.

[229] F. Weinhold. "Metric geometry of equilibrium thermodynamics. III. Elementary formal structure of a vector algebraic representation of equilibrium thermodynamics". In: *The Journal of Chemical Physics* 63.6 (July 1975), pp. 2488–2495. DOI: 10.1063/1.431636. URL: https://doi.org/10.1063/1.431636.

[230] F. Weinhold. "Metric geometry of equilibrium thermodynamics. IV. Vector algebraic evaluation of thermodynamic derivatives". In: *The Journal of Chemical Physics* 63.6 (July 1975), pp. 2496–2501. DOI: 10.1063/1.431637. URL: https://doi.org/10.1063/1.431637.

[231] F. Weinhold. "Metric geometry of equilibrium thermodynamics. V. Aspects of heterogeneous equilibrium". In: *The Journal of Chemical Physics* 65.2 (July 1976), pp. 559–564. DOI: 10.1063/1.433136. URL: https://doi.org/10.1063/1.433136.

[232] George Ruppeiner. "Thermodynamics: A Riemannian geometric model". In: *Phys. Rev. A* 20 (4 Oct. 1979), pp. 1608–1613. DOI: 10.1103/PhysRevA.20.1608. URL: https://link.aps.org/doi/10.1103/PhysRevA.20.1608.

[233] George Ruppeiner. "Application of Riemannian geometry to the thermodynamics of a simple fluctuating magnetic system". In: *Phys. Rev. A* 24 (1 July 1981), pp. 488–492. DOI: 10.1103/PhysRevA.24.488. URL: https://link.aps.org/doi/10.1103/PhysRevA.24.488.

[234] George Ruppeiner. "Riemannian geometry in thermodynamic fluctuation theory". In: *Rev. Mod. Phys.* 67 (3 July 1995), pp. 605–659. DOI: 10.1103/RevModPhys.67.605. URL: https://link.aps.org/doi/10.1103/RevModPhys.67.605.

[235] George Ruppeiner. "Thermodynamic curvature measures interactions". In: *American Journal of Physics* 78.11 (July 2010), pp. 1170–1180. DOI: 10.1119/1.3459936. URL: https://doi.org/10.1119/1.3459936.

[236] G. Ruppeiner et al. "Thermodynamic geometry, phase transitions, and the Widom line". In: *Phys. Rev. E* 86 (5 Nov. 2012), p. 052103. DOI: 10.1103/PhysRevE.86.052103. URL: https://link.aps.org/doi/10.1103/PhysRevE.86.052103.

[237] George Ruppeiner. "Thermodynamic curvature and phase transitions in Kerr-Newman black holes". In: *Phys. Rev. D* 78 (2 July 2008), p. 024016. DOI: 10.1103/PhysRevD.78.024016. URL: https://link.aps.org/doi/10.1103/PhysRevD.78.024016.

[238] Shao-Wen Wei, Yu-Xiao Liu, and Robert B. Mann. "Ruppeiner geometry, phase transitions, and the microstructure of charged AdS black holes". In: *Phys. Rev. D* 100 (12 Dec. 2019), p. 124033. DOI: 10.1103/PhysRevD.100.124033. URL: https://link.aps.org/doi/10.1103/PhysRevD.100.124033.

[239] F. Schlögl. "Thermodynamic metric and stochastic measures". In: *Zeitschrift für Physik B Condensed Matter* 59.4 (1985), pp. 449–454. DOI: 10.1007/BF01328857. URL: https://doi.org/10.1007/BF01328857.

[240] Gavin E. Crooks. "Measuring Thermodynamic Length". In: *Phys. Rev. Lett.* 99 (10 Sept. 2007), p. 100602. DOI: 10.1103/PhysRevLett.99.100602. URL: https://link.aps.org/doi/10.1103/PhysRevLett.99.100602.

[241] Peter Salamon and R. Stephen Berry. "Thermodynamic Length and Dissipated Availability". In: *Phys. Rev. Lett.* 51 (13 Sept. 1983), pp. 1127–1130. DOI: 10.1103/PhysRevLett.51.1127. URL: https://link.aps.org/doi/10.1103/PhysRevLett.51.1127.

[242] Karl Heinz Hoffmann. "An introduction to endoreversible thermodynamics". In: *Atti della Accademia Peloritana dei Pericolanti - Classe di Scienze Fisiche, Matematiche e Naturali* 1 (Feb. 2008), pp. 1–18. ISSN: 1825-1242. DOI: 10.1478/C1S0801011. URL: https://doi.org/10.1478/C1S0801011.

[243] Grant M. Rotskoff, Gavin E. Crooks, and Eric Vanden-Eijnden. "Geometric approach to optimal nonequilibrium control: Minimizing dissipation in nanomagnetic spin systems". In: *Phys. Rev. E* 95 (1 Jan. 2017), p. 012148. DOI: 10.1103/PhysRevE.95.012148. URL: https://link.aps.org/doi/10.1103/PhysRevE.95.012148.

[244] Heinz Schättler and Urszula Ledzewicz. *Geometric Optimal Control*. Springer New York, 2012. ISBN: 9781461438342. DOI: 10.1007/978-1-4614-3834-2. URL: http://dx.doi.org/10.1007/978-1-4614-3834-2.

[245] Paolo Abiuso et al. "Geometric Optimisation of Quantum Thermodynamic Processes". In: *Entropy* 22.10 (2020). ISSN: 1099-4300. DOI: 10.3390/e22101076. URL: https://www.mdpi.com/1099-4300/22/10/1076.

[246] Pablo Terren Alonso et al. "Geometric Optimization of Nonequilibrium Adiabatic Thermal Machines and Implementation in a Qubit System". In: *PRX Quantum* 3.1 (Feb. 2022), p. 010326.

[247] Dimitri Loutchko, Yuki Sughiyama, and Tetsuya J. Kobayashi. "Riemannian geometry of optimal driving and thermodynamic length and its application to chemical reaction networks". In: *Phys. Rev. Res.* 4 (4 Oct. 2022), p. 043049. DOI: 10.1103/PhysRevResearch.4.043049. URL: https://link.aps.org/doi/10.1103/PhysRevResearch.4.043049.

[248] Alberto Rolandi, Paolo Abiuso, and Martí Perarnau-Llobet. "Collective Advantages in Finite-Time Thermodynamics". In: *Phys. Rev. Lett.* 131 (21 Nov. 2023), p. 210401. DOI: 10.1103/PhysRevLett.131.210401. URL: https://link.aps.org/doi/10.1103/PhysRevLett.131.210401.

[249] I. A. Martínez et al. "Brownian Carnot engine". In: *Nature Physics* 12.1 (2016), pp. 67–70. DOI: 10.1038/nphys3518. URL: https://doi.org/10.1038/nphys3518.

[250] Massimiliano Esposito and Christian Van den Broeck. "Three Detailed Fluctuation Theorems". In: *Phys. Rev. Lett.* 104 (9 Mar. 2010), p. 090601. DOI: 10.1103/PhysRevLett.104.090601. URL: https://link.aps.org/doi/10.1103/PhysRevLett.104.090601.

[251] Takahiro Sagawa and Masahito Ueda. "Generalized Jarzynski Equality under Nonequilibrium Feedback Control". In: *Phys. Rev. Lett.* 104 (9 Mar. 2010), p. 090602. DOI: 10.1103/PhysRevLett.104.090602. URL: https://link.aps.org/doi/10.1103/PhysRevLett.104.090602.

[252] V. Blickle et al. "Thermodynamics of a Colloidal Particle in a Time-Dependent Nonharmonic Potential". In: *Phys. Rev. Lett.* 96 (7 Feb. 2006), p. 070603. DOI: 10.1103/PhysRevLett.96.070603. URL: https://link.aps.org/doi/10.1103/PhysRevLett.96.070603.

[253] Pedro A. Quinto-Su. "A microscopic steam engine implemented in an optical tweezer". In: *Nature Communications* 5.1 (2014), p. 5889. DOI: 10.1038/ncomms6889. URL: https://doi.org/10.1038/ncomms6889.

[254] Sudeesh Krishnamurthy et al. "A micrometre-sized heat engine operating between bacterial reservoirs". In: *Nature Physics* 12.12 (2016), pp. 1134–1138. DOI: 10.1038/nphys3870. URL: https://doi.org/10.1038/nphys3870.

[255] P. Salamon, J. Nulton, and E. Ihrig. "On the relation between entropy and energy versions of thermodynamic length". In: *The Journal of Chemical Physics* 80.1 (1984), pp. 436–437. DOI: 10.1063/1.446467. eprint: https://doi.org/10.1063/1.446467. URL: https://doi.org/10.1063/1.446467.

[256] Sebastian Deffner and Eric Lutz. "Thermodynamic length for far-from-equilibrium quantum systems". In: *Phys. Rev. E* 87 (2 Feb. 2013), p. 022143. DOI: 10.1103/PhysRevE.87.022143. URL: https://link.aps.org/doi/10.1103/PhysRevE.87.022143.

[257] Dibyendu Mandal and Christopher Jarzynski. "Analysis of slow transitions between nonequilibrium steady states". In: *Journal of Statistical Mechanics: Theory and Experiment* 2016.6 (June 2016), p. 063204. DOI: 10.1088/1742-5468/2016/06/063204. URL: https://doi.org/10.1088/1742-5468/2016/06/063204.

[258] Kosuke Ito, Chao Jiang, and Gentaro Watanabe. *Universal Bounds for Fluctuations in Small Heat Engines*. 2019. arXiv: 1910.08096 [cond-mat.stat-mech].

[259] Steven J. Large, Jannik Ehrich, and David A. Sivak. "Free-energy transduction within autonomous systems". In: *Phys. Rev. E* 103 (2 Feb. 2021), p. 022140. DOI: 10.1103/PhysRevE.103.022140. URL: https://link.aps.org/doi/10.1103/PhysRevE.103.022140.

[260] F. L. Curzon and B. Ahlborn. "Efficiency of a Carnot engine at maximum power output". In: *American Journal of Physics* 43.1 (1975), pp. 22–24. DOI: 10.1119/1.10023.

[261] C. Van den Broeck. "Thermodynamic Efficiency at Maximum Power". In: *Phys. Rev. Lett.* 95 (19 Nov. 2005), p. 190602. DOI: 10.1103/PhysRevLett.95.190602. URL: https://link.aps.org/doi/10.1103/PhysRevLett.95.190602.

[262] Massimiliano Esposito, Katja Lindenberg, and Christian Van den Broeck. "Universality of Efficiency at Maximum Power". In: *Phys. Rev. Lett.* 102 (13 Apr. 2009), p. 130602. DOI: 10.1103/PhysRevLett.102.130602. URL: https://link.aps.org/doi/10.1103/PhysRevLett.102.130602.

[263] Giuliano Benenti, Keiji Saito, and Giulio Casati. "Thermodynamic Bounds on Efficiency for Systems with Broken Time-Reversal Symmetry". In: *Phys. Rev. Lett.* 106 (23 June 2011), p. 230602. DOI: 10.1103/PhysRevLett.106.230602. URL: https://link.aps.org/doi/10.1103/PhysRevLett.106.230602.

[264] Kay Brandner and Udo Seifert. "Bound on thermoelectric power in a magnetic field within linear response". In: *Phys. Rev. E* 91 (1 Jan. 2015), p. 012121. DOI: 10.1103/PhysRevE.91.012121. URL: https://link.aps.org/doi/10.1103/PhysRevE.91.012121.

[265] Kay Brandner, Keiji Saito, and Udo Seifert. "Thermodynamics of Micro- and Nano-Systems Driven by Periodic Temperature Variations". In: *Phys. Rev. X* 5 (3 Aug. 2015), p. 031019. DOI: 10.1103/PhysRevX.5.031019. URL: https://link.aps.org/doi/10.1103/PhysRevX.5.031019.

[266] Naoto Shiraishi, Keiji Saito, and Hal Tasaki. "Universal Trade-Off Relation between Power and Efficiency for Heat Engines". In: *Phys. Rev. Lett.* 117 (19 Oct. 2016), p. 190601. DOI: 10.1103/PhysRevLett.117.190601. URL: https://link.aps.org/doi/10.1103/PhysRevLett.117.190601.

[267] Yu-Han Ma et al. "Optimal operating protocol to achieve efficiency at maximum power of heat engines". In: *Phys. Rev. E* 98 (2 Aug. 2018), p. 022133. DOI: 10.1103/PhysRevE.98.022133. URL: https://link.aps.org/doi/10.1103/PhysRevE.98.022133.

[268] Yu-Han Ma et al. "Universal constraint for efficiency and power of a low-dissipation heat engine". In: *Phys. Rev. E* 98 (4 Oct. 2018), p. 042112. DOI: 10.1103/PhysRevE.98.042112. URL: https://link.aps.org/doi/10.1103/PhysRevE.98.042112.

[269] Yu-Han Ma et al. "Experimental Test of the $1/\tau$-Scaling Entropy Generation in Finite-Time Thermodynamics". In: *Phys. Rev. Lett.* 125 (21 Nov. 2020), p. 210601. DOI: 10.1103/PhysRevLett.125.210601. URL: https://link.aps.org/doi/10.1103/PhysRevLett.125.210601.

[270] Harry J. D. Miller et al. "Thermodynamic Uncertainty Relation in Slowly Driven Quantum Heat Engines". In: *Phys. Rev. Lett.* 126 (21 May 2021), p. 210603. DOI: 10.1103/PhysRevLett.126.210603. URL: https://link.aps.org/doi/10.1103/PhysRevLett.126.210603.

[271] Ignacio A. Martínez et al. "Adiabatic Processes Realized with a Trapped Brownian Particle". In: *Phys. Rev. Lett.* 114 (12 Mar. 2015), p. 120601. DOI: 10.1103/PhysRevLett.114.120601. URL: https://link.aps.org/doi/10.1103/PhysRevLett.114.120601.

[272] Neha S. Wadia, Ryan V. Zarcone, and Michael R. DeWeese. "Solution to the Fokker-Planck equation for slowly driven Brownian motion: Emergent geometry and a formula for the corresponding thermodynamic metric". In: *Phys. Rev. E* 105.3 (Mar. 2022), p. 034130.

[273] Steven Blaber and David A. Sivak. "Skewed thermodynamic geometry and optimal free energy estimation". In: *The Journal of Chemical Physics* 153.24 (2020), p. 244119. DOI: 10.1063/5.0033405.

[274] Carlos A. Plata et al. "Finite-time adiabatic processes: Derivation and speed limit". In: *Phys. Rev. E* 101 (3 Mar. 2020), p. 032129. DOI: 10.1103/PhysRevE.101.032129. URL: https://link.aps.org/doi/10.1103/PhysRevE.101.032129.

[275] Carlos A Plata et al. "Building an irreversible Carnot-like heat engine with an overdamped harmonic oscillator". In: *Journal of Statistical Mechanics: Theory and Experiment* 2020.9 (Sept. 2020), p. 093207. DOI: 10.1088/1742-5468/abb0e1. URL: https://doi.org/10.1088/1742-5468/abb0e1.

[276] Olga Movilla Miangolarra et al. "Underdamped stochastic thermodynamic engines in contact with a heat bath with arbitrary temperature profile". In: *Phys. Rev. E* 103 (6 June 2021), p. 062103. DOI: 10.1103/PhysRevE.103.062103. URL: https://link.aps.org/doi/10.1103/PhysRevE.103.062103.

[277] Gentaro Watanabe and Yuki Minami. "Finite-Time Thermodynamics of Fluctuations in Microscopic Heat Engines". In: *Phys. Rev. Res.* 4.1 (Jan. 2022), p. L012008.

[278] Olga Movilla Miangolarra et al. "Energy harvesting from anisotropic fluctuations". In: *Phys. Rev. E* 104 (4 Oct. 2021), p. 044101. DOI: 10.1103/PhysRevE.104.044101. URL: https://link.aps.org/doi/10.1103/PhysRevE.104.044101.

[279] Patrick Pietzonka, Andre C Barato, and Udo Seifert. "Universal bound on the efficiency of molecular motors". In: *Journal of Statistical Mechanics: Theory and Experiment* 2016.12 (Dec. 2016), p. 124004. DOI: 10.1088/1742-5468/2016/12/124004. URL: https://doi.org/10.1088/1742-5468/2016/12/124004.

[280] Jae Sung Lee, Jong-Min Park, and Hyunggyu Park. "Brownian heat engine with active reservoirs". In: *Phys. Rev. E* 102 (3 Sept. 2020), p. 032116. DOI: 10.1103/PhysRevE.102.032116. URL: https://link.aps.org/doi/10.1103/PhysRevE.102.032116.

[281] L. E. Payne. "Isoperimetric Inequalities and Their Applications". In: *SIAM Review* 9.3 (1967). Publisher: Society for Industrial and Applied Mathematics, pp. 453–488. ISSN: 00361445.

[282] Robert Osserman. "The isoperimetric inequality". In: *Bulletin of the American Mathematical Society* 84.6 (1978), pp. 1182–1238. DOI: bams/1183541466. URL: https://doi.org/.

[283] Yunlong Huang and P. S. Krishnaprasad. "Sub-Riemannian geometry and finite time thermodynamics Part 1: The stochastic oscillator". In: *Discrete & Continuous Dynamical Systems - S* 13.4 (2020), pp. 1243–1268.

[284] Manuel Ritoré. "Constant geodesic curvature curves and isoperimetric domains in rotationally symmetric surfaces". In: *Communications in Analysis and Geometry* 9.5 (2001), pp. 1093–1138.

[285] Gatien Verley et al. "Universal theory of efficiency fluctuations". In: *Phys. Rev. E* 90 (5 Nov. 2014), p. 052145. DOI: 10.1103/PhysRevE.90.052145. URL: https://link.aps.org/doi/10.1103/PhysRevE.90.052145.

[286] Sushant Saryal et al. "Universal Bounds on Fluctuations in Continuous Thermal Machines". In: *Phys. Rev. Lett.* 127 (19 Nov. 2021), p. 190603. DOI: 10.1103/PhysRevLett.127.190603. URL: https://link.aps.org/doi/10.1103/PhysRevLett.127.190603.

[287] Frank Morgan. "Manifolds with density". In: *Notices of the American Mathematical Society* 52 (8 Sept. 2005), pp. 853–858.

[288] César Rosales et al. "On the isoperimetric problem in Euclidean space with density". In: *Calculus of Variations and Partial Differential Equations* 31.1 (2008), pp. 27–46. DOI: 10.1007/s00526-007-0104-y. URL: https://doi.org/10.1007/s00526-007-0104-y.

[289] Frank Morgan and Aldo Pratelli. "Existence of isoperimetric regions in $\mathbb{R}^n$ with density". In: *Annals of Global Analysis and Geometry* 43.4 (2013), pp. 331–365. DOI: 10.1007/s10455-012-9348-7. URL: https://doi.org/10.1007/s10455-012-9348-7.

[290] Ronnie Kosloff and Amikam Levy. "Quantum Heat Engines and Refrigerators: Continuous Devices". In: *Annual Review of Physical Chemistry* 65.1 (2014). PMID: 24689798, pp. 365–393. DOI: 10.1146/annurev-physchem-040513-103724. eprint: https://doi.org/10.1146/annurev-physchem-040513-103724. URL: https://doi.org/10.1146/annurev-physchem-040513-103724.

[291] Bartłomiej Gardas and Sebastian Deffner. "Thermodynamic universality of quantum Carnot engines". In: *Phys. Rev. E* 92 (4 Oct. 2015), p. 042126. DOI: 10.1103/PhysRevE.92.042126. URL: https://link.aps.org/doi/10.1103/PhysRevE.92.042126.

[292] Sebastian Deffner. "Efficiency of Harmonic Quantum Otto Engines at Maximal Power". In: *Entropy* 20.11 (2018). ISSN: 1099-4300. DOI: 10.3390/e20110875. URL: https://www.mdpi.com/1099-4300/20/11/875.

[293] Cédric Villani. *Optimal Transport*. Springer Berlin Heidelberg, 2009. ISBN: 9783540710509. DOI: 10.1007/978-3-540-71050-9. URL: http://dx.doi.org/10.1007/978-3-540-71050-9.

[294] Jean-David Benamou and Yann Brenier. "A computational fluid mechanics solution to the Monge-Kantorovich mass transfer problem". In: *Numerische Mathematik* 84.3 (2000), pp. 375–393. DOI: 10.1007/s002110050002. URL: https://doi.org/10.1007/s002110050002.

[295] Andreas Dechant and Yohei Sakurai. *Thermodynamic interpretation of Wasserstein distance*. 2019. arXiv: 1912.08405 [cond-mat.stat-mech]. URL: https://arxiv.org/abs/1912.08405.

[296] Muka Nakazato and Sosuke Ito. "Geometrical aspects of entropy production in stochastic thermodynamics based on Wasserstein distance". In: *Phys. Rev. Res.* 3 (4 Nov. 2021), p. 043093. DOI: 10.1103/PhysRevResearch.3.043093. URL: https://link.aps.org/doi/10.1103/PhysRevResearch.3.043093.